



National Library
of Canada

Bibliothèque nationale
du Canada

Canadian Theses Service

Services des thèses canadiennes

Ottawa, Canada
K1A 0N4

CANADIAN THESES

THÈSES CANADIENNES

NOTICE

The quality of this microfiche is heavily dependent upon the quality of the original thesis submitted for microfilming. Every effort has been made to ensure the highest quality of reproduction possible.

If pages are missing, contact the university which granted the degree.

Some pages may have indistinct print especially if the original pages were typed with a poor typewriter ribbon or if the university sent us an inferior photocopy.

Previously copyrighted materials (journal articles, published tests, etc.) are not filmed.

Reproduction in full or in part of this film is governed by the Canadian Copyright Act, R.S.C. 1970, c. C-30. Please read the authorization forms which accompany this thesis.

THIS DISSERTATION
HAS BEEN MICROFILMED
EXACTLY AS RECEIVED

AVIS

La qualité de cette microfiche dépend grandement de la qualité de la thèse soumise au microfilmage. Nous avons tout fait pour assurer une qualité supérieure de reproduction.

S'il manque des pages, veuillez communiquer avec l'université qui a conféré le grade.

La qualité d'impression de certaines pages peut laisser à désirer, surtout si les pages originales ont été dactylographiées à l'aide d'un ruban usé ou si l'université nous a fait parvenir une photocopie de qualité inférieure.

Les documents qui font déjà l'objet d'un droit d'auteur (articles de revue, examens publiés, etc.) ne sont pas microfilmés.

La reproduction, même partielle, de ce microfilm est soumise à la Loi canadienne sur le droit d'auteur, SRC 1970, c. C-30. Veuillez prendre connaissance des formules d'autorisation qui accompagnent cette thèse.

LA THÈSE A ÉTÉ
MICROFILMÉE TELLE QUE
NOUS L'AVONS REÇUE



National Library
of Canada

Bibliothèque nationale
du Canada

Ottawa, Canada
K1A 0N4

TC

ISI

0-315-23257-9

CANADIAN THESES ON MICROFICHE SERVICE - SERVICE DES THÈSES CANADIENNES SUR MICROFICHE

PERMISSION TO MICROFILM - AUTORISATION DE MICROFILMER

• Please print or type - Écrire en lettres moulées ou dactylographier

AUTHOR - AUTEUR

Full Name of Author - Nom complet de l'auteur

ROY NARTEN

Date of Birth - Date de naissance

SEPT 16, 1957

Canadian Citizen - Citoyen canadien

☒ Yes / Oui

☐ No / Non

Country of Birth - Lieu de naissance

CANADA

Permanent Address - Résidence fixe

7909-158 STR.
EDMONTON, ALBERTA
T5R 2B9

THESIS - THÈSE

Title of Thesis - Titre de la thèse

THE INFLUENCE OF SEVERAL FACTORS
ON THE LOCAL HEAT TRANSFER FROM
AN ISOTHERMAL CYLINDER

Degree for which thesis was presented
Grade pour lequel cette thèse fut présentée

M. Sc.

Year this degree conferred
Année d'obtention de ce grade

1985

University - Université

U. OF ALBERTA

Name of Supervisor - Nom du directeur de thèse

DR. E. M. GATES

AUTHORIZATION - AUTORISATION

Permission is hereby granted to the NATIONAL LIBRARY OF CANADA to
microfilm this thesis and to lend or sell copies of the film.

The author reserves other publication rights, and neither the thesis nor extensive extracts from it may be printed or otherwise reproduced without the author's written permission.

L'autorisation est, par la présente, accordée à la BIBLIOTHÈQUE NATIONALE DU CANADA de microfilmer cette thèse et de prêter ou de vendre des exemplaires du film.

L'auteur se réserve les autres droits de publication; ni la thèse ni de longs extraits de celle-ci ne doivent être imprimés ou autrement reproduits sans l'autorisation écrite de l'auteur.

ATTACH FORM TO THESIS - VEUILLEZ JOINDRE CE FORMULAIRE À LA THÈSE

Signature

R. Narten

Date

OCT 15, 85

THE UNIVERSITY OF ALBERTA

The Influence of Several Factors on the
Heat Transfer from an Isothermal Cylinder

by

(3) Roy Narten

A THESIS

SUBMITTED TO THE FACULTY OF GRADUATE STUDIES AND RESEARCH
IN PARTIAL FULFILMENT OF THE REQUIREMENTS FOR THE DEGREE
OF MASTER OF SCIENCE

DEPARTMENT OF MECHANICAL ENGINEERING

EDMONTON, ALBERTA

FALL, 1985

THE UNIVERSITY OF ALBERTA

RELEASE FORM

NAME OF AUTHOR: Roy Narten

TITLE OF THESIS: The Influence of Several Factors on the
Local Heat Transfer from an Isothermal
Cylinder.

DEGREE: Master of Science

YEAR THIS DEGREE GRANTED: Fall, 1985

Permission is hereby granted to THE UNIVERSITY OF
ALBERTA LIBRARY to reproduce single copies of this thesis
and to lend or sell such copies for private, scholarly or
scientific research purposes only.

The author reserves other publication rights, and
neither the thesis nor extensive extracts from it may be
printed or otherwise reproduced without the author's
written permission.

(SIGNED) _____

Roy Narten

PERMANENT ADDRESS:

7909 - 158 Street
Edmonton, Alberta
CANADA T5R 2B9

DATE: OCTOBER 15, 1985

THE UNIVERSITY OF ALBERTA
FACULTY OF GRADUATE STUDIES AND RESEARCH

The undersigned certify that they have read, and recommend to the Faculty of Graduate Studies and Research for acceptance, a thesis entitled

The Influence of Several Factors on the
Heat Transfer from an Isothermal Cylinder

submitted by Roy Narten in partial fulfillment of the requirements for the degree of Master of Science.

[Signature]
(Supervisor)

[Signature]

[Signature]

Date: OCTOBER 15, 1985

ABSTRACT

The object of the present study was to compare the effect of various factors on the local heat transfer distribution around an isothermal cylinder in crossflow. To this end, a laboratory apparatus was constructed to determine the local Nusselt number and its distribution around a cylinder. Tests were performed at Reynolds numbers of 40 000, 80 000, and 120 000 to determine the influence of three sizes of surface roughness, as well as the influence of water spray cooling with various airstream liquid water contents. The results of tests performed by others examining the effect of free stream turbulence and cross-sectional shape on the average heat transfer were also examined.

Exposing a cylinder to water spray cooling results in the largest increase in average heat transfer around the upstream side of a cylinder. Although heat transfer coefficients up to 30 times higher than those for single component (air) flow can be obtained with high liquid water contents, the measured increase can be explained or predicted using evaporation, convection, and other heat transfer terms contained in a surface energy balance. No other mechanism for enhanced heat transfer occurs with water spray cooling.

Free stream turbulence and cross-sectional shape both exhibited the smallest influence on the average heat

transfer. A rime icing shape produced the largest increase (22%) in average heat transfer over the corresponding heat transfer from a smooth, circular cylinder. Free stream turbulence, with turbulent intensities up to 5%, can also increase the average heat transfer by approximately 20% to 30%. This measured increase is virtually uniform over the perimeter of the cylinder for the region 0° to 50° from the stagnation line.

It was difficult to establish the relative effect of surface roughness, due to the limited range of Reynolds numbers examined in the present study. Roughness parameters, such as the size, shape, and surface distribution of roughness elements, also differed between studies, precluding any generalizations about the influence of roughness. Results by others suggest that the effect of surface roughness may produce the largest increase in the heat transfer distribution around a cylinder, especially at higher Reynolds numbers. To determine the relative contribution of roughness in an icing model, more tests should be conducted using surfaces which more accurately simulate the rough surfaces associated with atmospheric icing. The range of Reynolds numbers examined should also be restricted to the conditions expected for the particular type of icing being modelled.

An analysis of the data obtained for all water .

spray tests, conducted for the present study, indicated that the horizontal distribution of water spray was not uniform across the test section. Calculations comparing the evaporative mass flux with the mass influx of water droplets impacting on the model indicated that the data obtained for the measured liquid water contents may be questionable. A variation in water content along the horizontal length of the test model heaters would produce lower average liquid water contents than reported in the present study.

ACKNOWLEDGEMENTS

The author wishes to express his sincere appreciation to Dr. E. M. Gates, who supervised the preparation of this thesis. His expert guidance, encouragement, and advice were greatly appreciated.

The author would also like to thank Mr. A. Muir, Mr. T. Villett, and the technicians in the Department of Mechanical Engineering who contributed to the construction of various experimental apparatus. A special thanks are extended to machinist Tony Van Straten for his patience constructing the prototype test models, and to Terry Nord for his advice and assistance assembling the electronic equipment required for this project.

Funding for this project was supplied by a grant from the Department of National Defense, contract no. 2SU82-00334.

Finally, I would like to thank my family and friends for the overall support and encouragement they gave me during my study at the University of Alberta.

TABLE OF CONTENTS

CHAPTER	PAGE
1. INTRODUCTION	1
1.1 Background Information	1
1.2 Influence of Free Stream Turbulence	4
1.3 Influence of Cross-sectional Shape	8
1.4 Present Investigation	12
2. EXPERIMENTAL APPARATUS AND TEST PROCEDURE	14
2.1 The FROST Icing Wind Tunnel	14
2.2 The Test Model	16
2.3 Artificial Surface Roughness	23
2.4 Water Spray System	31
2.5 Instrumentation	32
2.5.1 Cylinder Temperature Measurement and Thermocouple Calibration	32
2.5.2 Air Velocity Measurement	32
2.5.3 Heater Power Supply and Temperature Controller	33
2.6 Test Procedure	36
3. DATA REDUCTION	39
3.1 Calculation of the Nusselt Number	39
3.2 Heat Loss in the Gaps Between Adjacent Heaters	39
3.3 The Local Convective Heat Transfer Coefficient	43
3.4 Heat Transfer Calculations for Smooth and Rough Cylinder Tests	45

CHAPTER	PAGE
4. PRESENTATION OF RESULTS	48
4.1 Heat Transfer Results for Smooth and Rough Cylinders	48
4.2 Influence of Water Spray Cooling	54
5. DISCUSSION	57
5.1 Smooth Cylinder	59
5.2 Influence of Surface Roughness	60
5.3 Influence of Water Spray Cooling	68
5.3.1 Introduction	68
5.3.2 Discussion of Spray Cooling Results..	71
5.3.3 Measurement of the Airstream Liquid Water Content	78
5.4 Heat Transfer Correlations for an Inclined Flat Plate	79
5.5 Summary	82
6. CONCLUSIONS AND RECOMMENDATIONS	86
6.1 Present Investigation	86
6.2 Tests Performed by Others	88
REFERENCES	89
APPENDIX A. Computer Program Listings	92
APPENDIX B. Electrical Schematic Diagram of the 12 Channel Heater Temperature Controller ...	114
APPENDIX C. Experimental Data	116
APPENDIX D. Finite Difference Analysis of the Heat Conduction in a Typical Cylinder Sector..	136
APPENDIX E. Steady State Heat Conduction Loss in the Gap Between Heaters. (Analytic Solution)	150
APPENDIX F. Derivation of the Heat Transfer Due to Evaporation of Water Vapour from The Cylinder Surface	158

LIST OF TABLES

TABLE		PAGE
2.1	Summary of the rough surfaces tested.....	29
3.1	Summary of tests performed and data reduction for the smooth and rough cylinder tests.....	47
5.1	The effect of relative humidity on the evaporation heat transfer.....	75
5.2	Average heat transfer from a spray cooled isothermal cylinder for the region 0° to 90° from the stagnation line. (Hodgson, et. al., 1968).....	76
D.1	Finite difference solution. Summary of the steady state heat losses from a typical nichrome strip heater.....	149

LIST OF FIGURES

FIGURE

PAGE

- 1.1 The influence of free stream turbulence on the local Nusselt number around a cylinder for various turbulence levels at $Re = 5300$ (Boulos & Pei, 1974)..... 7
- 1.2 Heat transfer distributions around typical ice accretion shapes. (Van Fossen, et. al., 1984)..... 9
- 1.3 Average heat transfer from typical smooth ice accretion shapes for the region 0° to 65° from the stagnation line (Van Fossen, et al., 1984)..... 11
- 2.1 A schematic drawing of the FROST icing wind tunnel..... 15
- 2.2 Model construction detail and location of strip heaters..... 21
- 2.3 Cylinder surface showing typical heater and thermocouple installation..... 23
- 2.4 Small scale surface roughness..... 25
- 2.5 Medium scale surface roughness..... 26
- 2.6 Large scale surface roughness..... 28
- 2.7 Schematic of the heater feedback control circuit..... 34
- 4.1 Local Nusselt number versus angular position comparing rough cylinder data with smooth cylinder data. ($Re = 40\ 000$)..... 49
- 4.2 Local Nusselt number versus angular position comparing rough cylinder data with smooth cylinder data. ($Re = 80\ 000$)..... 50
- 4.3 Local Nusselt number versus angular position comparing rough cylinder data with smooth cylinder data. ($Re = 120\ 000$)..... 51
- 4.4 Local Nusselt number versus angular position for a spray cooled cylinder with different airstream liquid water contents. ($Re = 40\ 000$)..... 55

4.5	Local Nusselt number versus angular position for a spray cooled cylinder with different airstream liquid water contents. ($Re = 80\,000$).....	56
5.1	Average heat transfer from a cylinder comparing data obtained for a smooth, rough, and water sprayed cylinder for the isothermal region 0° to 90° from the stagnation line.....	61
5.2	Average heat transfer from a rough circular cylinder for the region 0° to 50° from the stagnation line.....	66
5.3	Average heat transfer from an inclined flat surface for various angles of attack. (Lessmann and Test, 1984).....	81
D.1	Geometry of the finite difference model.....	137
D.2	Nodal numbering scheme for the finite difference grid.....	138
D.3	Corner node with a convective boundary and an insulated boundary.....	140
D.4	Node on a boundary separating regions with different thermal conductivities.....	141
D.5	Node intersecting an insulated boundary and two regions with different thermal conductivities.....	142
D.6	Nodal numbering scheme used with smaller grid increments.....	145
D.7	Nodes on the convective boundary.....	145
D.8	Contour plot solution of the finite difference analysis showing the temperature distribution in a typical cylinder sector....	146
D.9	Equations used in the numerical solution to calculate the heat loss from the side and bottom of the nichrome strip heater.....	148
E.1	Geometry for the analytical model.....	150
E.2	Boundary conditions for the analytical model.	151

LIST OF PHOTOGRAPHIC PLATES

PLATE		PAGE
2.1	Photograph of the wind tunnel test section and associated instrumentation.....	17
2.2	Photograph showing the test model installed in the wind tunnel. Side window has been removed for clarity. W.....	19
2.3	The test model.....	20
2.4	Fabric screen used to simulate small scale surface roughness.....	25
2.5	Photograph showing beads attached to the fabric screen to simulate medium scale surface roughness.....	26
2.6	Photograph showing beads attached to the fabric screen to simulate large scale surface roughness.....	28
2.7	Photograph of the large scale roughness screen wrapped around the test model. Medium scale roughness screen is shown in the foreground.....	30

NOMENCLATURE

<u>Symbol</u>		<u>Units</u>
a	depth of each strip heater.	[m]
A	exposed surface area of each heater.	[m ²]
α	thermal diffusivity.	[m ² /s]
b	half the width of the gap between adjacent heaters.	[m]
C _p	specific heat capacity at constant pressure.	[J/kg·K]
D	-diameter of test cylinder.	[m]
$D_{\text{H}_2\text{O}}$	-diffusivity of water vapour in air. (Appendix F)	[m ² /s]
Δ	increment in the variable.	
e	saturation vapour pressure of water vapour.	[Pa]
ϵ	ratio of the molecular weights of water vapour and dry air.	dimensionless
E	voltage.	[V]
f	friction factor.	dimensionless
h	local convective heat transfer coefficient.	[W/m ² ·°C]
h _D	mass transfer coefficient.	[m/s]
H _r	height of roughness element. (figure 5.2)	[mm]
i	numerical grid coordinate in the radial direction.	
j	numerical grid coordinate in the circumferential (y) direction.	
k	thermal conductivity.	[W/m·°C]
K ₁	conductivity of epoxy. (Appendix D)	[W/m·°C]
K	thermal conductivity of epoxy.	[W/m·°C]
K ₂	thermal conductivity of foam.	[W/m·°C]

<u>Symbol</u>		<u>Units</u>
l_v	latent heat of vaporization.	[J/kg]
L	length of the gap between heaters.	[m]
LWC	liquid water content in the airstream.	[g/m ³]
λ_n	positive roots of equation 3.3.	dimensionless
\dot{m}	mass flux per unit time.	[kg/s]
m	mass.	[kg]
M	molecular weight.	[g/mol]
v	specific volume.	[m ³ /kg]
Nu	Nusselt number.	dimensionless
Pr	Prandtl number for air.	dimensionless
p	partial pressure.	[Pa]
P	-electrical power.	[W]
	-air pressure.	[Pa]
q	heat flux.	[W]
Q	heat flux (total or per unit area).	[W] or [W/m ²]
R	-electrical resistance.	[ohms]
	-universal gas constant.	= 8.31441 [kJ/kg·K]
Re	Reynolds number.	dimensionless
RH	relative humidity.	dimensionless fraction
R_v	specific gas constant for water vapour.	[J/kg·K]
R_d	specific gas constant for dry air.	[J/kg·K]
ρ_{vs}	water vapour density at the cylinder surface temperature.	[kg/m ³]
ρ_{va}	water vapour density at ambient air temperature.	[kg/m ³]
ρ	density.	[kg/m ³]

SymbolUnits

Sc	Schmidt number for water vapour in air. dimensionless	
T	temperature.	[°C]
T _o	temperature normalized with respect to ambient temperature. ($T - T_a$)	[°C]
u _m	mean velocity.	[m/s]
v	air velocity.	[m/s]
V	total volume.	[m ³]
W	humidity ratio.	dimensionless
x	mole fraction.	dimensionless
x	coordinate in the radial direction. (Appendix D)	
y	coordinate in the circumferential direction. (Appendix D)	
ξ	distance along cylinder surface from the stagnation point non-dimensionalized by dividing by the diameter D.	dimensionless

Subscripts

sen	sensible heating component per unit area.
stat	static conditions.
total	total conditions.
θ	local position (angle) on the cylinder measured from the stagnation line.
a	ambient air.
c	convective component.
d	dry air.
e	evaporative component.
gap	region between heaters at the cylinder surface.
h	electrical heater on the cylinder.

Subscripts

I	the radial direction from the heater toward the cylinder centre.
J	the circumferential direction around the cylinder surface.
m	mean value.
n	nth root of equation 3.5
o	normalized with respect to ambient conditions.
s	cylinder surface (heater).
v	water vapour.
w	water (or water droplets).

Superscripts

r	iteration index.
---	------------------

CHAPTER 1

INTRODUCTION

1.1 Background Information

A field of study receiving increasing attention in recent years is the prediction of atmospheric ice accretion on surfaces. Atmospheric icing occurs when supercooled water droplets, suspended in the air, impact on a surface which is colder than the freezing point of water. The water droplets may be suspended in the air in the form of a cloud or generated by the wind as in sea spray. Significant accumulations of ice can occur on ships, off-shore structures, power lines, etc. causing structural damage. Helicopters and small aircraft are especially susceptible to icing problems since they fly at lower altitudes where they can be exposed to ice clouds. A knowledge of the anticipated additional loading due to ice accumulation must be incorporated into the initial design to avoid these potential problems.

Several attempts have been made to model the ice accretion process on structures to provide predictions or estimates of the increased loads and the effects of these loads. Computer programs have been developed for helicopter blades (Stallabrass, 1957, Cansdale and Gent, 1983) and airfoils (Lozowski and Oleskiw, 1981); however, most of the current work is concentrated on modelling ice

accretion on circular cylinders. Cylinder icing has been investigated by Lozowski, Stallabrass and Hearty (1983), Makkonen (1981, 1984), Ackley and Templeton (1979), and McComber (1982).

An analytic icing model is comprised of two distinct components. One component is purely dynamical, dealing with the airflow around the body, droplet trajectories, and the physics of impacting drops such as deformation and splashing. The other component accounts for the thermodynamics occurring at the surface, and is necessary to determine the local rate of ice accretion. In the icing models, a steady state energy balance is carried out at the surface to determine the fraction of the impinging water that freezes. This energy balance is comprised of many different terms (Lozowski, et. al., 1983) including radiative, convective, and conductive heat flux from the accretion to the airstream, evaporative heat flux, latent heat flux to the accretion due to freezing of some, or all, of the impinging water, and the sensible heat transfer between the impinging droplets and the surface. If the surface energy balance predicts that all the impinging water will freeze, the freezing fraction is equal to one. In this case, the local rate of ice accretion can easily be determined by using the local impingement parameters. However, if all the impinging water does not freeze, the accretion is said to be "glaze" or "wet" icing and a liquid layer will form at the

surface. In this case the surface temperature is assumed to be 0°C , and the energy balance then provides the freezing fraction and the local ice accretion rate.

It is not necessary to account for every term in the surface energy balance to obtain a good estimate of the local ice accretion rate. In most icing conditions, the important terms in the energy balance are the evaporative and convective terms.

The magnitudes of the evaporation and convection terms are directly dependent on the value of the local convective heat transfer coefficient (h) at the surface, since both terms are a linear function of this coefficient. A measure of the local heat transfer coefficient and its distribution around a cylinder or profile is therefore required in an icing model to accurately predict the local icing rate on a body. In some systems the quantity " h " can be calculated analytically; however, for most situations the heat transfer coefficient must be determined experimentally.

In order to make an icing model time dependent it is also important to account for any new surface or flow conditions which may influence the magnitude or distribution of the heat transfer coefficient at the surface. The introduction of water spray into the airstream and the presence of a liquid layer on the surface have been shown to greatly alter the heat transfer distribution around a cylinder (Hodgson, et. al., 1968,

Saterbak, 1967)). Two other factors which also influence the heat transfer are cross-sectional shape and surface roughness. As ice accumulates on a cylinder, the cross-section of the profile deviates further and further from a smooth circular cylinder. The surface may remain smooth or it may become very irregular and rough. The presence of a rough surface can influence the local heat transfer by changing the point at which the boundary layer undergoes transition from laminar to turbulent flow. No literature is available which compares the combined or separate effects of all of the various factors on the heat transfer from a cylinder. The relative effects of surface roughness, water spray cooling, etc. should be evaluated to determine which factor or factors represent the largest influence on the heat transfer distribution. The local ice accretion rate, predicted by models incorporating a surface energy balance calculation, may be in error if the influence of these factors is not accounted for. Therefore, an understanding of which factors have the largest influence on the local heat transfer distribution would increase the accuracy of many icing models presently being developed.

1.2 Influence of Free Stream Turbulence

The level of free stream turbulence present in the air stream can influence the heat transfer distribution around a cylinder. No experiments were conducted in the

present study to examine the effect of turbulence on the heat transfer distribution; however, the results of tests conducted by others are presented here.

Seban (1960) studied the effect of screen induced free stream turbulence on the local heat transfer distribution around 32 mm and 48 mm diameter cylinders. The turbulence was induced using a 6 mm screen mesh which produced a scale of turbulence of approximately 4 mm. This size screen only produced turbulent intensities as high as 1.6% at 46 m/s. Although Seban noted unusually high turbulent intensities in his clear wind tunnel without any screens, his results indicate a definite increase in the heat transfer in the region of laminar flow. The maximum heat transfer occurred at the stagnation point and decreased with position from the stagnation line. Seban concluded that, although the heat transfer is sensitive to variations in turbulence, only a slight increase in free stream turbulence over the clear tunnel value was required to increase the stagnation heat transfer by approximately 30%. Thereafter, the heat transfer increased only slightly when additional turbulence was introduced into the test section. Examination of data obtained by Seban showed that the average heat transfer over the entire front face of the cylinder increased by approximately 20% due to free stream turbulence. This calculation was based on data obtained over a range of Reynolds numbers from 137 000 to 214 000.

The influence of free stream turbulence on the heat transfer from an isothermal cylinder was also investigated by Boulos and Pei (1974). Their results for three different levels of turbulence at a Reynolds number of 5300 are presented in Figure 1.1. The exact solution of the laminar boundary layer equations for a cylinder with no free stream turbulence (Frossling, 1958) is also plotted in Figure 1.1. The results also indicate a definite increase in the heat transfer immediately downstream of the stagnation point. The average heat transfer for the region 0° to 60° from the stagnation line increased by approximately 25% for a turbulence level of 5.28%. The stagnation line heat transfer increased approximately 32% for this level of turbulence.

Boulos and Pei also conducted tests to determine the influence of Reynolds number on the stagnation line heat transfer for turbulence levels between 1% and 6%. They found that the stagnation Nusselt number varied linearly with Reynolds number with a positive slope of 0.5. This was based on data obtained at three Reynolds numbers between 3000 and 9000.

Tests were also performed by Van Fossen, et. al. (1984) to study the influence of free stream turbulence on the heat transfer from a circular cylinder. Heat transfer tests, performed over the range of Reynolds numbers from 50 000 to 180 000, indicated that a 3.5% turbulence level with a scale of 1 cm produced a 33% increase in average

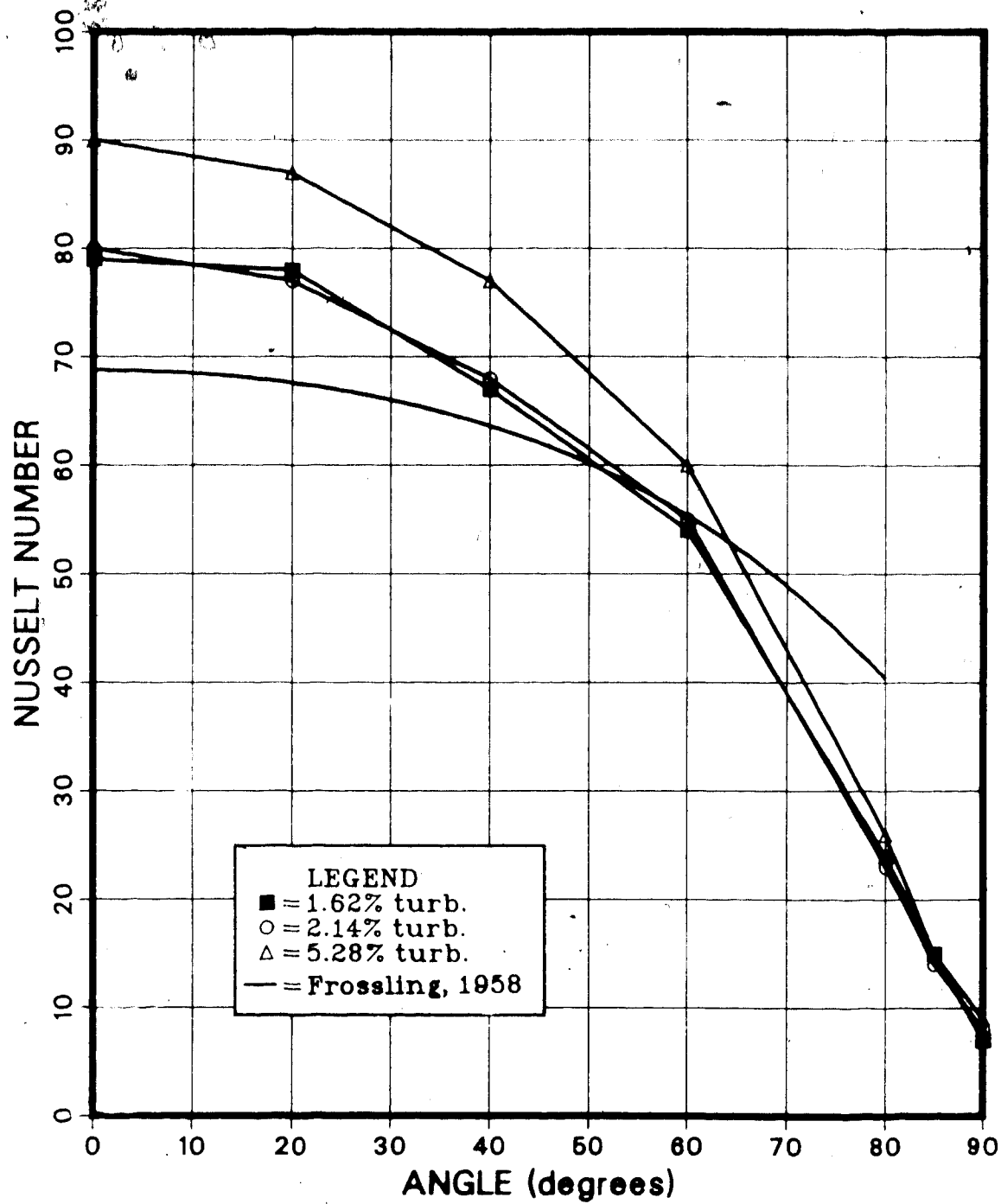


Figure 1.1 The influence of free stream turbulence on the local Nusselt number around a cylinder for various turbulence levels at $Re = 5300$. (Boulos and Pei, 1974)

heat transfer for the region 0° to 50° from the stagnation line. Local measurements made by Van Fossen showed that the increase in heat transfer was virtually uniform around the perimeter of the cylinder for the region specified.

The results due to Seban (1960), Van Fossen, et. al. (1984), and Boulos and Pei (1974) confirm that the average heat transfer from a cylinder will increase by approximately 20% to 30% due to the influence of free stream turbulent intensities up to 5%.

1.3 Influence of Cross-sectional Shape

The local heat transfer distribution around irregular cylindrical shapes has been investigated by Van Fossen, et. al. (1984), and Arimilli, et. al. (1984). The results due to Van Fossen are presented in Figure 1.2. The irregular cross-sections shown in Figure 1.2 are typical of shapes obtained by accreting ice on a circular cylinder. The shapes correspond to 2 minute, 5 minute, and 15 minute accumulations of ice in an icing wind tunnel.

The data plotted in Figure 1.2 was obtained at a Reynolds number of approximately 136 000. It is evident that the local heat transfer distribution around the cylinder is extremely sensitive to the cross-sectional shape. In order to effectively evaluate the influence of shape, the average heat transfer for the region 0° to 65° from the stagnation line was plotted versus the Reynolds

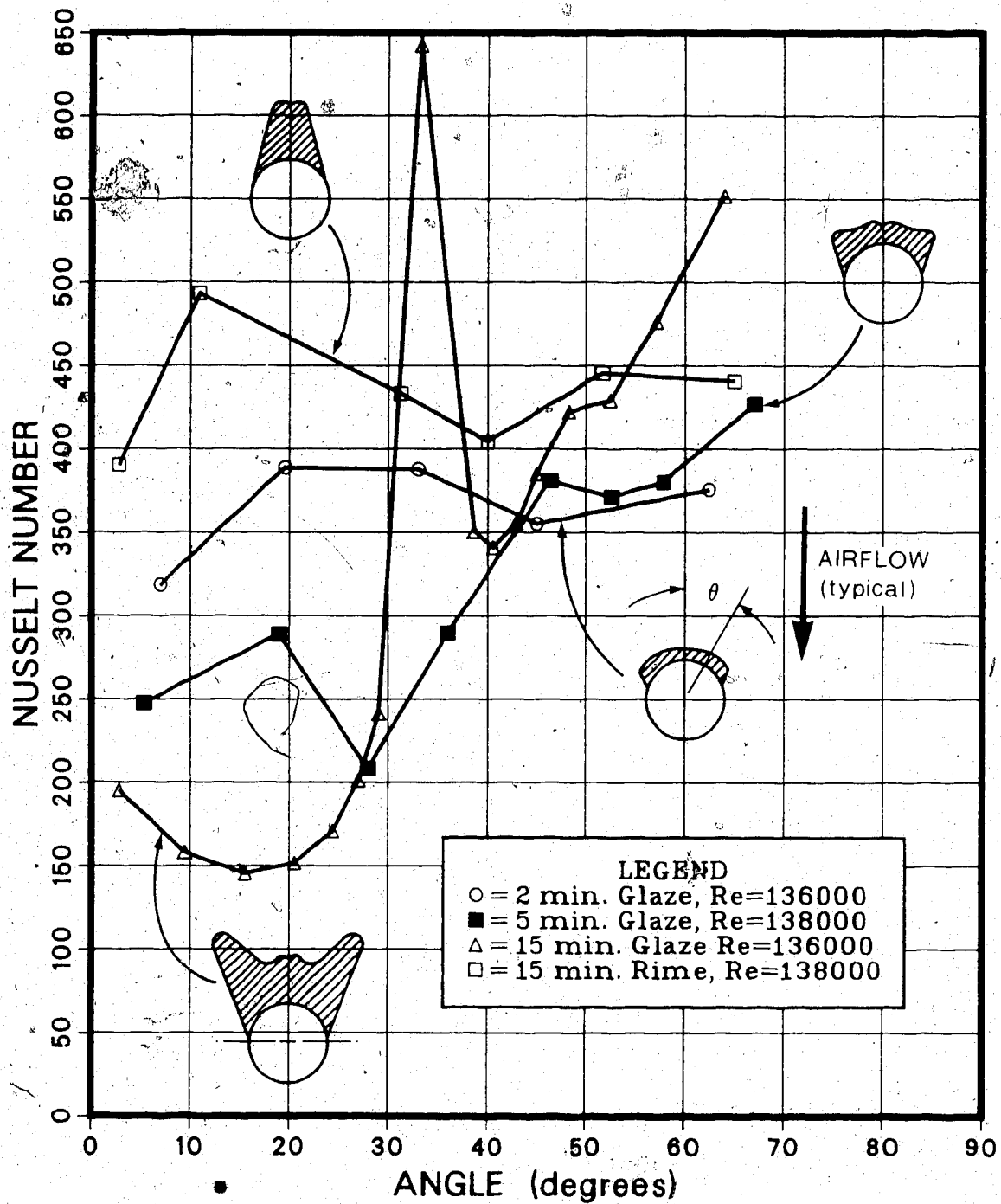


Figure 1.2 Heat transfer distributions around typical ice accretion shapes. (Van Fossen, et. al., 1984)

number for each icing shape. The results from tests performed over a range of Reynolds numbers from 50 000 to 180 000 are plotted in Figure 1.3. Figure 1.3 shows data obtained for each icing shape as well as a smooth circular cylinder. The average heat transfer for the smooth circular cylinder was consistently higher than both the 5 minute and 15 minute glaze ice shapes at all Reynolds numbers.

At a Reynolds number of 50 000, there was no noticeable increase in average heat transfer compared with circular cylinder results for either the 2 minute glaze or 15 minute rime icing shapes. Results indicated the average heat transfer for the region 0° to 65° from the stagnation line decreased by up to 20% with the 5 and 15 minute rime icing shapes; however, these shapes showed little or no difference from smooth cylinder heat transfer at the highest Reynolds number tested. The 15 minute rime ice shape exhibited the highest increase in average heat transfer for the entire range of Reynolds numbers tested. A 22% average increase was obtained for this shape for the range of Reynolds numbers between 50 000 and 180 000.

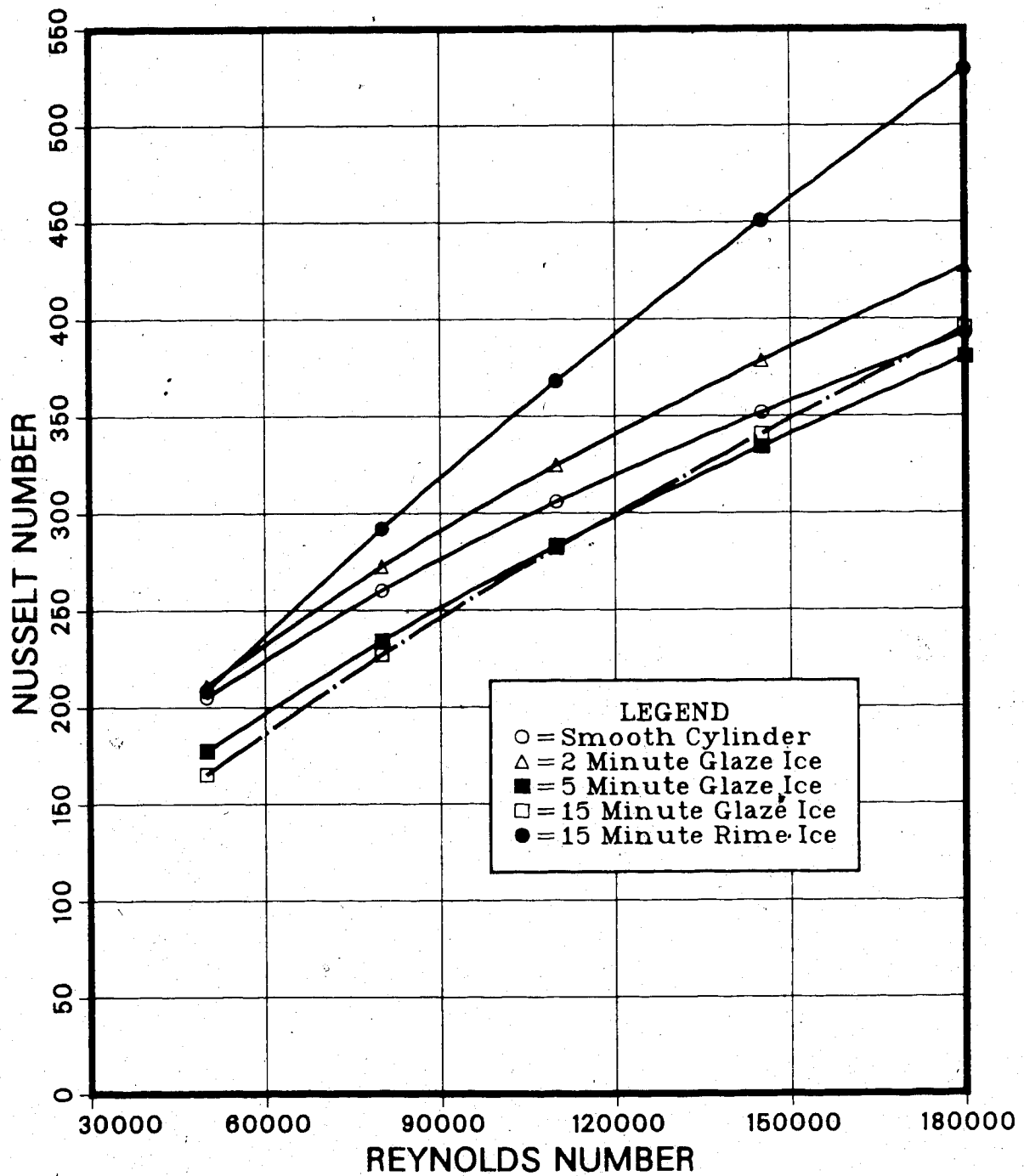


Figure 1.3 Average heat transfer from typical smooth ice accretion shapes for the region 0° to 65° from the stagnation line. (Van Fossen, et. al., 1984)

1.4 Present Investigation

The purpose of the present investigation was to compare the relative effects of the following four factors on the local heat transfer distribution around an isothermal cylinder:

1. Water spray cooling.
2. Surface roughness.
3. Cross-sectional shape.
4. Free stream turbulence.

The relative magnitude of the influence of each factor was examined to determine which factor or factors have the largest effect on the heat transfer distribution.

A test cylinder was constructed for the present study to experimentally determine the influence of water spray cooling and surface roughness on the local heat transfer distribution around a cylinder for the isothermal region 0° to 90° from the stagnation line. Results of tests conducted by others were also included to compare the effects of free stream turbulence and cross-sectional shape.

It has been suggested that the relatively large heat transfer rates associated with water spray cooling can not be predicted simply using terms contained in a standard surface heat balance formulation such as evaporation, convection, and sensible heat transfer. Another objective of the present investigation was to determine if an additional heat transfer mechanism occurs

in two component (water-in-air) flow due to splashing into a liquid layer on the surface. Results are presented as the local Nusselt number versus the angle from the stagnation line. The effect of Reynolds number on the average Nusselt number is also presented for some data. No attempt was made to produce correlations for the results obtained in this study.

Conclusions and recommendations for further study are included in Chapter 6.

CHAPTER 2

EXPERIMENTAL APPARATUS AND TEST PROCEDURE

2.1- The FROST Icing Wind Tunnel

All heat transfer tests were conducted in the FROST icing wind tunnel located in the Mechanical Engineering Building at the University of Alberta. FROST is an acronym for Fundamental Research on Solidification and Thawing. A schematic of the FROST tunnel is shown in Figure 2.1.

The FROST tunnel is a closed loop wind tunnel with a direct drive axial flow fan driven by a 22 kW constant speed electric motor. The fan (model V 421 - X 42) was designed by AEROVENT FAN Co., Inc., Pigua, Ohio, U.S.A. and manufactured under license by POWLES LAND ENGINEERING LTD., Woodbridge, Ontario. Air speed can be varied from 10 m/s to 40 m/s by adjusting a set of motorized dampers mounted directly upstream of the fan.

The air in the wind tunnel can be cooled down to -15°C if cold air temperatures are required. Cooling is provided by a 30 kW refrigeration system connected to cooling coils mounted in the tunnel. The refrigeration equipment was not utilized during any tests in this study since all tests were conducted with ambient air at room temperature.

A 16:1 area contraction ratio accelerates the air

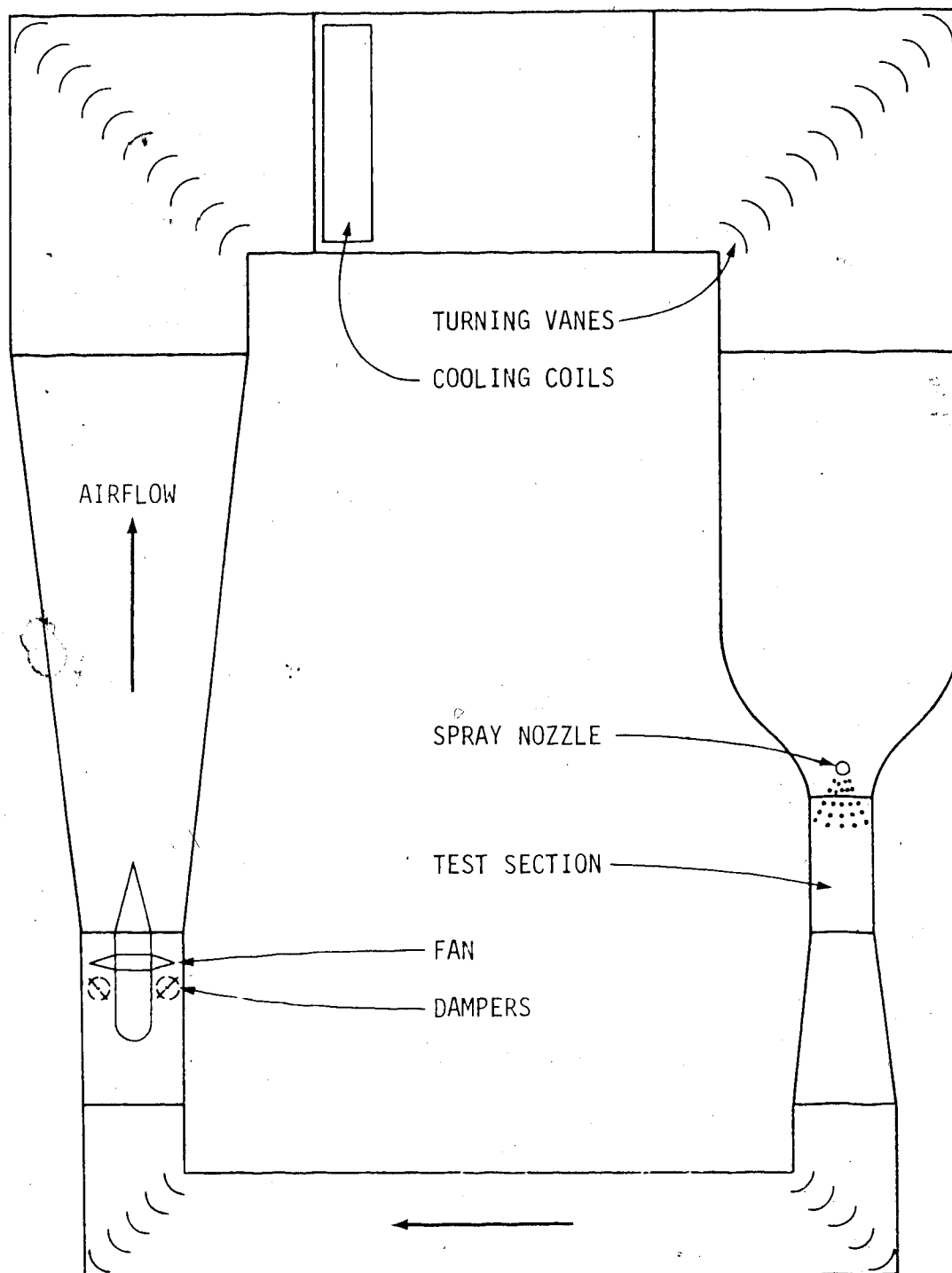


Figure 2.1 A schematic drawing of the FROST icing wind tunnel.

entering the high velocity test section (see Plate 2.1). The test section has an octagonal cross-section with a width of 460 mm. Single component air temperature in the test section was measured using a copper-constantan thermocouple mounted 335 mm downstream of the model. To monitor the temperature with the spray nozzle operating, a copper-constantan thermocouple was mounted upstream of the spray nozzle in the low velocity section of the wind tunnel.

The velocity in the test section was determined by measuring the static pressure drop across the contraction entering the test section. The method used to establish the air velocity is discussed in detail in Section 2.5.2 entitled "Air velocity measurement".

Tests were conducted by Sroka (1972) to determine the velocity profile in the working section of the wind tunnel. His tests indicated a uniform velocity profile over the working range of the tunnel with less than 0.2% variation from the mean velocity at 40 m/s. Sroka also determined the turbulence intensity at the centreline of the working section using a constant temperature hot wire anemometer. The turbulence intensity was found to be between 0.03% - 0.08% over the working range of the tunnel.

2.2 The Test Model

All heat transfer tests in this study were carried

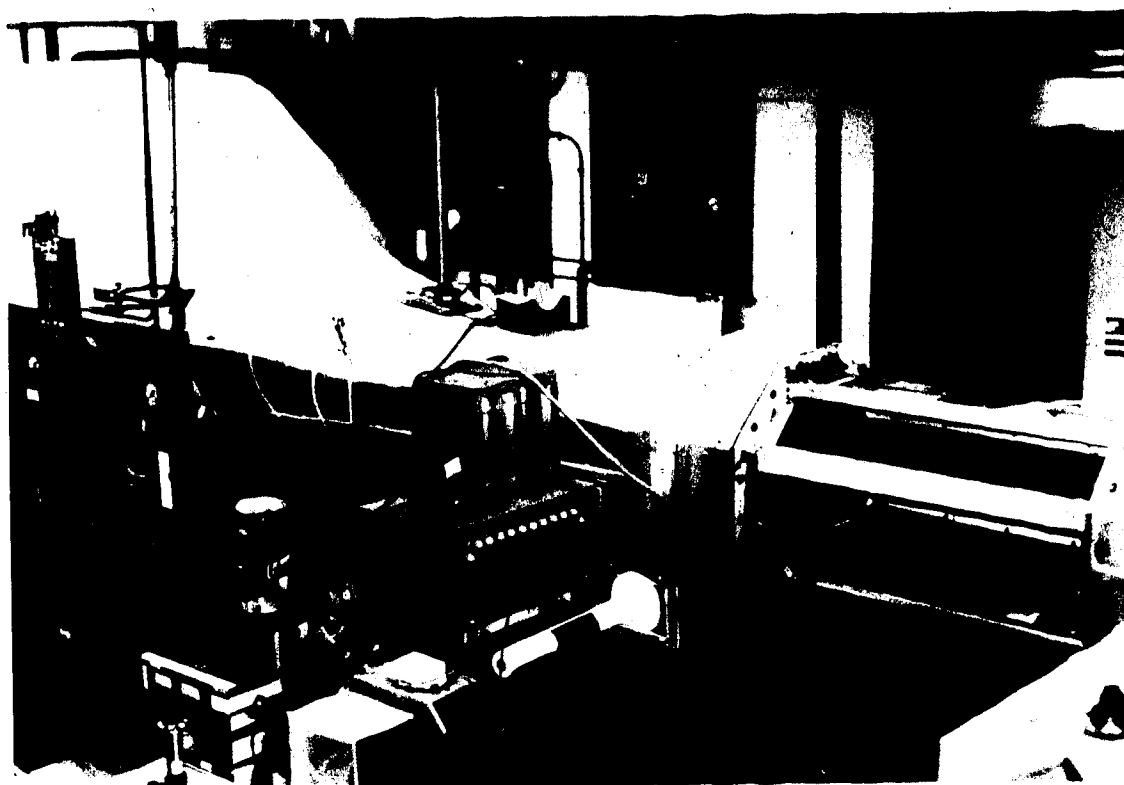


Plate 2.1 Photograph of the wind tunnel
test section and associated
test instrumentation..

out using a 60 mm diameter foam cylinder mounted horizontally in the tunnel (see Plate 2.2). The model was constructed of polystyrene foam and was 455 mm long (see Plate 2.3). Since the foam is very light, prototype models experienced vibration problems at higher velocities in the wind tunnel. To rectify this, a 25 mm diameter plexiglass tube with a 3.2 mm wall thickness was installed in the core of the foam cylinder for additional stiffness (see Figure 2.2). The tube was filled with expanded polyurethane foam to minimize the heat loss to the centre of the model.

An isothermal surface was simulated by attaching 12 electrically heated nichrome metal strips to the cylinder surface. The strip heaters were mounted with epoxy around the circumference from -10° to $+100^{\circ}$ from the stagnation line as shown in Figure 2.2. Each nichrome strip was 3.2 mm wide, 152.4 mm long, and 0.2 mm thick. To evaluate the local heat transfer coefficient around the cylinder, the heaters were mounted on the foam at 10 degree increments around the circumference of the cylinder. The heaters located at -10° and $+100^{\circ}$ from the stagnation line served as guard heaters to minimize the circumferential heat loss from the 0° and 90° heaters. After installation of the heaters, the gap between adjacent heaters at the surface was filled with an epoxy having a thermal conductivity of $1.13 \text{ W/m}\cdot^{\circ}\text{C}$, and the entire cylinder was sanded smooth and round to eliminate any surface



Plate 2.2 Photograph showing the test model installed in the wind tunnel. Side window has been removed for clarity.

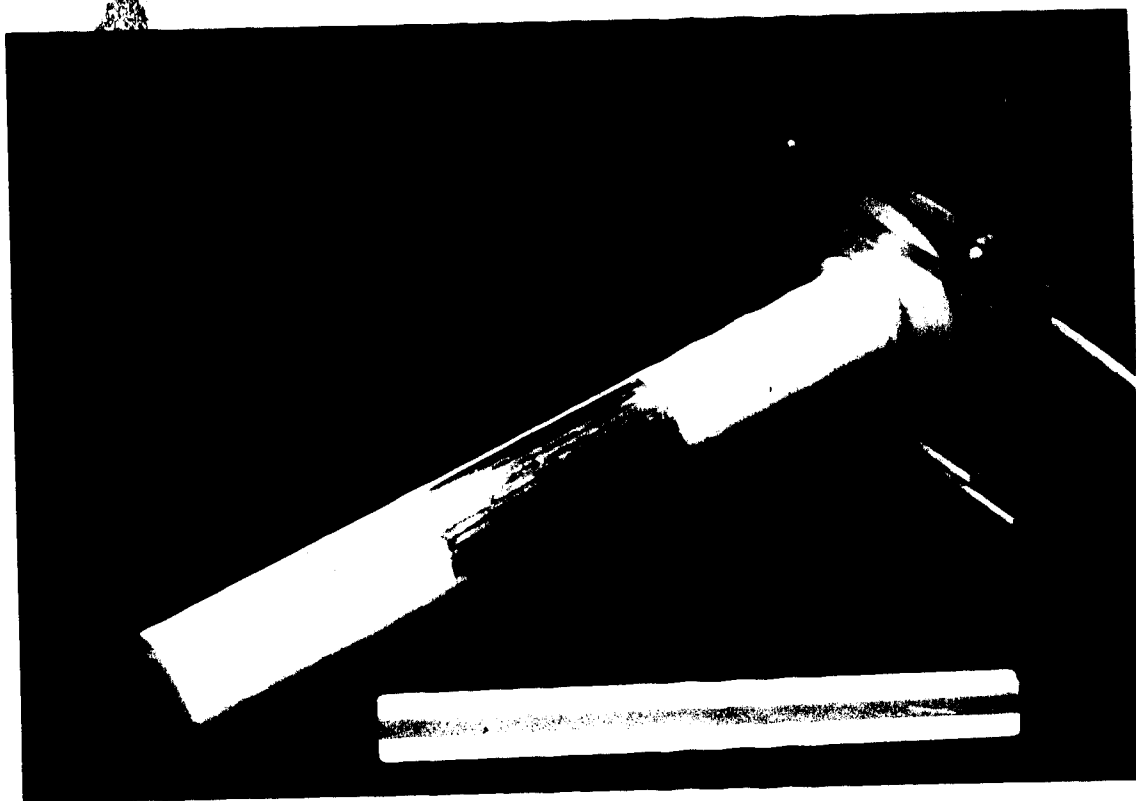


Plate 2.3 The test model.

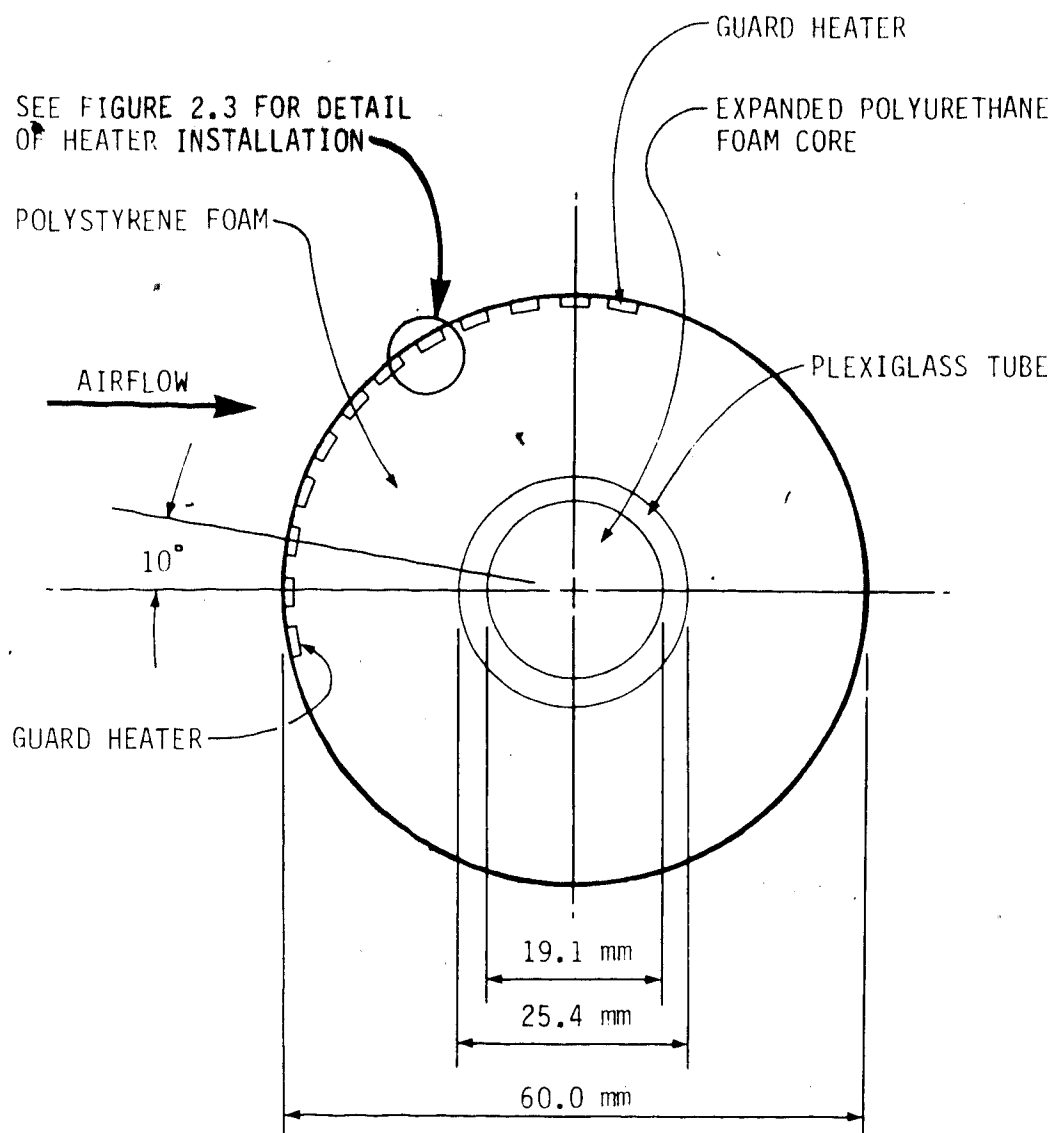


Figure 2.2 Model construction detail and location of strip heaters.

irregularities.

The temperature of each heater was monitored using 36 gauge (0.127 mm) teflon coated copper-constantan thermocouples. Each thermocouple junction (one for each heater) was positioned at the center of the heater and attached to the underside with epoxy. To electrically isolate the thermocouple junctions from the electric heaters, a thin layer of epoxy was applied to each heater before attaching the thermocouples (see Figure 2.3). The method used to calibrate the thermocouples is described in Section 2.5.1. A description of the power supply and temperature controller for the electric heaters is included in Section 2.5.3. Two pairs of wires were connected to each heater. One pair supplied the heater current while the second pair was attached to measure the voltage drop across the heater. The wires were run through the center core of the cylinder and out one end.

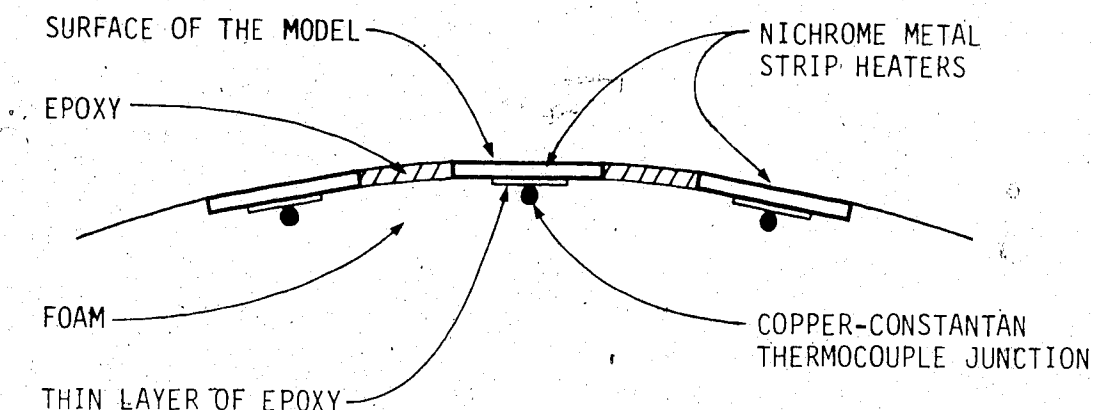


Figure 2.3 Cylinder surface showing typical heater and thermocouple installation.

2.3 Artificial Surface Roughness

The influence of a rough surface on the local convective heat transfer around the cylinder was investigated in this study. Three different scales of artificial surface roughness were tested using removable fabric screens.

To simulate small scale roughness elements, a fabric screen 265 mm long and 0.3 mm thick was wrapped around the model. A mesh was used since it was a simple method of creating a three-dimensional roughness element with minimal resistance to convective heat transfer at the surface (see Plate 2.4). Two 25 mm wide velcro strip fasteners were glued to the edges of the screen to join

the screen at the downstream side of the cylinder and also to facilitate easy removal (see Figure 2.4). The 0.3 mm screen simulates a surface roughness element corresponding to 0.5% of the bare cylinder diameter. The average spacing between roughness elements is approximately 1.6 times the element height (screen thickness). The screen was cut to extend approximately 55 mm beyond the ends of the heaters.

Medium and large surface roughness elements were simulated by attaching two different size beads to the fabric screen. A slightly larger fabric mesh was used to ease installation of the large beads on the screen. This screen was referred to as the "coarse screen" in this study, while the screen used with the small roughness elements was referred to as the "fine" screen. Only the data obtained using the fine fabric mesh was reported for the small scale roughness, since both screens produced approximately the same results. The clear space between beads in the axial direction was chosen to be approximately one element diameter for both the medium and large roughness elements.

To simulate medium scale roughness, 2.1 mm plastic beads (see Plate 2.5) were attached to the screen to cover an area that extended 40 mm beyond both ends of the heaters (see Figure 2.5). The average surface density of medium roughness elements was 8.6 elements/cm². Using this method of constructing surface roughness, both the

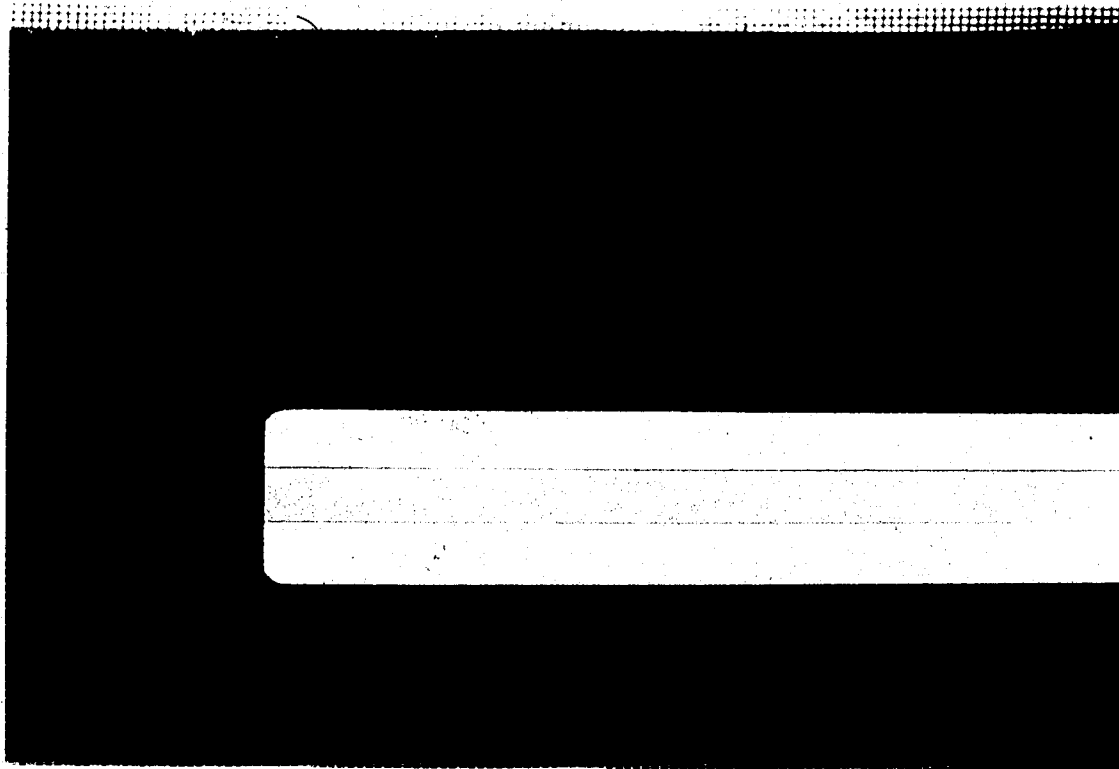


Plate 2.4 Fabric screen used to simulate small scale surface roughness.

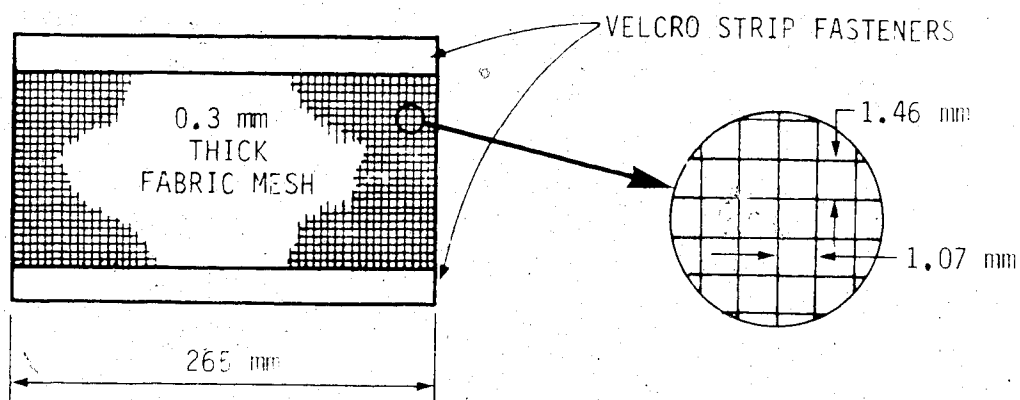


Figure 2.4 Small scale surface roughness.

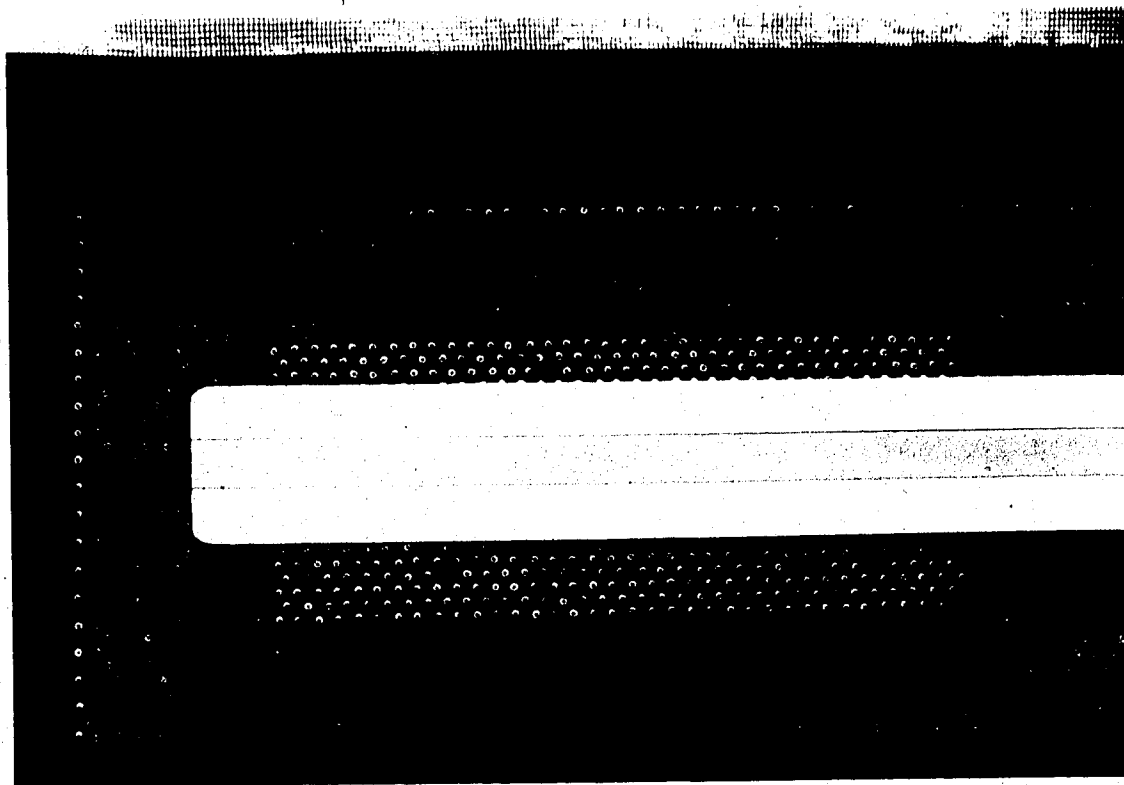


Plate 2.5 Photograph showing beads attached to the fabric screen to simulate medium scale surface roughness.

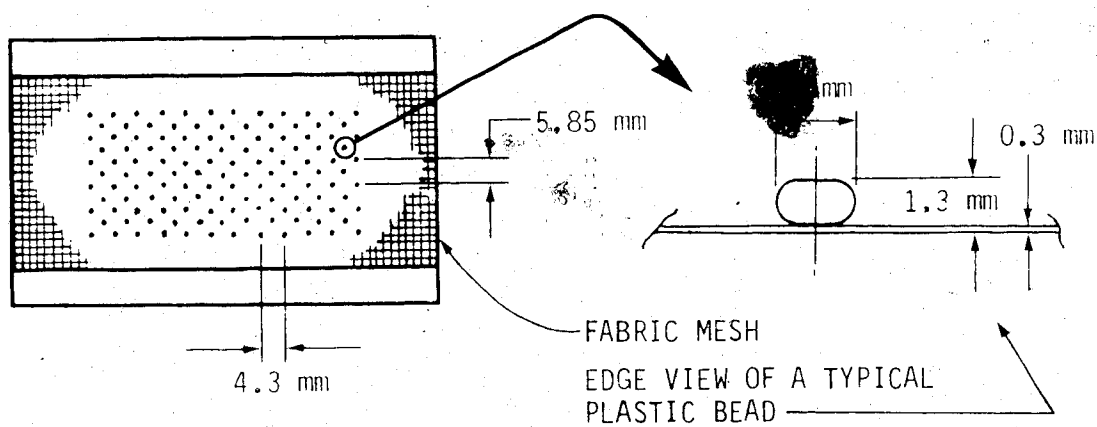


Figure 2.5 Medium scale surface roughness.

screen and the beads contribute to the increase in local convective heat transfer. To only consider the effect due to the plastic beads, the influence on the heat transfer due to the bare screens was subtracted from the overall results. See Section 3.4 for details of these calculations. The 2 mm element diameter simulates a surface roughness corresponding to 3.5% of the bare cylinder diameter.

Large scale surface roughness was constructed similar to the medium roughness, using 4.6 mm diameter glass beads to represent large roughness elements (see Plate 2.6). Each bead was approximately hemispherical in shape as shown in Figure 2.6. A sufficient number of elements were used to cover an area which extended 50 mm beyond both ends of the heaters. The 4.6 mm element diameter simulates a three-dimensional surface roughness corresponding to 7.7% of the bare cylinder diameter. The average surface density of large scale roughness elements was 2.0 elements/cm². A summary of the three different surface roughnesses tested is shown in Table 2.1.

Plate 2.7 is a photograph showing the medium roughness screen with the white velcro strips attached to each side. This photo also shows the large roughness screen wrapped around the test model.

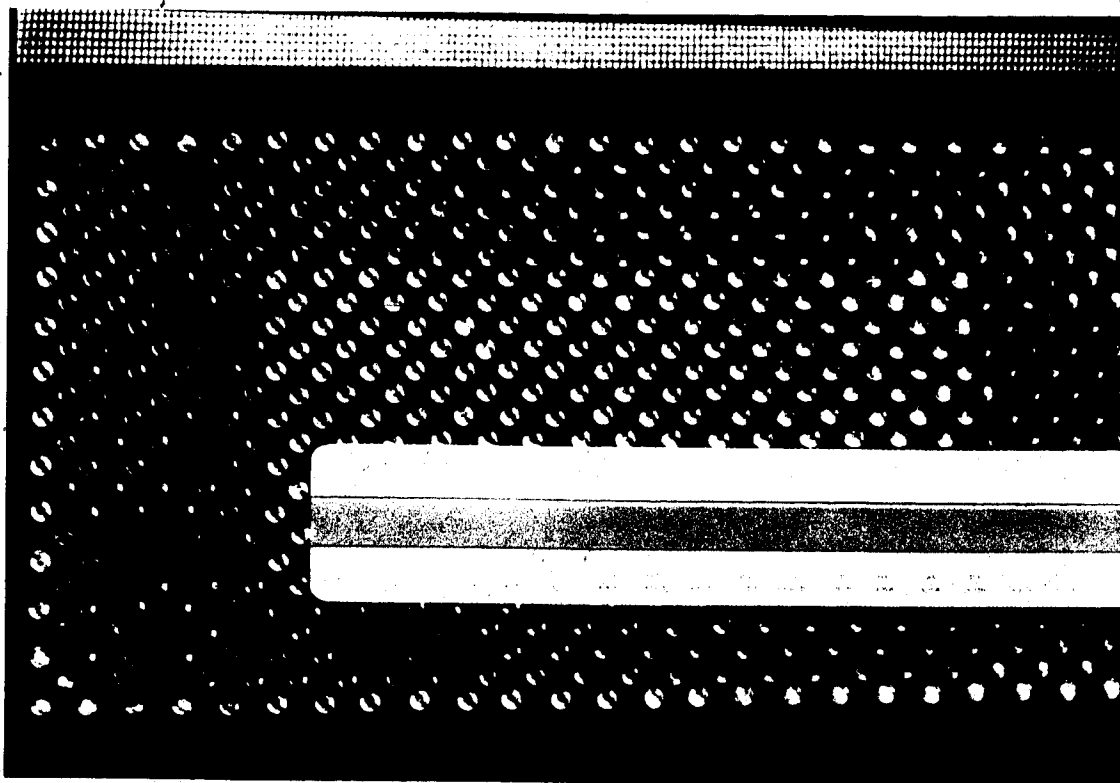


Plate 2.6 Photograph showing beads attached to the fabric screen to simulate large scale surface roughness.

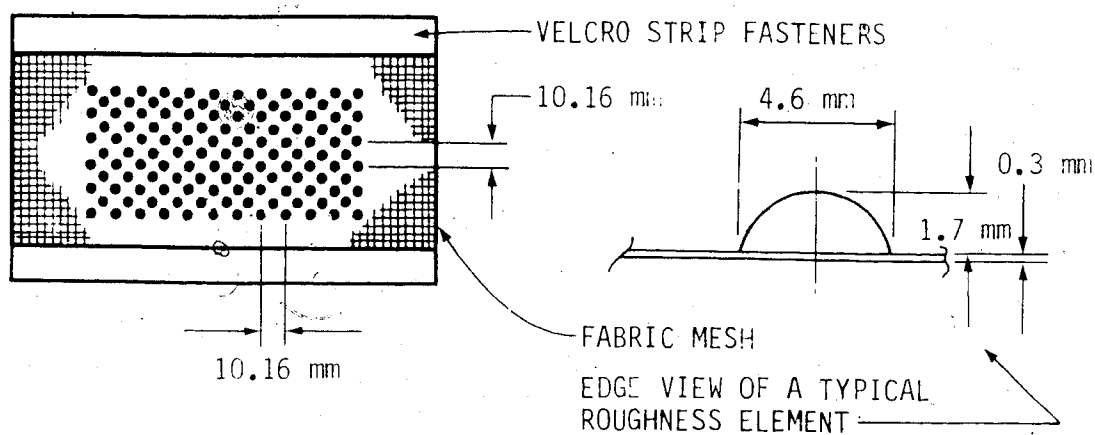


Figure 2.6 Large scale surface roughness.

Table 1.1 Summary of the rough surfaces tested.

	Small scale roughness	Medium scale roughness	Large scale roughness
Material: paper fabric mesh	spherical (flattened)	hemispherical	
Element height: mm	1.5 mm	1.5 mm	
Element diameter: mm	2.2 mm	1.8 mm	
Element dia.: mm	2.1 mm	4.0 mm	
Element diameter: mm	1.5 mm	7.5 mm	
Average spacing between element centers: mm	4.0 mm	9.0 mm	
Surface density of roughness elements: 17/cm ²	8.6/cm ²	2.0/cm ²	
Increase in surface area: —	0.7 cm ² /cm ²	0.3 cm ² /cm ²	

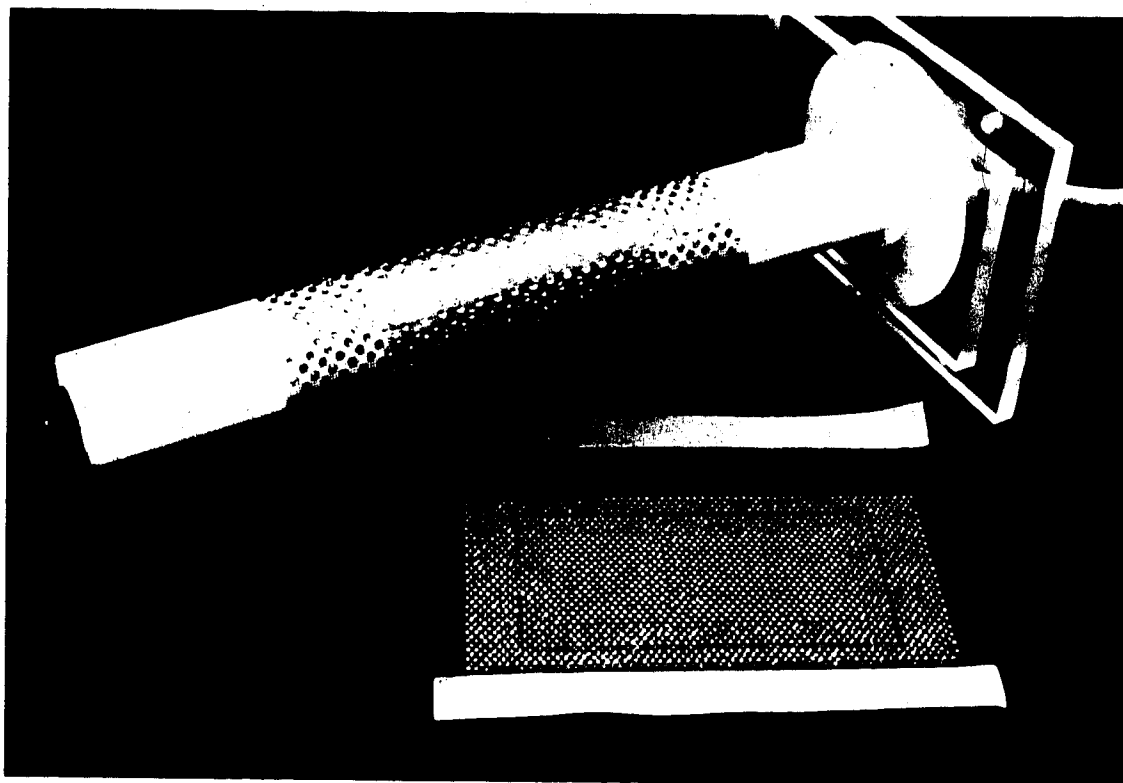


Plate 2.7 Photograph of the large scale roughness screen wrapped around the test model. Medium scale roughness screen is shown in the foreground.

2.4 Water Spray System

The influence of water spray cooling on the local convective heat transfer was also investigated in this study. A single pneumatic atomizing spray nozzle manufactured by SPRAYING SYSTEMS COMPANY was used to introduce water droplets into the airstream for all spray cooling tests. The nozzle was equipped with a type 2050 fluid cap and air cap number 120 also manufactured by SPRAYING SYSTEMS Co.

The spray nozzle was mounted on the tunnel centreline at the entrance to the test section 220 mm upstream of the cylinder. Water was supplied to the nozzle from a reservoir maintained at 275 kPa. After filtering, the water was passed through a GILMONT rotameter to monitor the flow rate. The liquid water content in the airstream was measured using a CSIRO-KING liquid water content probe manufactured by PARTICLE MEASURING SYSTEMS, INC.. The air pressure supplied to the nozzle was set for different tests between 138 kPa and 345 kPa to vary the droplet size distribution. The oil slide method utilizing microphotography was used to determine the associated water droplet size distribution for each flow setting. This method is discussed in detail by Golitzine (1951).

2.5 Instrumentation

2.5.1 Cylinder temperature measurement and thermocouple calibration

The temperature of each heater cylinder was monitored using copper-constantan thermocouples as described in Section 2.2 labelled "The Test Model". The output from each of the 12 thermocouples was fed into an amplifier with an integral cold junction. The precalibrated amplifier and electronic ice point reference were both contained in an integrated circuit manufactured by ANALOG DEVICES, Massachusetts. Each chip (one for each thermocouple) provided a high level output of 10 mV/°C from the thermocouple signal.

After all the thermocouples were mounted on the heaters, the thermocouples were immersed in a ROSEMOUNT Model 910AC constant temperature calibration bath. The output from each thermocouple amplifier was calibrated against a FLUKE 2180A RTD digital thermometer with a resolution of 0.01°C and a system accuracy of $\pm 0.15^\circ\text{C}$. Calibration was performed from 20°C to 45°C in 2.5°C increments.

2.5.2 Air velocity measurement

The velocity of the test section was determined by measuring the static pressure drop across the contraction entering the test section. In order to compare tests at the same Reynolds number, a program was written to

calculate the required contraction pressure drop corresponding to any desired Reynolds number. At any given Reynolds number, the pressure drop was not necessarily the same for all tests since the air temperature and barometric pressure changed between tests. The air velocity (pressure drop) was adjusted to compensate for changes in air density due to changes in temperature and pressure. The FORTRAN computer program entitled FROST, detailing the algorithm, is included in Appendix A.

2.5.3 Heater power supply and temperature controller

During each test, the power to each strip heater was adjusted to maintain all heaters at the desired setpoint temperature. To obtain an equilibrium setpoint temperature for all 12 heaters is difficult and time consuming if all heater currents are adjusted manually. As each heater temperature is adjusted, it influences the temperature of the heaters immediately adjacent to it on the model. To overcome this problem an electronic feedback control circuit was constructed to reduce the time necessary to attain equilibrium during a test. A feedback control circuit as shown schematically in Figure 2.7 was constructed for each of the 12 heaters and thermocouples on the model. The output from the thermocouple amplifier was compared with a reference setpoint voltage, which was adjustable to set the desired

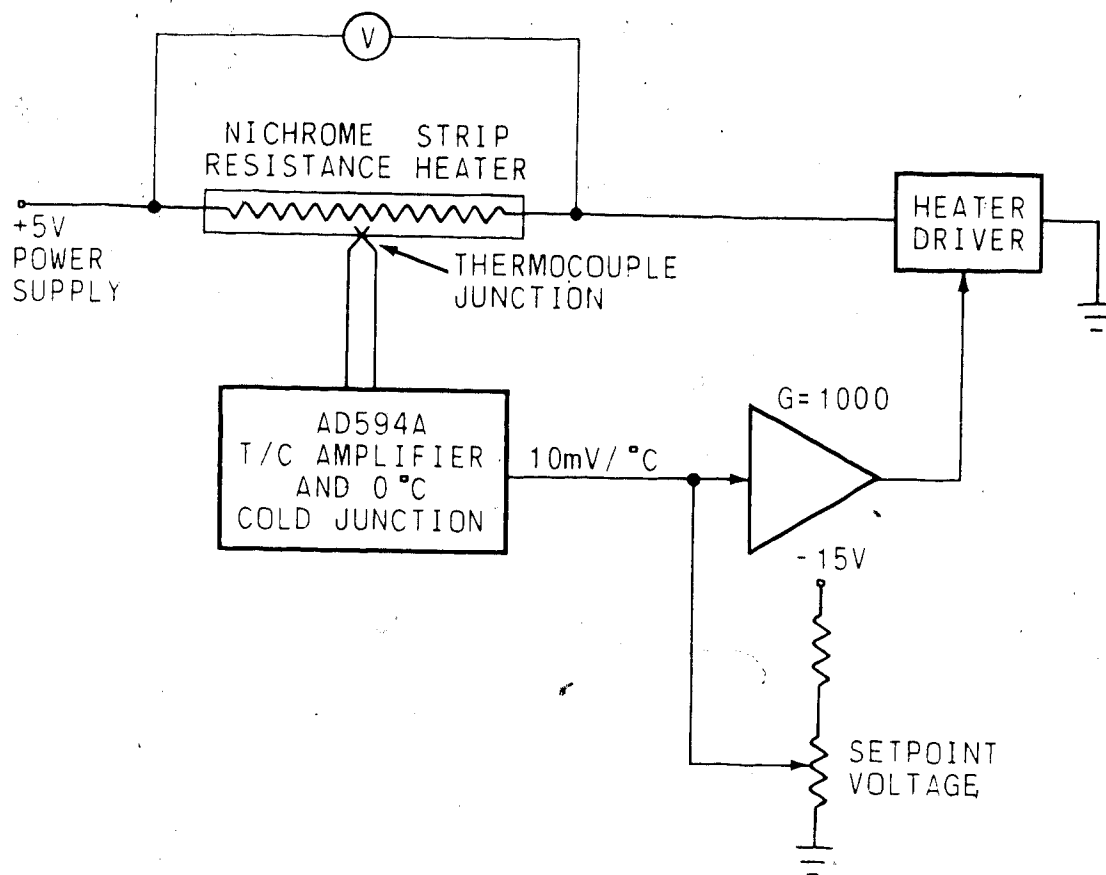


Figure 2.7 Schematic of the heater feedback control circuit.

heater temperature. The difference between these two voltages was amplified and this signal was used to control the current through the heater. A constant voltage (+5V) power supply provided up to 30 amps of current (total) to all heaters if required. The overall amplification from the thermocouple output voltage to the heater current controller was 200 000. An electrical schematic diagram for the 12 channel temperature controller is included in Appendix B of this thesis. Interpolation between calibration points was not required since the exact calibration temperatures chosen, during thermocouple calibration, could be used.

An extra pair of wires was connected to each heater to measure the voltage drop across each heater during each test. The resistance of each heater was measured prior to installation, thus the electrical power dissipated in each heater was easily calculated using the relation:

$$P = \frac{E^2}{R} \quad (2.1)$$

2.6 Test Procedure

The procedure followed for each heat transfer test consisted of adjusting the air speed through the test section to obtain the chosen test Reynolds number, ensuring that the system had reached steady state operation, and calculating the heat flux from the cylinder.

All tests were run with ambient air at approximately room temperature. Since the FROST wind tunnel is a closed loop wind tunnel, the air temperature in the tunnel gradually increases during operation due to internal friction and heat imparted by the fan. Preliminary tests indicated that the air temperature in the test section would increase from room temperature (20°C) to over 40°C after 3 hours of operation and the temperature would continue to increase at a rate of 0.3°C every 5 minutes. In order to keep the airstream temperature constant during tests, it was necessary to remove a section of the wind tunnel. The straight diffuser immediately upstream of the fan was removed for all subsequent tests. By removing this section out of the circuit, the tunnel air was allowed to mix and recirculate with the room air. With the open circuit, the air temperature in the test section was found to increase from 20°C to only 24°C after 2 hours of operation. The maximum steady state air temperature achieved varied with the air velocity; however, the rate of increase was limited to

approximately 0.1°C every 10 minutes at any speed.

The three Reynolds numbers chosen for tests were 40 000 , 80 000, and 120 000. These Reynolds numbers corresponded to air velocities of approximately 12 m/s, 24 m/s, and 36 m/s respectively. Water spray tests were only carried out at Reynolds numbers of 40 000 and 80 000 since the heater temperature controller was limited to 30 amps of total current supply. The heat transfer associated with higher Reynolds numbers and water spray cooling required higher heater currents to maintain the heater setpoint temperature.

After allowing the wind tunnel to reach a steady state operating temperature (approximately 2-3 hours), measurements of barometric pressure, test section air temperature, and contraction pressure drop (air speed) ensured that the required Reynolds number was set for each test. The conditions measured for each heat transfer test are shown in Appendix C of this thesis. To establish the Reynolds number, the density of air was evaluated at the cylinder film temperature and static pressure in the test section. Since the static pressure was not measured, Bernoulli's equation for incompressible flow (Equation 2.2 below) was used to estimate the static pressure.

$$P_{\text{stat}} = P_{\text{total}} - \frac{1}{2} \rho_a v^2 \quad (2.2)$$

Iteration of Equation 2.2 was required since the density is a function of the static pressure P_{stat} . The total pressure P_{total} was assumed to be the local barometric pressure. The method used to measure the velocity in the test section was described in Section 2.5.2.

The nichrome strip heaters were maintained at a temperature approximately 15°C warmer than the free stream air temperature. All smooth and rough cylinder tests were carried out using a 15°C temperature differential. Since the heater currents increased substantially with water spray cooling, the temperature differential was decreased to approximately 5°C for all water spray tests. This was done to ensure that the heater temperature controller had sufficient power to maintain the heaters at the desired setpoint temperature. After the desired setpoint temperature was chosen, the heaters attained equilibrium after approximately 2 minutes. The heat flux at each angle was then determined by recording the voltage drop across each heater.

CHAPTER 3

DATA REDUCTION

3.1 Calculation of the Nusselt Number

The main objective of this study was to determine the variation of the local heat transfer with position around the upstream half of a smooth and rough isothermal cylinder, as well as a smooth cylinder exposed to a water in air spray. This chapter details the calculations required to convert the recorded voltage drops across each heater to dimensionless values of the Nusselt number corresponding to the actual heat flux from the surface.

By definition:

$$Nu_{\theta} = \frac{h_{\theta} D}{k_a} \quad (3.1)$$

where D = cylinder diameter. [m]
 k_a = thermal conductivity of air at the film temperature. [W/m \cdot °C]
 h_{θ} = local heat transfer coefficient. [W/m²·°C]

The Nusselt number was calculated using Equation 3.1, with the thermal conductivity of air for all tests.

3.2 Heat Loss in the Gaps Between Adjacent Heaters

In order to evaluate the Nusselt Number at any angle, the local convective heat transfer coefficient (h_{θ})

is required. The convective heat transfer coefficient can be calculated using:

$$h_{\theta} = \frac{P_{\theta} - Q_{\text{gap}}}{A(T_h - T_a)} \quad (3.2)$$

where Q_{gap} = Correction for the heat loss from the sides of the heater, dissipated via convection at the surface of the gap between adjacent heaters. [W]

P = electrical power dissipated in the heater. [W]

A = exposed surface area of the heater. [m^2]

T_h = heater temperature. [$^{\circ}\text{C}$]

T_a = ambient air temperature. [$^{\circ}\text{C}$]

The heat transfer due only to convection at the heater surface was desired; therefore, a correction was made for the convective heat loss in the gap between adjacent heaters. Corrections for the heat loss due to radiation were not included in Equation 3.2. Neglecting the radiation component may influence the results for single component (air) flow tests by up to 8%. Calculations revealed the radiation contribution for water spray tests was approximately 3%. Using Equation 2.1, the electrical power dissipated in any heater could easily be calculated using the measured voltage drop (E) across the heater. This electrical power is dissipated as heat energy lost through convection at the surface as well as conduction through the edges and bottom of the heater. In order to estimate the convective heat loss at the surface of the heater, a correction was made to subtract the

conduction losses within the cylinder. As described in Chapter 2; the heaters were mounted on a polystyrene foam cylinder and the 2 mm gap between the heaters was filled with epoxy glue. Since the thermal conductivity of epoxy is 40 times greater than the conductivity of foam, this study assumed that the heat loss from the underside of the heaters was negligible compared with the heat loss from the edges. To verify this assumption, a finite difference analysis of the heat conduction in a typical cylinder sector was carried out. The calculations are included in Appendix D of this thesis. Typical test conditions were used as constants in the finite difference analysis. The constants as well as the results of the analysis are summarized in Table D.1 in Appendix D. They show that the heat loss from the bottom of the heater represents approximately 9% of the total conductive heat loss within the cylinder, and approximately 3% of the total heat dissipated in the heater.

A finite difference solution is not required if the heat loss from the bottom of the heaters is neglected. The steady state conduction heat loss from the edges of the heaters can be estimated analytically by solving the Laplace equation for two dimensional temperature distribution in the region between adjacent heaters. The region represents a rectangle with a constant temperature boundary (the edge of the heater), two adjacent insulated boundaries, and a convective boundary (see Figure E.1).

The solution assumed that the value of the local convective heat transfer coefficient at the surface of the gap was the same as the heat transfer coefficient at the heater surface. The heat loss from the ends of each heater is also ignored since the area was negligible compared with the surface area of the heater. The total steady state heat loss from both sides of a heater through two semi-gaps is given by:

$$Q_{\text{gap}} = 4Lh(T_h - T_a) \sum_{n=1}^{\infty} \frac{\tan \lambda_n a \tanh \lambda_n b}{\{\lambda_n^2 + (h/K)^2\}a + h/K} \quad (3.3)$$

where Q_{gap} = correction for the gap heat loss. [W]
 L = length of gap between heaters. [m]
 a = depth of heater. [m]
 b = semi-gap width. [m]
 h = local heat transfer coefficient. [W/m²·°C]
 T_a = ambient air temperature. [°C]
 T_h = heater temperature. [°C]
 K = thermal conductivity of epoxy. [W/m·°C]
 λ_n = positive roots of equation 3.5.

The complete derivation of Equation 3.3 is given in Appendix E of this thesis. The test parameters used in the finite difference analysis were substituted into Equation 3.3 to compare the exact solution with the finite difference solution. Using a heat transfer coefficient of 132.6 W/m²·°C, the exact solution yielded a gap heat loss of 491 mW which differed from the finite difference solution by 4%.

3.3 The Local Convective Heat Transfer Coefficient

An iterative solution is required to solve Equation 3.2 since Q_{gap} (Equation 3.3) is also a function of the local convective heat transfer coefficient "h". The Gauss-Seidel method of iteration was used with relaxation. A relaxation factor of 1.0 proved adequate for fast convergence, so essentially no relaxation was used during iteration.

To solve Equation 3.2 at any angle, Q_{gap} was initially assumed to be zero. The initial value of "h" calculated with $Q_{gap} = 0$ was used in Equation 3.3 to calculate a value for Q_{gap} . The value of "h" was then recalculated in Equation 3.2 using this updated value for Q_{gap} . This sequence was repeated until the value of "h" differed from its previous value by less than a specified tolerance of 0.001:

$$\text{ie. } |h(r+1) - h(r)| < 0.001 \quad (3.4)$$

After the specified tolerance was obtained, the associated Nusselt number was calculated using Equation 3.1. The FORTRAN computer program entitled "QGAP" containing these algorithms is included in Appendix A.

It should be noted that the expression for Q_{gap} (Equation 3.3) is a series solution requiring the positive roots λ_n of the equation:

$$\lambda_n \tan(\lambda_n a) = \frac{h}{K} \quad (3.5)$$

a = depth of the heater. [m]

K = conductivity of the epoxy in the gap. [W/m·°C]

Equation 3.5 is the transcendental equation derived in Appendix E. Iteration using Gauss-Seidel with relaxation was also required to solve for the positive roots (λ_n) of Equation 3.5. This process is carried out in the subroutine called "BETA" which is part of the FORTRAN program "QGAP" included in Appendix A. Only the first three positive roots were calculated since the inclusion of higher roots did not significantly improve the accuracy of the final solution. A check carried out at the highest Reynolds number using only the first two roots confirmed that the final calculated value of the Nusselt number changed by 0.005% when the third root was included in the solution.

To begin the Gauss-Seidel iteration of Equation 3.5, an initial guess for each of the first three roots was required. For small angles ($\lambda_n a$), $\tan(\lambda_n a)$ can be approximated by ($\lambda_n a$). In general, for any interval:

$$\tan(\lambda_n a) = \lambda_n a - (n-1)\pi \quad n=1,2,\dots$$

or
$$\lambda_n \tan(\lambda_n a) = \lambda_n^2 a - \lambda_n(n-1)\pi \quad (3.6)$$

Combining Equations 3.5 and 3.6 yields:

$$a\lambda_n^2 - (n-1)\pi\lambda_n - \frac{h}{K} = 0$$

The solution to this quadratic equation gives an approximate value for the first three roots of Equation 3.5 with $n=1, 2$, and 3 :

$$\lambda_n = \frac{(n-1)\pi}{2a} + \sqrt{\frac{(n-1)^2\pi^2}{4a^2} + \frac{h}{aK}} \quad (3.7)$$

3.4 Heat Transfer Calculations for Smooth and Rough Cylinder Tests

After obtaining the voltage drop measurements for each test, the data was reduced to values of the Nusselt number at each angular position around the cylinder. This procedure was described in detail in the previous Sections 3.1 to 3.3. The results of this data reduction are summarized in Appendix C entitled "Experimental Data". Tests carried out on both smooth and rough cylinders were designated as test numbers 1 through 15.

No further calculations were required to reduce the Nusselt number data for the smooth cylinder tests. The results obtained for each rough surface test required some additional manipulation to determine the actual heat transfer due only to the rough surface elements. The construction of each scale of surface roughness was

described in Section 2.3. Nusselt number data for the medium and large roughness tests reflects the influence of both the roughness elements and the fabric mesh. To determine the heat transfer due only to the roughness elements, the influence of the bare screen was subtracted from the overall results. This difference was then added to the Nusselt number data obtained for the corresponding smooth cylinder test. It would be expected that the heat transfer at the cylinder stagnation point should be the same for both a smooth and rough cylinder since the flow is still laminar. Therefore, after subtracting the bare screen data from the medium and large roughness data, a further correction was made to shift the entire curve vertically such that the value at the 0° position (stagnation point) coincided with the smooth cylinder stagnation value. A summary of the data reduction performed on the surface roughness tests at each Reynolds number is shown in Table 3.1. No attempt was made to normalize the small roughness data with respect to the smooth cylinder stagnation value. The corresponding depression which results at the stagnation point is discussed in Chapter 4.

Table 3.1 Summary of tests performed and data reduction for the smooth and rough cylinder tests.

Re=40 000

	Corresponding Tests	Add Smooth Cylinder Data and Correction
Smooth cylinder	Test#1	n/a
Small roughness	Test#2	n/a
Medium roughness	Test#4 - Test#2	+ Test#1 + 0.73
Large roughness	Test#5 - Test#3	+ Test#1 + 10.53

Re=80 000

	Corresponding Tests	Add Smooth Cylinder Data and Correction
Smooth cylinder	Test#6	n/a
Small roughness	Test#7	n/a
Medium roughness	Test#9 - Test#7	+ Test#6 - 2.11
Large roughness	Test#10 - Test#8	+ Test#6 + 4.26

Re=120 000

	Corresponding Tests	Add Smooth Cylinder Data and Correction
Smooth cylinder	Test#11	n/a
Small roughness	Test#12	n/a
Medium roughness	Test#14 - Test#12	+ Test#11 + 10.49
Large roughness	Test#15 - Test#13	+ Test#11 + 16.01

CHAPTER 4

PRESENTATION OF RESULTS

The experimental tests performed for this study were classified into two separate groups. The first series of tests was conducted to determine the effect of surface roughness on the local heat transfer around the isothermal test model. The local heat transfer distribution around a smooth cylinder with no roughness elements added was also obtained during these experiments. The second series of tests was carried out with the smooth cylinder exposed to a two-component (water-in-air) crossflow. A data sheet for each test performed is included in Appendix C of this thesis. Each data sheet lists the test conditions and the reduced Nusselt number data for the respective heat transfer test.

4.1 Heat Transfer Results for Smooth and Rough Cylinders

Figures 4.1, 4.2, and 4.3 show the experimental results obtained for both a smooth and rough cylinder for the isothermal region 0° to 90° from the stagnation line. Results are presented for three different Reynolds numbers (40 000, 80 000, and 120 000). All figures plot the dimensionless Nusselt number as a function of the angular position measured from the stagnation line. The Nusselt numbers were calculated using Equation 3.1 with the

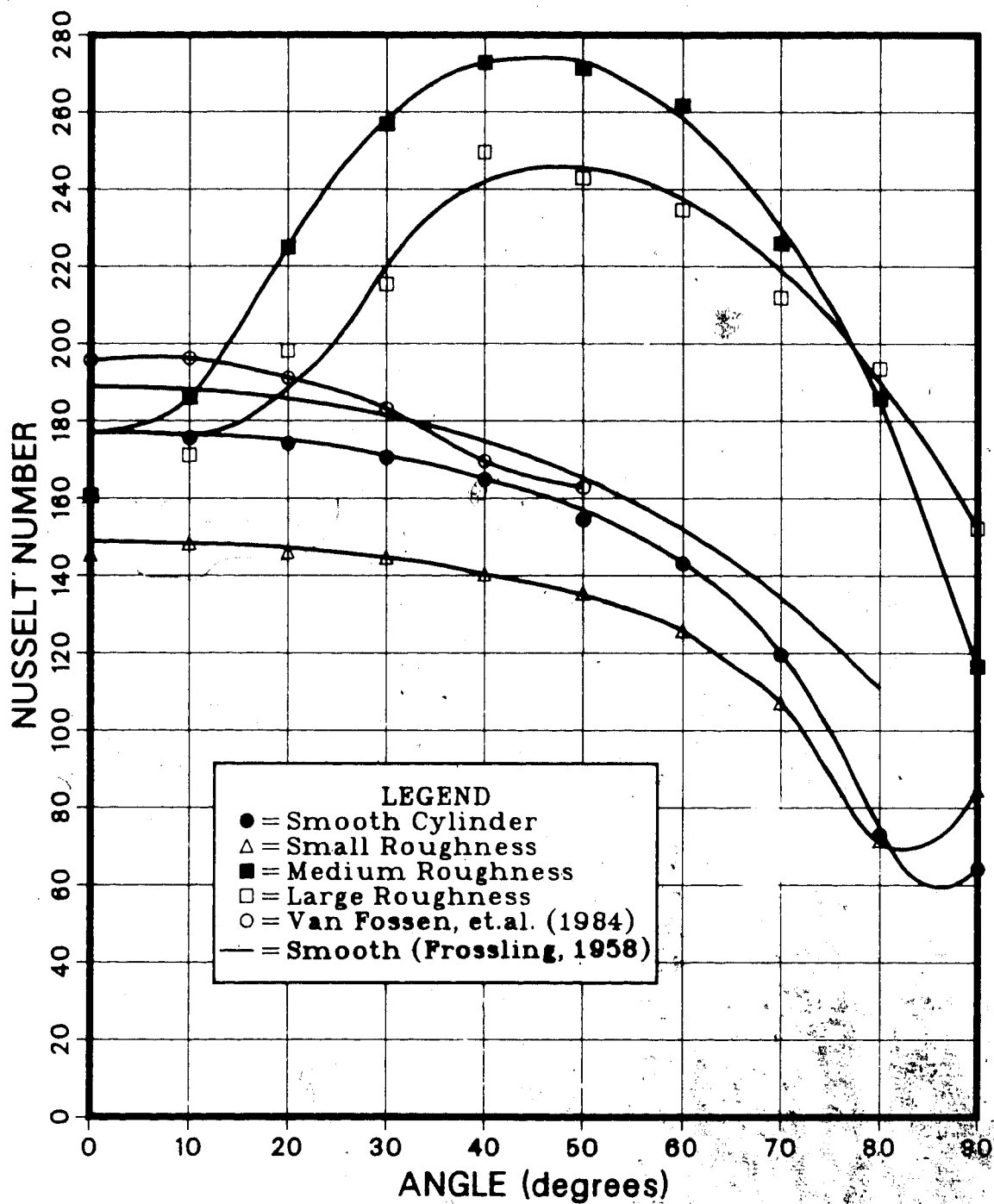


Figure 4.1 Local Nusselt number versus angular position comparing rough cylinder data with smooth cylinder data. ($Re = 40,000$)

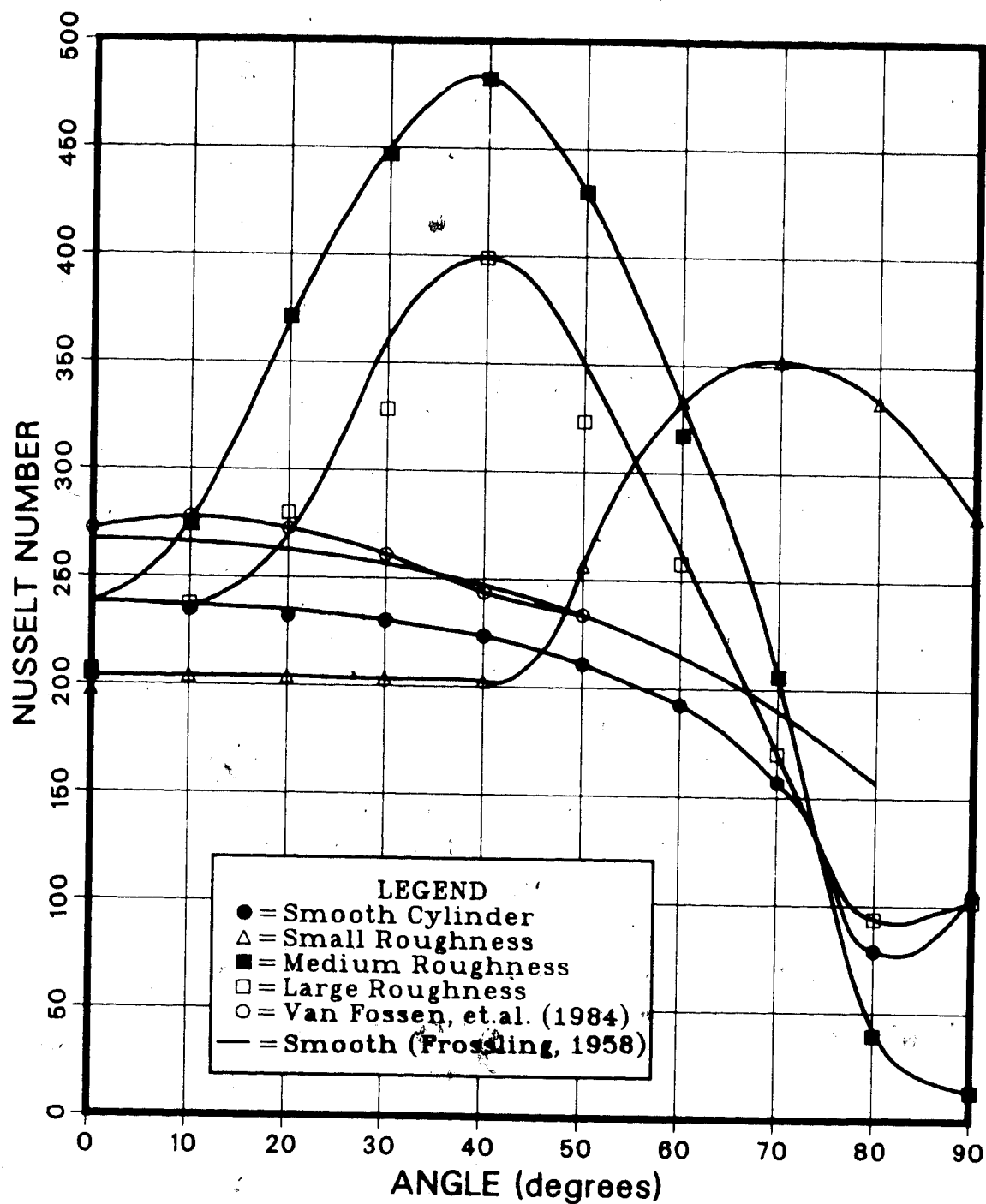


Figure 4.2 Local Nusselt number versus angular position comparing rough cylinder data with smooth cylinder data. ($Re = 80,000$)

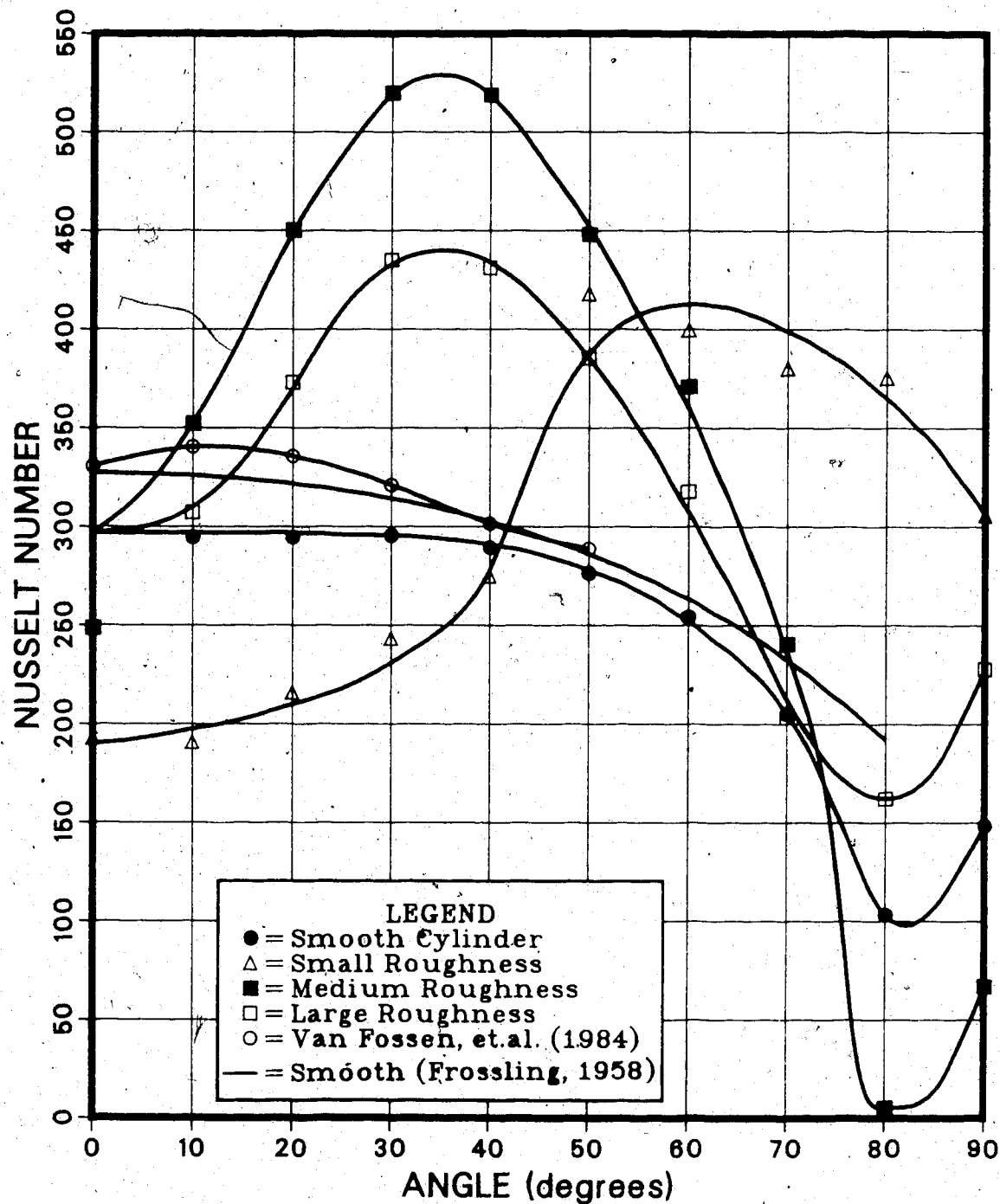


Figure 4.3 Local Nusselt number versus angular position comparing rough cylinder data with smooth cylinder data. ($Re = 120\,000$)

cylinder diameter and the thermal conductivity of air. An analytical solution of the laminar boundary layer equations for the heat transfer from a smooth cylinder was developed by Frossling (1958). Frossling's exact solution given by Equation 4.1 was also plotted for each Reynolds number.

$$\frac{Nu}{\sqrt{Re}} = 0.9449 - 0.5100 \xi + 0.5956 \xi^4 \quad (4.1)$$

Frossling's solution was shown plotted only up to 80° since the exact solution is not valid for the transition to a turbulent boundary layer or for a separated boundary layer. Experimental data obtained by Van Fossen, et. al. (1984) for a smooth, circular cylinder in crossflow was also plotted for comparison. The method used by Van Fossen to measure local the heat transfer was described in Section 5.1. Smooth cylinder data were compared with Van Fossen's data to verify the accuracy of the experimental technique employed.

The method used to determine the final Nusselt number data for the rough cylinder tests was described in detail in Section 3.4. A smooth, best-fit curve was generated for each group of data. Experimental data obtained from the smooth test model showed a continuously decreasing trend for angles greater than 10°. The data obtained at the stagnation point was consistently lower than the value obtained at the 10° position adjacent to

it. .Due to symmetry, the heat transfer distribution must be continuous about the stagnation point; therefore, the stagnation data point was ignored to plot the curves. It would be expected that the heat transfer at the stagnation point should be the same for both a smooth and rough cylinder; therefore, the data obtained for medium and large surface roughness was shifted vertically to include the stagnation value for the smooth cylinder curve. The maximum correction required at the stagnation point was 7.0%, 2.1% and 6.9% for Reynolds numbers of 40 000, 80 000, and 120 000 respectively. The medium and large roughness data was obtained by subtracting the bare screen data from the results obtained with roughness elements glued on the screen. These calculations were described in detail in Section 3.4. The measured difference between the smooth and rough cylinder data at the stagnation point can be attributed, in part, to the insulating effect of the roughness elements attached to the screens. Nusselt number data for small surface roughness was obtained by using the fabric screen alone without any roughness elements attached. The data obtained in this manner was not normalized with respect to the smooth cylinder stagnation values as was done with the medium and large roughnesses. The corresponding lower values can be attributed to the insulating effect of the fabric screen covering the heaters.

4.2 Influence of Water Spray Cooling

Figures 4.4, and 4.5 show the results with water spray cooling on the smooth isothermal cylinder. Figure 4.4 shows the results at a Reynolds number of 40 000 for three different liquid water contents in the airstream. Figure 4.5 shows the results at a Reynolds number of 80 000 with a liquid water content of 0.1 g/m^3 . Both figures also include the data obtained with no liquid water entrained in the airstream. A spline curve was fitted through all data points for the spray cooling data.

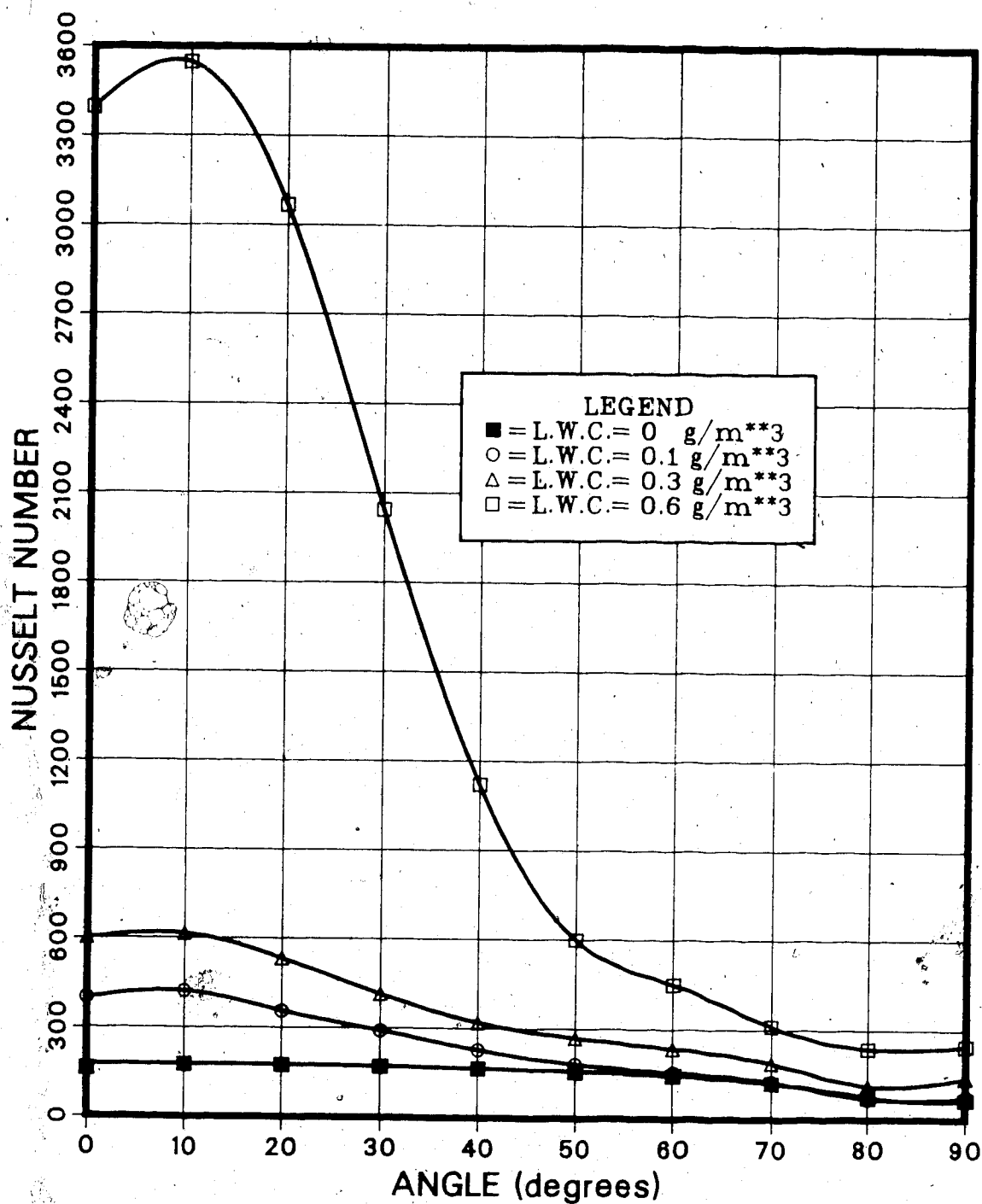


Figure 4.4 Local Nusselt number versus angular position for a spray cooled cylinder with different airstream liquid water contents ($Re = 40\,000$)

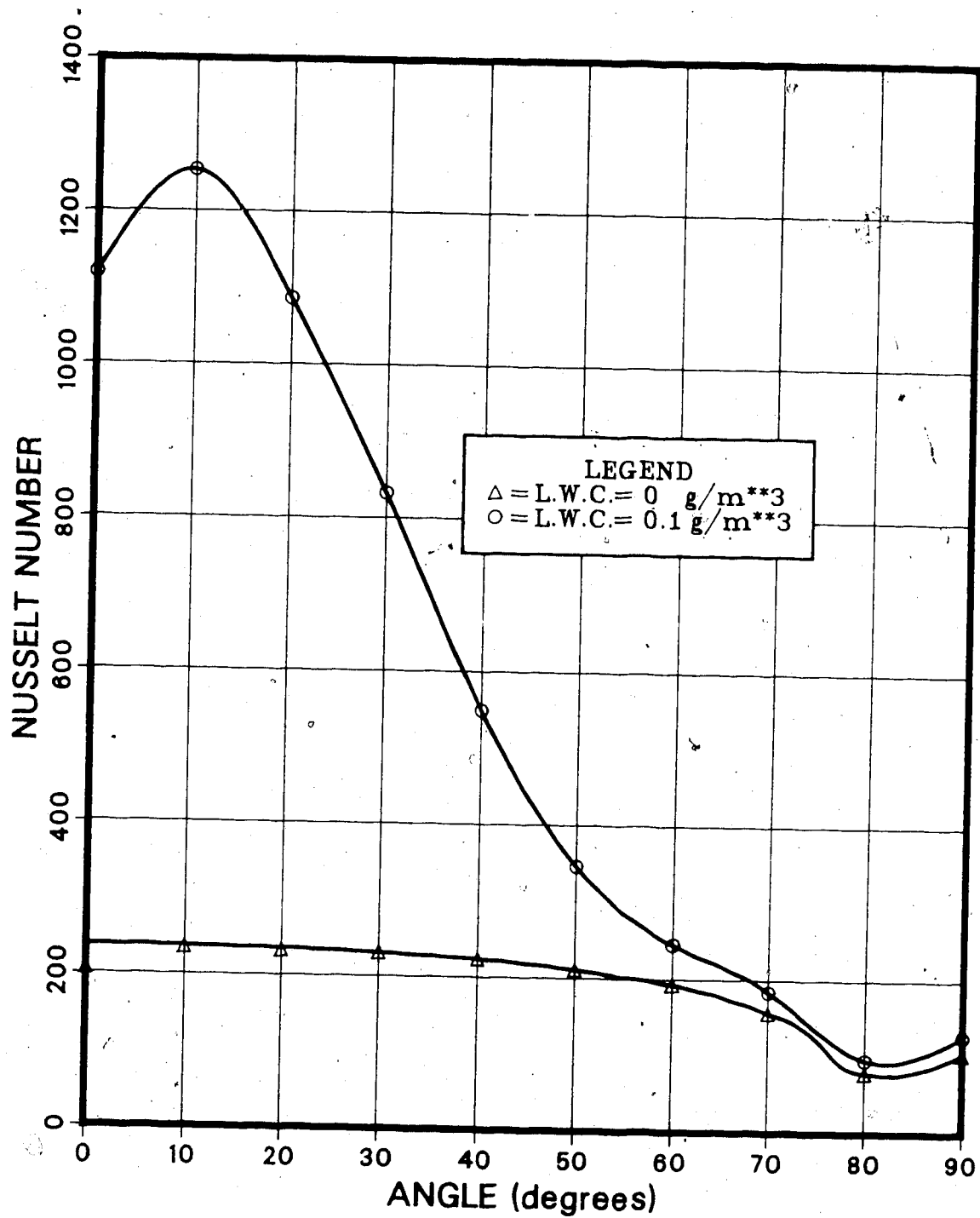


Figure 4.5 Local Nusselt number versus angular position for a spray cooled cylinder with different airstream liquid water contents ($Re = 80,000$)

CHAPTER 5

DISCUSSION

Icing models presently being developed rely on a surface energy balance calculation to determine the local rate of ice accretion on the body. Many factors can influence the local heat transfer rate at the surface of a cylinder or ice profile. For example, the presence of a rough surface can alter the heat transfer by changing the point at which the boundary layer undergoes transition from laminar to turbulent flow. An increase in heat transfer is also realized with an increase in the level of free-stream turbulence or the introduction of water spray into the airstream. The purpose of the present investigation was to compare the relative effects of the following four factors on the local heat transfer distribution around a cylinder:

1. Surface roughness.
2. Water spray cooling.
3. Free stream turbulence.
4. Cross-sectional shape.

The local ice accretion rate predicted by models incorporating a surface energy balance calculation may be in error if the influence of these factors is not accounted for. It is desirable to know the relative effect of each factor, as well as their limits of

influence, to increase the accuracy of icing models presently being developed.

An apparatus was constructed for the present study to experimentally determine the influence of spray cooling and surface roughness on the heat transfer distribution around the upstream half of a cylinder in crossflow. To obtain data for comparison, the results of other investigations were reviewed to examine the influence of free stream turbulence and cross-sectional shape on the local heat transfer distribution around a cylinder. Results due to Seban (1960) and Boulos and Pei (1974) for airstream turbulence and Van Fossen, et. al. (1984) for irregular cylindrical shapes were examined. Results due to Hodgson, et. al. (1968) for water spray cooling with very high airstream liquid water contents, and Achenbach (1977) for surface roughness are also presented to supplement the experimental results obtained for the present study.

For all tests performed without water spray cooling, the most predominant heat transfer mechanism was forced convection. With the addition of spray cooling, evaporation became the dominant mode of cooling. The surface energy balance calculation incorporated in icing models contains both the evaporative and convective heat transfer terms. Both terms are a linear function of the local heat transfer coefficient (h); therefore, a measure of the heat transfer coefficient is required to determine

the ice accretion rate at the surface. The variation of the local convective heat transfer coefficient around the upstream half of a cylinder was determined for the present study.

All results were plotted showing the variation of the local Nusselt number versus the angle from the stagnation line. The effect of the Reynolds number on the average Nusselt number was also presented.

5.1 Smooth Cylinder

Figures 4.1, 4.2, and 4.3 show the experimental results obtained for a smooth cylinder at Reynolds numbers of 40 000, 80 000, and 120 000 respectively. Also plotted in each figure is the exact solution of the laminar boundary layer equations due to Frossling (1958) and experimental data obtained by Van Fossen, et. al. (1984). Van Fossen measured the local heat transfer by using electrically heated copper strips embedded in a wooden cylinder similar to the method used for the present study. The heat flux gauges were mounted at 10° intervals around the circumference of the cylinder up to 50° from the stagnation line. Smooth cylinder data obtained for the present study showed good agreement with Van Fossen's results; however, the experimental data was consistently lower than both Van Fossen's data and Frossling's analytical solution. Experimental results differed by less than 15%, with the maximum difference occurring near

the stagnation point.

For a smooth cylinder in cross flow, maximum heat transfer occurred at the stagnation point and decreased to a minimum at the point of laminar boundary layer separation. The subsequent increase in convective heat transfer following flow separation was observed to occur at approximately 80° for the range of Reynolds numbers tested. This agrees with results obtained by Achenbach (1975) and Giedt (1949).

The average heat transfer or Nusselt number over the front half of the cylinder was plotted versus each test Reynolds number. The results are shown in Figure 5.1. The exact solution due to Frossling (1958) was also plotted in Figure 5.1.

5.2 Influence of Surface Roughness

The influence of surface roughness on the local heat transfer is also presented in Figures 4.1, 4.2, and 4.3. Three different sizes of artificial surface roughness were tested at three different Reynolds numbers.

The method used to simulate a rough cylinder surface was described in detail in Section 2.3. A major difficulty encountered with using a removeable, screen type, artificial surface roughness was attempting to measure the effect due only to the rough surface and not the effect of the screen itself. The calculations carried out to overcome this problem were described in

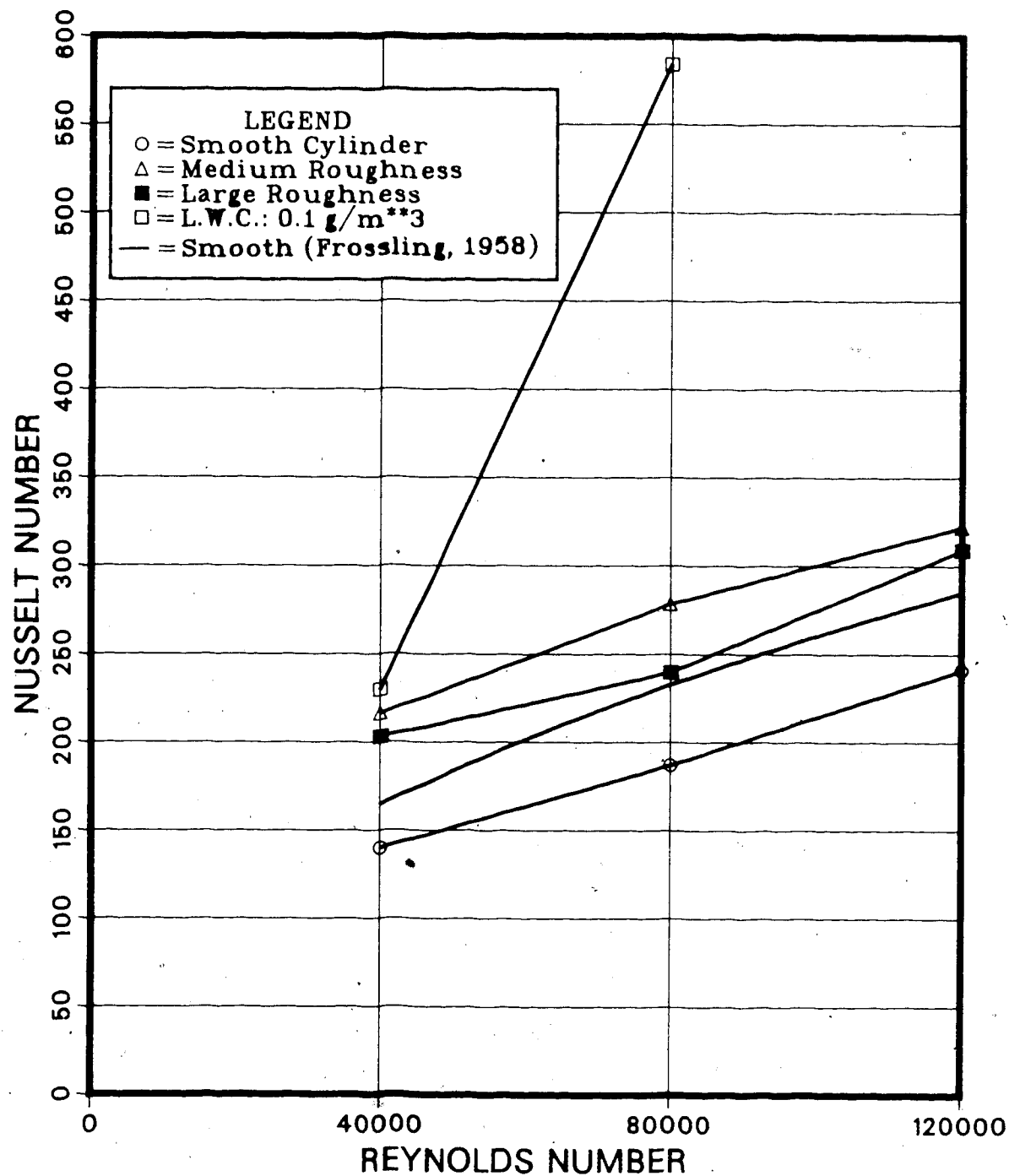


Figure 5.1 Average heat transfer from a cylinder comparing data obtained for a smooth, rough, and water sprayed cylinder for the isothermal region 0° to 90° from the stagnation line.

Section 3.4. The medium and large scale roughnesses were constructed by attaching two different size beads to a fine fabric mesh. In order to subtract the influence of the screen, a series of heat transfer tests were conducted using the bare screen with no roughness elements attached. This procedure worked well for the medium and large scale roughness; however, this correction could not be applied to the small scale roughness, since the small scale roughness was simulated using the fabric screen alone. An estimate of the error incurred by using the fabric screens was obtained from the stagnation point data. It would be expected that the heat transfer at the stagnation point should be the same for both a smooth and rough cylinder, since the flow is still laminar. The measured difference between the stagnation values for the smooth and rough cases was attributed, in part, to the insulating effect of the roughness elements (beads) attached to the fabric screen. The finite width of the electrical heater mounted on the cylinder would also affect the data at the stagnation point. The data for medium and large scale roughness in Figures 4.1, 4.2, and 4.3 was shifted vertically to coincide with the smooth cylinder data point at the stagnation point. Maximum corrections of 6.6%, 2.1%, and 6.4% were required at Reynolds numbers of 40 000, 80 000, and 120 000 respectively. No attempt was made to shift the data obtained for small scale roughness, thus the data presented in Figures 4.1 to 4.3 includes any

insulating effects of the fabric screen. Results shown in Figure 5.1 indicate that the medium scale roughness produced a higher average heat transfer than the large scale roughness at all three Reynolds numbers. Although the diameter of the large roughness elements was significantly larger than the medium elements, both roughnesses had approximately the same height. An alternate method of defining the three-dimensional roughness scale is the surface density or spacing of the roughness elements. The higher heat transfer associated with the medium scale roughness could be attributed to the larger number of roughness elements per unit area on the surface. Table 2.1 also includes the calculated increase in surface area due to the addition of roughness elements. The medium and large roughness elements increased the surface area by 70% and 30% respectively. The increased heat transfer associated with the smaller (medium scale) roughness elements may be attributed, in part, to the corresponding increase in surface area.

Figure 4.1 shows the results for a rough cylinder at a Reynolds number of 40 000. The results using small scale roughness at this Reynolds number have the same heat transfer characteristics as those associated with a laminar boundary layer. At higher Reynolds numbers, the transition from a laminar to turbulent boundary layer occurred further upstream. Figure 4.2 shows a distinct transition at 40° for a Reynolds number of 80 000, while

the transition point appears to occur almost immediately downstream of the stagnation point for a Reynolds number of 120 000. As the Reynolds number increases, the transition from a laminar to turbulent boundary layer approaches the stagnation point. These results are consistent with boundary layer theory. At lower Reynolds numbers, the boundary layer thickness increases; therefore, the relative height of the small roughness elements does not affect the transition to turbulence.

Within the turbulent boundary layer, the heat transfer increased with position from the stagnation line. Maximum heat transfer occurred approximately 40° to 50° from the stagnation point. This trend compares favorably with results obtained by Achenbach (1977). The maximum values attained also increased with increasing Reynolds number.

The effect of surface roughness on the heat transfer from a circular cylinder has also been investigated by Van Fossen, et. al. (1984), Arimilli, et. al. (1984), and Achenbach (1977). Van Fossen and Arimilli also reported the influence of surface roughness on the heat transfer from irregular cross-sections representing ice accretion shapes on cylinders. It is difficult to compare results with other investigations since the roughness parameters are defined differently in each investigation. Van Fossen applied a thin layer of sand to his test models to simulate small scale surface

roughness associated with ice accretion. This produced roughness elements with an average height of 0.33 mm. Arimilli, et. al. (1984) chose to create a "two-dimensional" roughness element by attaching wires axially to the cylinder surface, equally spaced around the circumference. Achenbach manufactured a rough surface by knurling the surface of his copper test cylinder. This technique produced a regular arrangement of pyramids, each having a rhomboidal base. In this study, individual round beads were utilized as medium and large roughness elements, to simulate a "three-dimensional" roughness typical of atmospheric ice accretion. The size of the roughness elements was defined in terms of their height, width (or diameter), and the average spacing between elements (pitch). A summary of the parameters used for each size of roughness was presented in Table 2.1. Figure 5.2 shows the results obtained by Van Fossen and results obtained by Achenbach (1977) for two sizes of surface roughness. The average heat transfer from a rough cylinder, for the region 0° to 50° from the stagnation line, is presented as a function of the Reynolds number. The results obtained from the present study and the exact solution for a smooth cylinder due to Frossling (1958), are also reproduced in Figure 5.2 for comparison.

For the sizes and types of surface roughnesses examined in the present study, the medium scale roughness increased the average heat transfer from the cylinder by

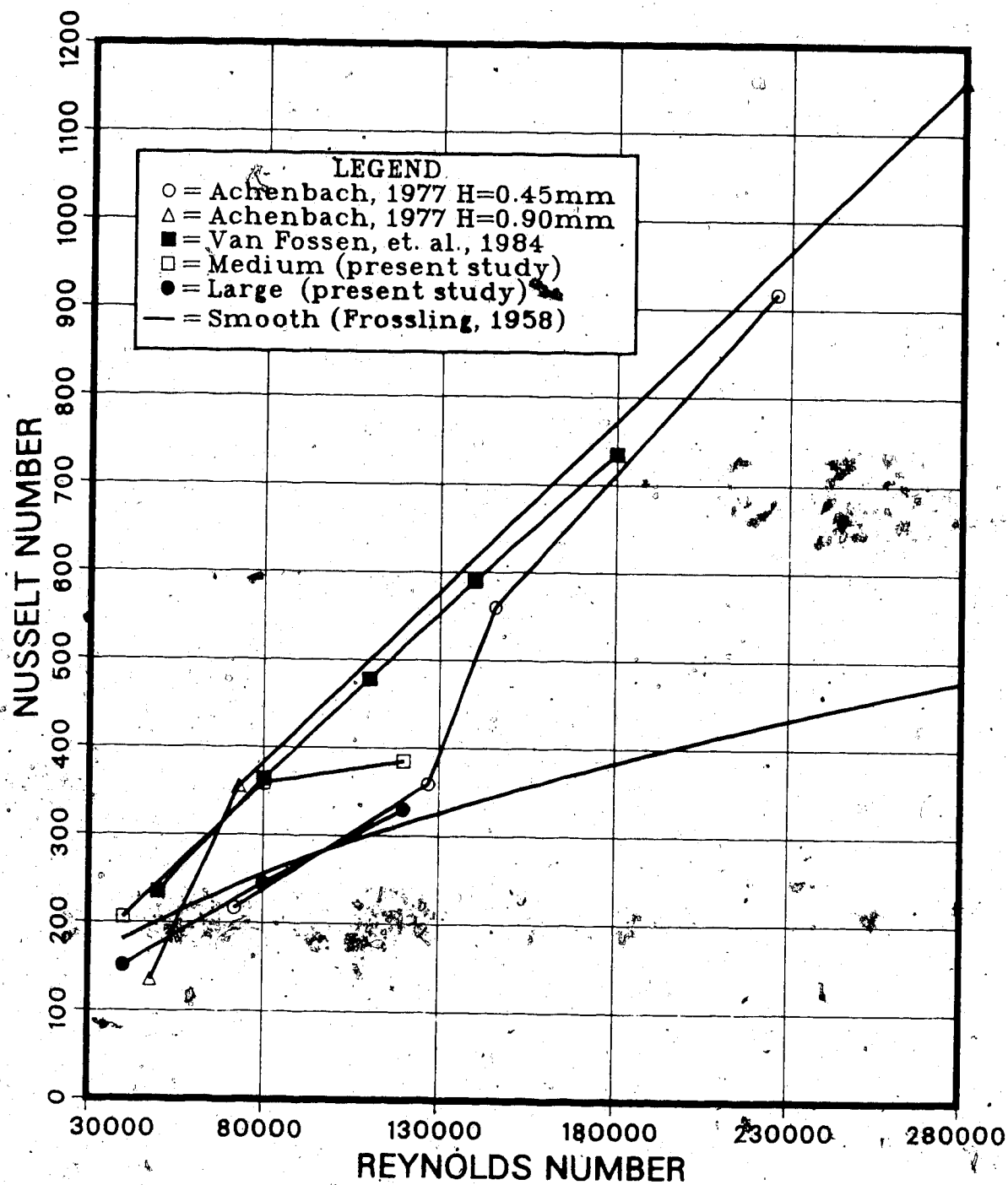


Figure 5.2 Average heat transfer from a rough circular cylinder for the region 0° to 50° from the stagnation line.

44%. This average is based on the data obtained for the region 0° to 90° from the stagnation line at all three Reynolds numbers tested. The large scale surface roughness increased the average heat transfer by approximately 32%. This value approximately corresponds to the 30% increase in surface area of the cylinder due to the addition of large scale roughness elements. This suggests that the increase in surface area due to the roughness elements may be a parameter required to quantify the effect of roughness on the heat transfer.

The results shown in Figure 5.2 can not be compared directly since test parameters were different for each investigation. The results suggest that other parameters, in addition to Reynolds number, may be important when comparing or scaling results for surface roughness. The size, shape, and surface distribution of roughness elements should all be considered to specify the type of roughness being examined. In order to incorporate the influence of surface roughness into an icing model, it would be highly desirable to attempt to more closely simulate the actual rough surfaces associated with atmospheric ice accretions. It should be noted that Achenbach's results were obtained using a 150 mm diameter cylinder. It is difficult to make quantitative comparisons with Achenbach's results since the test cylinder used for the present study was much smaller (60 mm diameter).

The limited range of Reynolds numbers examined in the present study also precluded any useful comparison with Achenbach's results. Achenbach's test's, performed at much higher Reynolds numbers (up to 40 000), indicate that the influence of surface roughness on the average heat transfer increases with increasing Reynolds number. This suggests that the effects of surface roughness may constitute the largest influence on the heat transfer at higher Reynolds numbers.

5.3 Influence of Water Spray Cooling

5.3.1 Introduction

Heat transfer tests with water spray cooling were only conducted at Reynolds numbers of 40 000 and 80 000 since the heater power supply was limited in the total heater current available. The temperature differential between the cylinder surface (heaters) and the ambient airstream was also decreased to approximately 5°C to ensure that the heater temperature controller had sufficient power to maintain all the heaters at the desired setpoint temperature. Due to these equipment restrictions, only relatively low airstream liquid water contents could be examined in this study. Maximum liquid water contents of 0.6 g/m³ and 0.1 g/m³ were possible at Reynolds numbers of 40 000 and 80 000 respectively.

The introduction of water spray into the airstream

can significantly increase the local heat transfer around a cylinder. The energy balance calculation, used in icing models to determine the local surface ice accretion rate, is strongly dependent on additional terms due to the presence of water drops or a liquid layer at the surface. The energy balance must account for evaporative heat transfer, as well as other possible heat transfer mechanisms not explained by mass transfer. It has been suggested by Launiainen and Lyyra (1985) that an additional heat transfer mechanism may occur with water spray cooling that can not be explained simply using terms contained in a standard surface energy balance. Heat transfer terms including evaporation and convection could not explain the experimental ice growth they observed on their test cylinder. They have speculated that heat transfer mechanisms, such as those associated with splashing into a liquid layer at the surface may account for the high local ice accretion rates observed. The validity of these assumptions are examined later in this chapter using results from the present investigation and results due to Hodgson, et. al. (1968).

Evaporation was the most significant mechanism for heat transfer present during all water spray tests conducted for this study. The expression for the heat transfer per unit area due to evaporation of water vapour from the cylinder surface can be expressed as:

$$Q_e = h \left(\frac{Pr}{Sc} \right)^{2/3} \frac{\epsilon l_v}{C_{pa} P} [e_s - (RH)e_a] \quad (5.1)$$

Equation 5.1 was derived in detail in Appendix F of this study. A description of each of the variables used in Equation 5.1 is also included in Appendix F. It should be noted that this derivation assumes that the relative humidity of the air immediately adjacent to the cylinder surface is 100%; therefore, the saturated value for the vapour pressure of water (e_s) is used at the surface. Since the wind tunnel was operated in an open circuit configuration, the tunnel air was allowed to mix with the room air. As a result, it was impossible to saturate the air before it entered the test section. Since the air was not saturated, the saturated vapour pressure of water at the ambient air temperature (e_a in Equation 5.1) was multiplied by the relative humidity.

The total heat transfer measured during all spray tests included the sensible heat flux required to warm up the impinging droplets from ambient air temperature up to the cylinder surface temperature. The sensible heat flux per unit area was calculated using:

$$Q_{sen} = \dot{m}_w (C_{pw}) (T_h - T_a) \quad (5.2)$$

where Q_{sen} = sensible heat flux per unit area. $[W/m^2]$
 \dot{m}_w = mass flux of water droplets impinging on the cylinder surface per unit area. $[kg/m^2 \cdot s]$
 C_{pw} = specific heat capacity of water at constant pressure and film temperature. $[J/kg \cdot K]$
 T_h = heater temperature. $[^{\circ}C]$
 T_a = ambient air temperature. $[^{\circ}C]$

The mass flux of water droplets per unit area (\dot{m}_w) in Equation 5.2 was calculated using:

$$\dot{m}_w = (v)(LWC)(\text{overall collision frequency}) \quad (5.3)$$

where LWC = airstream liquid water content. $[g/m^3]$
 v = air velocity. $[m/s]$

The overall collision frequency required in Equation 5.3 was calculated using correlations due to Lozowski, et. al. (1983).

The relative magnitudes of the sensible, convective, and evaporative heat transfer components were calculated for one spray test conducted for the present investigation. The results are presented and discussed in Section 5.3.2.

5.3.2 Discussion of Spray Cooling Results.

Figures 4.4 and 4.5 show the experimental results for a smooth cylinder exposed to a water-in-air crossflow. The local Nusselt number is plotted versus the angle from the stagnation line for various liquid water contents. Both figures also include data obtained for a smooth

cylinder without spray cooling. Although the median volume droplet diameter of the water spray varied between $25\mu\text{m}$ and $49\mu\text{m}$ from test to test, the effect of droplet diameter on the heat transfer was not included in the scope of this investigation. The present study was limited to examining the effects of different liquid water contents on the local heat transfer. The Nusselt number in both figures was calculated using the cylinder diameter and the thermal conductivity of air at the film temperature. A summary of the test conditions recorded for each test run is included in Appendix C of this study. Water spray tests were designated as test numbers 16 through 19.

The heat transfer measured with water spray cooling is extremely sensitive to the liquid water content in the airstream. Small changes in the water flow rate to the spray nozzle were detected by the heater temperature controller. With spray cooling at a liquid water content of 0.6 g/m^3 , the average heat transfer over the upstream face of the cylinder was 10 times higher than without spray at Reynolds number of 40 000. Both Figures 4.4 and 4.5 show an increasing trend immediately downstream of the stagnation point reaching a maximum value at the 180° position. This trend is misleading due to the uncertainty of the stagnation data point. Results presented for a smooth cylinder in Chapter 4 indicated that the data obtained using the stagnation line heater was much lower.

than expected. This conclusion was drawn from comparisons made between the smooth cylinder data and Frossling's exact solution. For this reason and because of the inherent symmetry of the problem, it was deduced that the maximum heat transfer for spray cooling also occurs at the stagnation point and decreases with position around the cylinder. At higher angles, the measured heat transfer differed very little with water spray cooling. Thus, at any given Reynolds number, the heat transfer was almost independent of the liquid water content for angles greater than approximately 70° from the stagnation line. This agrees with results obtained by Hodgson, et. al. (1968).

Hodgson, et. al. (1968) conducted tests using very high liquid water contents in the airstream. This produced a continuous liquid layer on the surface of his test cylinder. Relatively low airstream liquid water contents were studied in the present investigation; consequently, no continuous liquid film was present on the surface of the cylinder during any spray tests. Only some scattered beading of water droplets was observed on the cylinder at a Reynolds number of 40 000. At this Reynolds number, some accumulation of water was observed on the cylinder 90° from the stagnation line where some shedding of droplets was occurring.

Since it was impossible to saturate the air entering the test section, the amount of evaporative cooling was strongly dependent on the relative humidity of

the airstream. To demonstrate the importance of the relative humidity on the proportion of heat transfer due to evaporation, a sample calculation is presented using data from test #18 ($Re = 40\,000$, $LWC = 0.6\text{ g/m}^3$). The results of this test yielded the highest increase in average heat transfer with spray cooling. The average heat transfer contribution per unit area due to convection alone was obtained from test #1 at the same Reynolds number without spray cooling. This was calculated to be 267 W/m^2 . The sensible heating component required to warm up the impacting water droplets was calculated to be 62 W/m^2 based on an overall collision efficiency of 0.48. The FORTRAN computer program entitled EVAP detailing these calculations is included in Appendix A. The values calculated for convective, evaporative, and sensible heat transfer are summarized in Table 5.1. Values for each heat transfer mechanism were calculated in an attempt to explain or predict the total measured heat transfer. It can be seen quite clearly from Table 5.1 that the evaporation component varies significantly over the range of relative humidities chosen. This is expected since high ambient temperatures (28°C) were used in the present study. The influence of airstream relative humidity on the evaporative component is much smaller at lower temperatures associated with atmospheric icing. Using the same test conditions, with a surface temperature of 0°C and an ambient temperature of -10°C , the evaporative

Table 5.1 The effect of relative humidity on the evaporation heat transfer.

Calculated heat fluxes: $[W/m^2]$

	RH of the airstream			
	0%	50%	70%	100%
Q_e (evaporation)	5375	3272	2442	1180
Q_c (convection)	267	267	267	267
Q_{sen} (sensible heating)	62	62	62	62
Total $[W/m^2]$	5704	3601	2771	1509

Total measured heat flux = $2770 W/m^2$

component only varied between $620 W/m^2$ and $330 W/m^2$ for relative humidities between 0% and 100% respectively. It is important to note that the values listed for the evaporative heat flux in Table 5.1 were calculated assuming that the relative humidity of the air immediately adjacent to the cylinder surface was 100%. Since the cylinder surface was not flooded during any spray tests conducted for the present study, surface vapour pressure term in Equation 5.1 should be corrected to include the RH at the cylinder surface.

The average measured heat flux per unit area for test #18 with a liquid water content of $0.6 g/m^3$ was $2770 W/m^2$. By trial and error, it was determined that a relative humidity of 70% would generate a total predicted (calculated) heat flux equal to the measured value. RH measurements made in the test section confirmed that the relative humidity was approximately 65% during this test.

Thus, for this test, nearly all the measured heat transfer can be explained or predicted by the calculated values of the convective, evaporative, and sensible heat transfer occurring at the cylinder surface.

The effect on the local heat transfer due to spray cooling with much higher liquid water contents was studied by Hodgson, et. al. (1968). His results for three different Reynolds numbers and various water-to-air mass flow ratios are presented in Table 5.2. Hodgson studied liquid water contents up to 100 times higher than those

Table 5.2 Average heat transfer from a spray cooled isothermal cylinder for the region 0° to 90° from the stagnation line. (Hodgson, et.al., 1968)

Water-to-air mass flow ratio	Nusselt number
Re = 30 000	
0.0	143
0.028	1722
0.057	2682
0.097	4020
0.13	5512
Re = 75 000	
0.0	225
0.013	2853
0.024	4225
0.045	5422
0.061	5748
Re = 118 000	
0.0	283
0.012	3793
0.018	4326
0.024	5227
0.036	6623
0.044	7643

Note:

1. Nusselt numbers were calculated based on the cylinder diameter and the conductivity of air at the film temperature.
2. Average Nusselt numbers corresponding to a water-to-air mass flow ratio = 0 were calculated using the exact solution due to Frossling (1958).

used in the present study. These very high water contents resulted in a flooded cylinder surface for all his spray cooling tests. Based on data from Table 5.2, Hodgson's results indicate the average heat transfer with spray cooling may be up to 30 times higher than the corresponding single component (air) heat transfer.

Icing tests on circular cylinders have been conducted by Launiainen and Lyyra (1985) to study heat transfer coefficients associated with atmospheric icing. The ice accretion rates they observed were significantly higher than those predicted using a standard surface energy balance formulation. They have suggested that additional heat transfer mechanisms such as those associated with splashing into a liquid film at the surface may account for these unusually high heat transfer coefficients. To examine this hypothesis, a sample calculation is presented here using data obtained from tests performed by Hodgson, et. al. (1968). For Hodgson's test performed at a Reynolds number of 30 000 and a water-to-air mass flow ratio of 0.13, the average measured heat transfer per unit area for the upstream side of his test cylinder was 65 000 W/m². Using test data reported by Hodgson, the heat transfer contribution due to convection and evaporation were calculated to be approximately 800 W/m² and 4000 W/m² respectively based on an airstream relative humidity of 93%. The sensible heat flux was calculated to be approximately 55 000 W/m² based

on a local collision efficiency of 75% calculated using correlations due to Lozowski, et. al. (1983). Thus, for this test, nearly all the measured heat transfer can be explained using the convective, evaporative, and sensible heat flux terms. These results indicate that no other significant mechanism for enhanced heat transfer is associated with water spray cooling for the range of airstream liquid water contents examined in the present study. The sensible heating term, calculated in this example, is much larger than the evaporative and convective terms. Under normal icing conditions, the contribution of the sensible heating term in the surface energy balance is usually negligible.

5.3.3 Measurement of the Airstream Liquid Water Content

The relative contribution of the sensible heating term was small for all water spray tests, since low liquid water contents were examined in the present study. Therefore, if the relative humidity of the air immediately adjacent to the cylinder surface was 100%, the evaporative heat transfer would not vary with airstream liquid water content, and the total measured heat transfer would be approximately constant at all liquid water contents examined. This was not observed during any spray tests. The measured heat transfer for liquid water contents of 0.1 g/m^3 and 0.3 g/m^3 was much lower than the data for a liquid water content of 0.6 g/m^3 , which suggests that the

air at the cylinder surface was not saturated. Since no liquid layer was present at the cylinder surface, all the water droplets impacting at the surface should evaporate immediately. Calculations showed that the mass transfer associated with the evaporative heat transfer did not entirely account for the mass influx of water droplets impacting at the surface. This discrepancy suggests that the data obtained for the measured liquid water contents reported in the present study may be questionable. Further tests should be conducted to determine if the horizontal distribution of water spray is uniform across the test section. The technique used to measure the airstream liquid water content was described in Section 2.4. Since the CSIRO-KING liquid water content probe was mounted vertically on the centreline of the tunnel, measurements were only obtained at the centre of the test model. A variation in water content along the horizontal length of the test model heaters would produce lower average liquid water contents than reported in the present study.

5.4 Heat Transfer Correlations for an Inclined Flat Plate

Analytical modelling of the heat transfer from irregular shaped profiles can sometimes be simplified by applying heat transfer correlations for simple shapes such as ellipses, hexagons, or flat plates. To illustrate this, the results for a flat plate exposed to a crossflow

are presented here. The average heat transfer from a flat plate for various angles of attack was calculated using correlations due to Lessmann and Test (1984). The results are plotted in Figure 5.3. In order to make a direct comparison with Figure 1.3, the average Nusselt number in Figure 5.3 was plotted versus the Reynolds number using the same horizontal and vertical scales. The average heat transfer for an inclined flat plate also increases linearly with increasing Reynolds number. Since the slope of the curves for the flat plate are approximately the same as the heat transfer curves for the ice accretion shapes, the results for a flat plate inclined at 30° could be used, for example, to predict the average heat transfer from 5 and 15 minute glaze ice shapes for the range of Reynolds numbers presented.

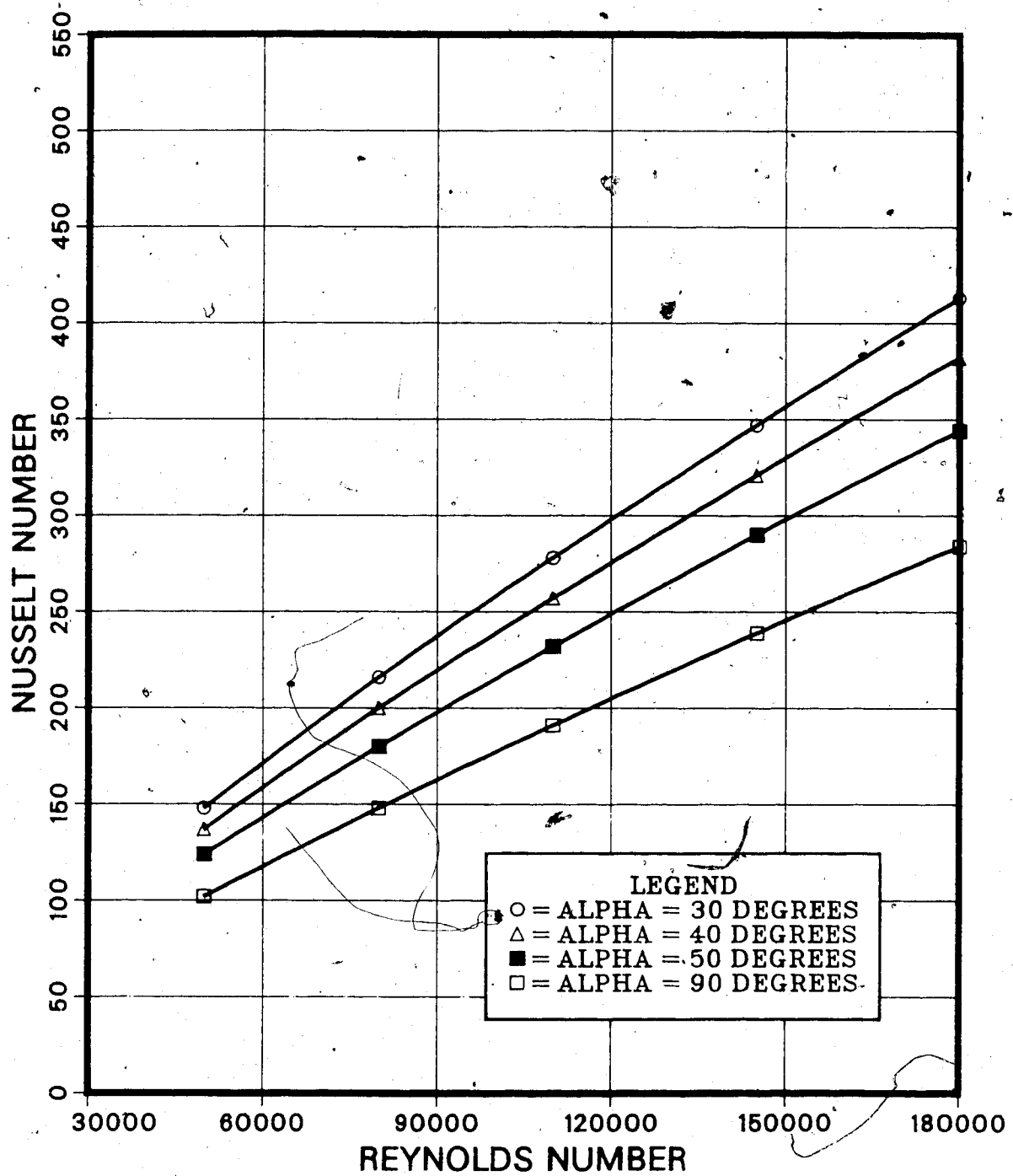


Figure 5.3 Average heat transfer from an inclined flat surface for various angles of attack. (Lessmann and Test, 1984)

5.5 Summary

The influence of various factors on the heat transfer distribution around an isothermal, circular cylinder was examined in the present study. Although many different parameters can influence the heat transfer, the present investigation was limited to examining the effects of surface roughness and water spray cooling. Results of tests conducted by others were also included in the present study to compare the relative influence of free stream turbulence and cross-sectional shape on the heat transfer distribution around a cylinder.

Exposing the test cylinder to a water spray resulted in the largest increase in average heat transfer. For the range of liquid water contents examined in the present study, the measured average heat transfer was 10 times higher than single component (air) flow. These figures pertain to the upstream (forward) half of the cylinder surface, since measurements were only made in the region 0° to 90° from the stagnation line. Average heat transfer coefficients up to 30 times higher were obtained by Hodgson, et. al. (1968) by using much higher airstream liquid water contents.

Although the influence of water spray cooling produced significantly higher heat transfer coefficients, the measured increase can be entirely explained or predicted using the calculated values for the corresponding evaporative, convective, and sensible heat

transfer. The evaporative component was the predominant term in the energy balance for water spray tests conducted for the present study. With higher liquid water contents, such as those examined by Hodgson, et. al. (1968), the sensible heating term was the most significant mode of heat transfer. In both cases, it was determined that no other complex mechanism for enhanced heat transfer occurs with water spray cooling, and all measured heat transfer could be accounted for using mass transfer, convection, etc.. This result can be readily incorporated into an icing model to account for the influence of water spray cooling on the local ice accretion rate. The need still exists to compare the relative influence of surface roughness, free stream turbulence, and cross-sectional shape on the heat transfer distribution around a cylinder.

It was determined from the present investigation that other parameters are required to adequately quantify the influence of surface roughness on the heat transfer from a cylinder. Although the rough surfaces tested for the present study increased the average heat transfer coefficients up to 45%, this figure is specific to the types of roughnesses tested and the limited range of Reynolds numbers examined. No comparisons were made with other investigations since roughness parameters such as the size, shape, and surface distribution of roughness elements or cylinder diameter differed between studies.

The limited range of Reynolds numbers examined in

the present study also precluded any useful comparisons. Results due to Achenbach (1977) for higher Reynolds numbers indicated that the influence of surface roughness on the average heat transfer from a cylinder increases with increasing Reynolds number. This suggests that the influence of surface roughness may represent the largest contributing factor at higher Reynolds numbers. To determine the relevant contribution of surface roughness in an icing model, more tests should be done using surfaces which more accurately simulate the rough surfaces associated with atmospheric icing. The range of Reynolds numbers examined should also be restricted to the conditions expected for the particular type of icing being modelled.

Calculations comparing the evaporative mass flux with the influx of water droplets impacting on the test model indicated that the data obtained for the measured liquid water contents may be questionable. Since no continuous liquid layer was present at the cylinder surface during any spray tests, the mass transfer associated with the evaporative heat transfer should be approximately equal to the mass influx of water droplets impacting at the surface. The liquid water contents, measured for the present study, were much higher than those predicted by the calculated mass transfer associated with the evaporative heat transfer. This suggests that the horizontal distribution of spray was not uniform

across the test section. A variation in liquid water content along the length of the test model would produce lower average liquid water contents than reported in the present study.

CHAPTER 6

CONCLUSIONS AND RECOMMENDATIONS

6.1 Present Investigation

The purpose of this study was to experimentally determine the relative influence of surface roughness and water spray cooling on the heat transfer distribution around an isothermal cylinder. The influence of free stream turbulence and cross-sectional shape was also examined using results from other investigations.

Results from this study and other investigations suggest that surface roughness produces the largest increase in heat transfer around a cylinder. The influence of roughness increases with increasing Reynolds number; therefore, the effects may become very significant at higher Reynolds numbers. Although water spray tests with both low and high liquid water contents produced significantly higher heat transfer coefficients, the measured increase could be entirely explained or predicted using evaporation, convection, and other heat transfer terms contained in a surface heat balance formulation. No other mechanism for enhanced heat transfer occurs with water spray cooling for the range of airstream liquid water contents examined. To determine the contribution of surface roughness in an icing model, more tests should be done using surfaces which more accurately simulate the

roughnesses associated with atmospheric icing. The range of Reynolds numbers should also be restricted to the conditions expected for the particular type of icing being modelled.

Due to equipment limitations, relatively low airstream liquid water contents were examined in the present study. Tests using higher liquid water contents should be conducted to determine the upper limits of heat transfer associated with water spray cooling. For some of the factors examined in the present study, it was also complex and difficult to determine the local effects on the heat transfer coefficient. More studies should be made to examine the effects on the average or overall heat transfer from a cylinder.

Calculations comparing the evaporative mass flux with the mass influx of water droplets impacting on the test model indicated that the data obtained for the liquid water contents may be questionable. The measured liquid water contents were higher than those predicted by the calculated mass transfer associated with the evaporative heat transfer. This suggests that the horizontal distribution of water spray was not uniform across the test section. A variation in liquid water content along the horizontal length of the test model would produce lower average water contents than reported in the present study.

6.2 Tests Performed by Others

Shape effects and free stream turbulence effects produced the smallest increase in local and average heat transfer from a cylinder. It was determined that turbulent intensities up to 5% can increase the average heat transfer by approximately 20% to 30% over the upstream perimeter of the cylinder. It was difficult to summarize the effects of shape since the heat transfer data was limited to the particular profiles examined. An analysis of the overall heat transfer from an inclined flat plate indicated that heat transfer correlations for symmetric bluff bodies can be used to predict the average heat transfer from irregular profiles associated with atmospheric icing.

More studies are also required to examine the combined influence of factors examined in the present investigation.

REFERENCES

- Achenbach, E., "The Effect of Surface Roughness on the Heat Transfer from a Circular Cylinder to the Cross Flow of Air", Int. J. Heat Mass Transfer, Vol. 20, p.359-369, 1977.
- Achenbach, E., "Total and Local Heat Transfer from a Smooth Circular Cylinder in Cross Flow at High Reynolds Number", Int. J. Heat Mass Transfer, Vol. 18, p.1387-1396, 1975.
- Ackley, S.F., Templeton, K., "Computer Modelling of Atmospheric Ice Accretion", CRREL Report 79.4, 1979.
- Arimilli, R.V., Smith, M.E., Keshock, E.G., "Measurements of Local Convective Heat Transfer Coefficients on Ice Accretion Shapes", American Institute of Aeronautics and Astronautics, Inc., 1984.
- ASHRAE Handbook (Fundamentals), American Society of Heating, Refrigeration, and Air-Conditioning Engineers, Inc., 3rd Printing, 1978.
- Boulos, M.I., Pei, D.C.T., "Dynamics of Heat Transfer From Cylinders in a Turbulent Air Stream", Int. J. Heat Mass Transfer, Vol. 17, p.767-785, 1974.
- Cansdale, J.T., Gent, R.W., "Ice Accretion on Aerofoils in Two-Dimensional Compressible Flow: A Theoretical Model", RAE Tech. Report 82128, 1983.
- Van Fossen, G.J., Simoneau, R.J., Olsen, W.A., and Shaw, R.J., "Heat Transfer Distributions Around Nominal Ice Accretion Shapes Formed on a Cylinder in the NASA Lewis Icing Research Tunnel", Report TM-83557, National Aeronautics and Space Administration, 1984.
- Frossling, N., "Evaporation, Heat Transfer, and Velocity Distribution in Two-Dimensional & Rotationally Symmetrical Laminar Boundary-Layer Flow", NACA TM 1432, 1958 (English translation).
- Giedt, W.H., "Investigation of Variation of Point Unit Heat Transfer Coefficient Around a Cylinder Normal to an Airstream", Trans. ASME, Vol 71, p.375, 1949.

Golitzine, N., "Method for Measuring the Size of Water Droplets in Clouds, Fogs, and Spray", Report ME-177, National Aeronautical Establishment, Canada, 1951.

Hodgson, J.W., Saterbak, R.T., Sunderland, J.E., "An Experimental Investigation of Heat Transfer From a Spray Cooled Isothermal Cylinder", J. Heat Transfer, Vol. 90, p.457-463, Nov 1968.

Holman, J.P., "Heat Transfer", Fourth Edition, McGraw-Hill Book Company, New York, 1976.

Launiainen, J., Lyyra, M., "Ice Accretion on a Non-Rotating Cylinder Under Conditions of High Atmospheric Liquid Water Contents. Part II: Heat Transfer and Rate of Ice Growth"; Accepted for publication in the J. of Glaciology., 1985.

Lessman, R.C., Test, F.L., "Heat Transfer Coefficients for the Faces of a Rectangular Cylinder in a Cross Stream", Accepted for publication in Journal of Heat Transfer, Trans. ASME., 1984

Lowe, P.R., "An Approximating Polynomial for the Computation of Saturated Vapour Pressure", J. Appl. Meteor., Vol. 16, p.100-103, 1977.

Lozowski, E.P., Oleskiw, M.M., "Computer Simulation of Airfoil Icing Without Runback", AIAA paper no. 81-0404, 8 p., 1981.

Lozowski, E.P., Stallabrass, J.R., Hearty, P.F., "The Icing of an Unheated, Nonrotating Cylinder. Part I: A Simulation Model", J. Climate & Appl. Meteorology, Vol. 22, No. 12, p.2053-2062, 1983.

Makkonen, L., "Estimating Intensity of Atmospheric Ice Accretion on Stationary Structures", J. Appl. Meteor., Vol. 20, p.595-600, 1981.

Makkonen, L., "Modelling of Ice Accretion on Wires", Accepted for publication in J. Appl. Meteor., 1984.

McComber, P., "Numerical Simulation of Ice Accretion on Cables", First International Workshop on Atmospheric Icing of Structures, 51-58, 1982.

Pruppacher, H.R., Klett, J.D., "Microphysics of Clouds and Precipitation", D. Reidel Publishing Company, Mass., U.S.A., 1978.

Saterbak, R.T., "An Experimental Investigation of Heat Transfer from an Isothermal Cylinder Exposed to Two-Component Crossflow", MS Thesis, Georgia Institute of Technology, Atlanta, Georgia, 1967.

Seban, R.A., "The Influence of Free Stream Turbulence on the Local Heat Transfer From Cylinders", J. Heat Transfer, Vol. 82, p.101-107, May 1960.

Sroka, M., "Design of an Atmospheric Icing Tunnel", M.Sc. Thesis, University of Alberta, Edmonton, Alberta, 1972.

Stallabrass, J.R., "Icing Flight Trials of a Bell HTL-4 Helicopter", National Research Council Report, NRC-NAE-LR-97, 1957.

APPENDIX A

COMPUTER PROGRAM LISTINGS

This appendix contains the listings of the
FORTRAN computer programs used in this thesis.

```

C*****
C  FILENAME: HEATFLUX
C
C  THIS PROGRAM READS A DATA FILE CONTAINING THE
C  SOLUTION FOR THE TEMPERATURE DISTRIBUTION IN THE
C  319 x 53 GRID (OUTPUT FROM THE PROGRAM "COND.B").
C  THE PROGRAM THEN CALCULATES THE FOLLOWING HEAT FLUX
C  DATA USING THE GRID TEMPERATURES:
C  1. THE HEAT LOSS FROM THE SIDES OF THE HEATER.
C  2. THE HEAT LOSS FROM THE BOTTOM OF THE HEATER.
C  3. THE HEAT LOSS AT THE GAP SURFACE (BY CONVECTION).
C  4. THE HEAT LOSS AT THE SURFACE OF THE HEATER.
C
C  EXECUTION COMMAND:
C  $R -LOAD# T=1 2=INPUTFILE 3=OUTPUTFILE
C*****
C  CONSTANTS AND VARIABLES USED IN MAIN PROGRAM:
C  -----
C  T(I,J) = NODAL TEMPERATURES. (C)
C  DX = SQUARE GRID SPACING = 50.80 microns
C  TA = AMBIENT TEMPERATURE. (C)
C  TH = HEATER TEMPERATURE. (C)
C  TK1 = THERMAL CONDUCTIVITY OF EPOXY. (W/m-C)
C  TK2 = THERMAL CONDUCTIVITY OF FOAM. (W/m-C)
C  H = SPECIFIED LOCAL CONVECTIVE HEAT TRANSFER
C      COEFFICIENT. (W/m**2-C)
C  M = TOTAL NUMBER OF NODES IN THE "I" DIRECTION.
C  N = TOTAL NUMBER OF NODES IN THE "J" DIRECTION.
C  QHTSUR = HEAT LOSS AT HEATER SURFACE. (mW)
C  HTFLXI = HEAT LOSS FROM THE BOTTOM OF THE HEATER. (mW)
C  HTFLXJ = HEAT LOSS FROM THE SIDES OF THE HEATER. (mW)
C  HTFLXT = HTFLXI + HTFLXJ
C  HTFLXR = HEAT LOSS TOWARDS THE CYLINDER CENTRE. (mW)
C  QSUR = GAP HEAT LOSS (BY CONVECTION). (mW)
C  PER = RATIO OF THE HEAT LOSS IN THE GAP TO THE HEAT
C        LOSS AT THE SURFACE OF THE HEATER.
C*****

```

DIMENSION T(319,53)

DATA M/319/,N/53/,TK1/1.1344/,TK2/0.026/,H/132.623/,

@ TA/23.8/,TH/38.0/,DX/50.80E-6/,

@ SUM1/0./,SUM2/0./,SUM3/0./,SUM4/0./

```

C  READ DATA FILE CONTAINING NODAL TEMPERATURES:
C  -----

```

READ(2,1000)((T(I,J),J=1,N),I=1,M)

```

C  CALCULATE THE HEAT LOSS AT THE SURFACE OF THE HEATER:
C  -----

```

QHTSUR=H*0.003175*0.1524*(TH-TA)*1000.

C CALCULATE QSUR, HTFLXI, HTFLXJ, AND HTFLXR:

```

C -----
DO 100 J=2,20
100 SUM1=SUM1+(I(1,J)-TA)
   QSUR=H*DX*0.1524*(SUM1+0.5*(T(1,1)-TA))*2.*1000.
   DO 200 I=2,4
200 SUM2=SUM2+TH-T(I,20)
   DO 300 J=22,52
300 SUM3=SUM3+TH-T(6,J)
   HTFLXI=TK2*(SUM3+0.5*(TH-T(6,N)+TH-T(6,21)))
   @ *0.1524*2.*1000.
   HTFLXJ=TK1*(SUM2+0.5*(TH-T(1,20)+TH-T(5,20)))
   @ *0.1524*2.*1000.
   HTFLXT=HTFLXI+HTFLXJ
   DO 400 J=2,52
400 SUM4=SUM4+T(318,J)-T(319,J)
   HTFLXR=TK2*0.1524*2.*1000.*(SUM4+.5*(T(318,1)-
   @ T(319,1)+T(318,53)-T(319,53)))

   PER=(QSUR/QHTSUR*100.)
   WRITE(3,2000)H,TA,TH,TK1,TK2,QSUR,HTFLXI,
   @ HTFLXJ,HTFLXT,HTFLXR,QHTSUR,PER

```

C FORMAT STATEMENTS:

```

C -----
1000 FORMAT(53F10.5)
2000 FORMAT(/////9X,'FINITE DIFFERENCE SOLUTION: '//
   @9X,27(' - '),//
   @9X,'CONVECTIVE HEAT TRANSFER COEFFICIENT = ',F7.2,
   @' W/m**2-C' /
   @9X,'AMBIENT TEMPERATURE = '
   @,F5.1,' C' /
   @9X,'HEATER TEMPERATURE = '
   @,F5.1,' C' /
   @9X,'GAP THERMAL CONDUCTIVITY (EPOXY) = ',F6.3,
   @' W/m-C' /
   @9X,'CYLINDER THERMAL CONDUCTIVITY (FOAM) = ',F6.3,
   @' W/m-C' //
   @9X,'HEAT LOSS SUMMARY: '//,9X,18(' - '),/
   @9X,'A. SURFACE (GAP HEAT LOSS) = ',F8.3,' mW' //
   @9X,'B. HEAT LOSS FROM BOTTOM OF HEATER = ',F8.3,' mW' /
   @9X,'C. LOSS FROM SIDES OF THE HEATER = ',F8.3,' mW' //
   @9X,'D. TOTAL = ',F8.3,' mW' //
   @9X,'E. LOSS TO INTERIOR OF THE CYLINDER = ',F8.3,' mW' //
   @9X,'F. LOSS FROM SURFACE OF THE HEATER = ',F8.3,' mW' //
   @9X,'GAP LOSS REPRESENTS',F6.2,' % OF HEATERS SURFACE'
   @,' LOSS.')
   STOP
   END

```

```

C*****
C  FILENAME:  COND
C
C  THIS PROGRAM SOLVES FOR THE STEADY STATE TEMPERATURE
C  DISTRIBUTION IN A TYPICAL 5 DEGREE SECTOR OF THE
C  CYLINDER. THE TEMPERATURE DISTRIBUTION IS OBTAINED
C  NUMERICALLY USING THE METHOD OF FINITE DIFFERENCES.
C  THIS PROGRAM UTILIZES A ROUGH GRID OF 296 x 27 NODES.
C  SPECIFIED TOLERANCE FOR T(I,J) = 0.0005.
C
C  EXECUTION COMMAND:
C  $R -LOAD# T=10 3=OUTPUT
C*****
C  CONSTANTS AND VARIABLES USED IN MAIN PROGRAM:
C  -----
C  T(I,J) = NODAL TEMPERATURES (C) AFTER ITERATION
C           NUMBER r.
C  TEMP(I,J) = NODAL TEMPERATURES AFTER ITERATION (r+1).
C  DX = SQUARE GRID SPACING = 101.60 microns
C  TOL = SPECIFIED TOLERANCE USED FOR THE DIFFERENCE
C        (T(I,J)-TEMP(I,J)).
C  W = RELAXATION FACTOR USED WITH GAUSS-SEIDEL
C       ITERATION.
C  TA = AMBIENT TEMPERATURE. (C)
C  TH = HEATER TEMPERATURE. (C)
C  TK1 = THERMAL CONDUCTIVITY OF EPOXY. (W/m-C)
C  TK2 = THERMAL CONDUCTIVITY OF FOAM. (W/m-C)
C  H = SPECIFIED LOCAL CONVECTIVE HEAT TRANSFER
C       COEFFICIENT. (W/m**2-C)
C  M = TOTAL NUMBER OF NODES IN THE "I" DIRECTION.
C  N = TOTAL NUMBER OF NODES IN THE "J" DIRECTION.
C  MM = M-1
C  NN = N-1
C  ITER = NUMBER OF ITERATIONS COMPLETED.
C  DIFF = T(I,J)-TEMP(I,J) CALCULATED FOR EVERY NODE
C         AFTER EACH ITERATION.
C  DIFFL= LARGEST ITERATION DIFFERENCE "DIFF".
C  (IL,JL) = NODAL COORDINATE OF DIFFL.
C  FLAG = 0.0 (OFF) WHEN "DIFF" IS LESS THAN TOLERANCE.
C         = 1.0 (TURNED ON) WHEN "DIFF" IS GREATER THAN
C         TOLERANCE.
C*****

```

```

      DIMENSION T(296,27),TEMP(296,27)
      DATA M/296/,N/27/,DX/101.60E-6/,TOL/.0005/,TA/23.8/,
      @ TH/38.0/,TK1/1.1344/,TK2/0.026/,H/132.623/
      MM=M-1
      NN=N-1

```

C READ IN VALUE FOR THE RELAXATION FACTOR:
C -----

READ(5,1000)W

C INITIAL GUESSES FOR T(I,J):
C -----

DO 100 J=1,N
DO 100 I=1,M
100 T(I,J)=TA

C SPECIFIED BOUNDARY TEMPERATURES:
C -----

DO 200 J=1,N
200 T(M,J)=TA
DO 300 J=11,N
DO 300 I=1,3
300 T(I,J)=TH
DO 400 I=1,M
DO 400 J=1,N
400 TEMP(I,J)=T(I,J)

ITER=0
WRITE(6,3000)

C 920 DO-LOOP IS A GLOBAL DO-LOOP WITH AN OUTPUT
C STATEMENT WHICH PRINTS EVERY 5 ITERATIONS.
C 910 DO-LOOP ALLOWS 5 ITERATIONS BEFORE
C ENCOUNTERING THE 920 DO-LOOP OUTPUT STATEMENT.
C FOR EACH ITERATION IN THE 910 DO-LOOP, NEW VALUES FOR
C THE NODAL TEMPERATURES TEMP(I,J) ARE CALCULATED USING
C THE PREVIOUS VALUES T(I,J) FROM THE PREVIOUS ITERATION:
C -----

DO 920 KK=1,5000
DO 910 IT=1,5
ITER=ITER+1
DIFFL=0.0
FLAG=0.0
TEMP(1,1)=(T(2,1)+T(1,2)+H*TA/TK1*DX)/
(2.+H/TK1*DX)
DO 500 J=2,10
500 TEMP(1,J)=(T(1,J+1)+T(1,J-1)+2.*(T(2,J)+
@ TA*H/TK1*DX))/4.+2.*H/TK1*DX)
TEMP(2,1)=(T(1,1)+T(3,1)+2.*T(2,2))/4.
DO 600 J=2,10
600 TEMP(2,J)=(T(3,J)+T(1,J)+T(2,J+1)+
@ T(2,J-1))/4.0
TEMP(3,1)=(TK1*(T(2,1)+T(3,2))+TK2*
@ (T(3,2)+T(4,1)))/(2.*(TK1+TK2))

```

DO 700 J=2,10
700   TEMP(3,J)=(TK1*(T(2,J)+0.5*(T(3,J+1)+
@      T(3,J-1)))+TK2*(T(4,J)+0.5*
@      (T(3,J+1)+T(3,J-1))))/
@      (2.*(TK1+TK2))
DO 900 I=4,MM
TEMP(I,1)=(T(I-1,1)+T(I+1,1)+2.*T(I,2))/4.
DO 800 J=2,NN
800   TEMP(I,J)=(T(I+1,J)+T(I-1,J)+T(I,J+1)+
@      T(I,J-1))/4.
TEMP(I,N)=(T(I-1,N)+T(I+1,N)+2.*T(I,NN))/4.
900   CONTINUE

C      COMPARE TEMP(I,J) WITH PREVIOUS VALUES FOR
C      T(I,J). CHECK IF T(I,J)-TEMP(I,J) IS
C      GREATER THAN TOLERANCE FOR ANY NODE (I,J):
C      -----

      CALL DIFF(T,TA,TEMP,M,N,I,J,IL,JL,
               TOL,FLAG,DIFFL,W)
      IF(FLAG.EQ.0.0) GOTO 10
910   CONTINUE
      WRITE(6,4000)ITER,IL,JL,DIFFL
920   CONTINUE
10    WRITE(3,2000)((T(I,J),J=1,N),I=1,M)

C  FORMAT STATEMENTS:
C  -----

1000  FORMAT(F15.5)
2000  FORMAT(27F10.5)
3000  FORMAT('/ NUMBER OF ITERATIONS',6X,
@      ' MAXIMUM ITERATION DIFFERENCE' /,54(' '),/)
4000  FORMAT(I11,20X,' (',I3,',',I2,') = ',F10.5)
      STOP
      END

```

C***** CONTINUED *****

```

C*****
C S/R TO EVALUATE THE LARGEST ITERATION DIFFERENCE, TO *
C COMPARE THE CURRENT ITERATION DIFFERENCE TO TOLERANCE, *
C AND TO RELAX THE NEW CALCULATED VALUE OF T(I,J). *
C*****

```

```

SUBROUTINE DIFF(T,TA,TEMP,M,N,I,J,IL,JL,
@      TOL,FLAG,DIFFL,W)
REAL T(M,N),TEMP(M,N)
DO 100 I=1,M
  DO 100 J=1,N
    IF(I.GT.3)GOTO 10
    IF(J.GE.11)GOTO 100
    DIFF=ABS(T(I,J)-TEMP(I,J))
    IF(DIFF.LT.DIFFL)GOTO 20
    DIFFL=DIFF
    IL=I
    JL=J
    IF(DIFF.GT.TOL)FLAG=1.0
    T(I,J)=T(I,J)+W*(TEMP(I,J)-T(I,J))
  100 CONTINUE
  RETURN
END

```

```

C*****
C  FILENAME:  COND.B
C
C  THIS PROGRAM READS A DATA FILE CONTAINING A 296 x 27
C  TEMPERATURE MATRIX (OUTPUT FROM PROGRAM "COND").
C  THIS PROGRAM THEN SOLVES FOR THE STEADY STATE
C  TEMPERATURE DISTRIBUTION USING A FINER GRID SIZE.
C  THE FINER GRID CONSISTS OF A 319 x 53 MATRIX WHICH
C  REPRESENTS 160 x 27 NODES OF THE GRID USED IN "COND".
C  COLUMN 319 OF THE FINE GRID IS SPECIFIED BY COLUMN
C  160 (23.8780 C) OF THE 296 x 27 ROUGH GRID.
C  *SPECIFIED TOLERANCE FOR T(I,J)= 0.0005
C
C  EXECUTION COMMAND:
C  R -LOAD# T=10 2=INPUT 3=OUTPUT
C*****
C
C  CONSTANTS AND VARIABLES USED IN MAIN PROGRAM:
C  -----
C  T(I,J)      = NODAL TEMPERATURES (C) AFTER ITERATION
C                NUMBER r.
C  TEMP(I,J)   = NODAL TEMPERATURES AFTER ITERATION (r+1).
C  T2(I,J)     = NODAL TEMPERATURES OF THE 296 x 27 ROUGH
C                GRID OUTPUT FROM PROGRAM "COND".
C  DX          = SQUARE GRID SPACING = 50.80 microns
C  TOL         = SPECIFIED TOLERANCE USED FOR THE DIFFERENCE
C                (T(I,J)-TEMP(I,J)).
C  W           = RELAXATION FACTOR USED WITH GAUSS-SEIDEL
C                ITERATION.
C  TA          = AMBIENT TEMPERATURE. (C)
C  TH          = HEATER TEMPERATURE. (C)
C  TK1         = THERMAL CONDUCTIVITY OF EPOXY. (W/m-C)
C  TK2         = THERMAL CONDUCTIVITY OF FOAM. (W/m-C)
C  H           = SPECIFIED LOCAL CONVECTIVE HEAT TRANSFER
C                COEFFICIENT. (W/m**2-C)
C  M           = TOTAL NUMBER OF NODES IN THE "I" DIRECTION.
C  N           = TOTAL NUMBER OF NODES IN THE "J" DIRECTION.
C  MM          = M-1
C  NN          = N-1
C  ITER        = NUMBER OF ITERATIONS COMPLETED.
C  DIFF        = T(I,J)-TEMP(I,J) CALCULATED FOR EVERY NODE
C                AFTER EACH ITERATION.
C  DIFFL       = LARGEST ITERATION DIFFERENCE "DIFF".
C  (IL,JL)     = NODAL COORDINATE OF DIFFL.
C  FLAG        = 0.0 (OFF) WHEN "DIFF" IS LESS THAN TOLERANCE.
C                = 1.0 (TURNED ON) WHEN "DIFF" IS GREATER THAN
C                TOLERANCE.
C*****

```

```

DIMENSION T(319,53),T2(296,27),TEMP(319,53)
DATA M/319/,N/53/,DX/50.80E-6/,TOL/.0005/,H/132.623/,
@      TK1/1.1344/,TK2/0.026/,TA/23.8/,TH/38.0/

```

MM=M-1

NN=N-1

C READ IN VALUE FOR THE RELAXATION FACTOR:

C -----

READ(5,1000)W

C READ DATA FILE AND SPECIFY T(I,J):

C -----

READ(2,2000)((T2(I,J),J=1,27),I=1,296)

DO 100 II=1,160

DO 100 JJ=1,27

I=2.*II-1.

J=2.*JJ-1.

100 T(I,J)=T2(II,JJ)

C SPECIFIED BOUNDARY TEMPERATURES:

C -----

DO 200 J=1,N

200 T(M,J)=23.8780

DO 300 J=21,N

DO 300 I=1,5

300 T(I,J)=TH

DO 400 I=1,M

DO 400 J=1,N

400 TEMP(I,J)=T(I,J)

ITER=0

WRITE(6,4000)

C 930 DO-LOOP IS A GLOBAL DO-LOOP WITH AN OUTPUT

C STATEMENT WHICH PRINTS EVERY 5 ITERATIONS.

C 920 DO-LOOP ALLOWS 5 ITERATIONS BEFORE ENCOUNTERING

C THE 930 DO-LOOP OUTPUT STATEMENT.

C FOR EACH ITERATION IN THE 920 DO-LOOP, NEW VALUES FOR

C THE NODAL TEMPERATURES TEMP(I,J) ARE CALCULATED USING

C THE PREVIOUS VALUES T(I,J) FROM THE PREVIOUS ITERATION:

C -----

DO 930 KK=1,5000

DO 920 IT=1,5

ITER=ITER+1

DIFFL=0.0

FLAG=0.0

TEMP(1,1)=(T(2,1)+T(1,2)+H*TA/TK1*DX)/
@ (2.+H/TK1*DX)

DO 500 J=2,20

500 TEMP(1,J)=(T(1,J+1)+T(1,J-1)+2.*(T(2,J)+
@ TA*H/TK1*DX))/4.+2.*H/TK1*DX)

```

DO 700 I=2,4
  TEMP(I,1)=(T(I-1,1)+T(I+1,1)+2.*T(I,2))/4.
DO 600 J=2,20
  TEMP(I,J)=(T(I+1,J)+T(I-1,J)+T(I,J+1)+
    T(I,J-1))/4.
@
700 CONTINUE
  TEMP(5,1)=(TK1*(T(4,1)+T(5,2))+TK2*(T(5,2)+
    T(6,1)))/(2.*(TK1+TK2))
@
DO 800 J=2,20
  TEMP(5,J)=(TK1*(T(4,J)+0.5*(T(5,J+1)+
    T(5,J-1)))+TK2*(T(6,J)+0.5*
    (T(5,J+1)+T(5,J-1))))/
    (2.*(TK1+TK2))
@
@
DO 910 I=6,MM
  TEMP(I,1)=(T(I-1,1)+T(I+1,1)+2.*T(I,2))/4.
DO 900 J=2,NN
  TEMP(I,J)=(T(I+1,J)+T(I-1,J)+T(I,J+1)+
    T(I,J-1))/4.
@
  TEMP(I,N)=(T(I-1,N)+T(I+1,N)+2.*T(I,NN))/4.
910 CONTINUE

C COMPARE TEMP(I,J) WITH PREVIOUS VALUES FOR
C T(I,J). CHECK IF T(I,J)-TEMP(I,J)
C GREATER THAN TOLERANCE FOR ANY NODE (I,J)
C -----
@
CALL DIFF(T,TA,TEMP,M,N,I,J,IL,JL,
  TOL,FLAG,DIFFL,W)
IF(FLAG.EQ.0.0) GOTO 10
@
920 CONTINUE
  WRITE(6,5000)ITER,IL,JL,DIFFL
930 CONTINUE
10 WRITE(3,3000)((T(I,J),J=1,N),I=1,M)

C FORMAT STATEMENTS:
C -----
1000 FORMAT(F15.5)
2000 FORMAT(27F10.5)
3000 FORMAT(53F10.5)
4000 FORMAT(/'NUMBER OF ITERATIONS',6X,
  'MAXIMUM ITERATION DIFFERENCE',54(' '),/)
@
5000 FORMAT(I11,20X,'('',I3,'',',',I2,'') = ',F10.5)
STOP
END

```

C***** CONTINUED *****


```

C*****
C S/R TO EVALUATE THE LARGEST ITERATION DIFFERENCE, TO *
C COMPARE THE CURRENT ITERATION DIFFERENCE TO TOLERANCE, *
C AND TO RELAX THE NEW CALCULATED VALUE OF T(I,J). *
C*****

```

```

      SUBROUTINE DIFF(T,TA,TEMP,M,N,I,J,IL,JL;
@      TOL,FLAG,DIFFL,W)
      REAL T(M,N),TEMP(M,N)
      DO 100 I=1,M
        DO 100 J=1,N
          IF(I.GT.5)GOTO 10
          IF(J.GE.21)GOTO 100
10         DIFF=ABS(T(I,J)-TEMP(I,J))
          IF(DIFF.LT.DIFFL)GOTO 20
          DIFFL=DIFF
          IL=I
          JL=J
20         IF(DIFF.GT.TOL)FLAG=1.0
          T(I,J)=T(I,J)+W*(TEMP(I,J)-T(I,J))
100        CONTINUE
      RETURN
      END

```

```

C*****
C  FILENAME:  EVAP
C
C  THIS PROGRAM CALCULATES THE EVAPORATIVE HEAT TRANSFER
C  FOR A WATER-SPRAY COOLED ISOTHERMAL CYLINDER. THIS
C  PROGRAM ALSO CALCULATES THE TOTAL HEAT TRANSFER AS
C  WELL AS THE CONVECTIVE HEAT TRANSFER TO COMPARE TO
C  THE EVAPORATIVE COMPONENT.
C  TEST DATA USED: (REFERENCE: TEST #18)
C      RE= 40000
C      L.W.C.= 0.6 g/m**3
C      AIR VELOCITY= 11.9 m/s
C  AVERAGE HEAT TRANSFER COEFFICIENT = 636.73 W/m**2-C
C  AVERAGE (DRY) HEAT TRANSFER COEFFICIENT
C      (REFERENCE: TEST #1) = 61.29 W/m**2-C
C*****
C
C  CONSTANTS AND VARIABLES USED IN THE MAIN PROGRAM:
C  -----
C  HC = AVERAGE HEAT TRANSFER COEFFICIENT. (W/m**2-C)
C  HT = AVERAGE HEAT TRANSFER COEFFICIENT WITH SPRAY
C      COOLING. (W/m**2-C)
C  QC = AVERAGE HEAT FLUX PER UNIT AREA DUE TO
C      CONVECTION. (W/m**2)
C  QE = AVERAGE HEAT FLUX PER UNIT AREA DUE TO
C      EVAPORATION. (W/m**2)
C  QT = QC + QE
C  TA = AMBIENT AIR TEMPERATURE. (C)
C  TD = DROPLET TEMPERATURE AT CYLINDER SURFACE. (C)
C  RH = RELATIVE HUMIDITY OF AIRSTREAM. (Decimal)
C  P = STATIC AIR PRESSURE. (Pa)
C  EP = (EPSILON) = RATIO OF THE MOLECULAR WEIGHTS OF
C      WATER VAPOUR AND DRY AIR. (Mv/Md)
C  CPD = CONSTANT PRESSURE SPECIFIC HEAT CAPACITY OF
C      DRY AIR. (J/kg-K)
C  CPM = CONSTANT PRESSURE SPECIFIC HEAT CAPACITY OF
C      MOIST AIR. (J/kg-K)
C  W = HUMIDITY RATIO FOR MOIST AIR.
C  RHOA = DENSITY OF MOIST AIR. (kg/m**3)
C  CONDA = THERMAL CONDUCTIVITY OF MOIST AIR AT
C      AMBIENT AIR TEMPERATURE. (W/m-C)
C  CONDAF = THERMAL CONDUCTIVITY OF MOIST AIR AT
C      THE FILM TEMPERATURE. (W/m-C)
C  ALPHA = THERMAL DIFFUSIVITY. (m**2/s)
C  DIFF = DIFFUSIVITY OF WATER VAPOUR IN AIR. (m**2/s)
C  VAP = SATURATED VAPOUR PRESSURE OF WATER VAPOUR. (Pa)
C  LV = SPECIFIC LATENT HEAT OF VAPORIZATION. (J/kg)
C*****

```

```

REAL*8 LV, COND
DATA HT/636.73/, HC/61.29/, TA/301.2/,
@ TD/305.55/, RH/0.70/, P/92728.3/
TFILM=(TA+TD)/2

```

RA=8314.41/28.9645
 EP=18.01534/28.9645
 CPD=1005.0

C
 C CALCULATE THE SATURATED VAPOUR PRESSURE OF WATER @TFILM:
 C-----
 C

C VAPTF=VAP(TFILM)

C
 C CALCULATE THE MIXING RATIO FOR MOIST AIR (W):
 C-----
 C

C C1=RH*VAP(TFILM)
 C W=EP*C1/(P-C1)

C
 C CALCULATE CP OF MOIST AIR:
 C-----
 C

C CPM=CPD*(1.0+(1850./1005.-1.)*(W/(W+1.)))

C
 C CALCULATE THE DENSITY OF MOIST AIR:
 C-----
 C

C RHOA=P*(1.+W)/((287.055*TA*(1.+1.6078*W))

C
 C CALCULATE THE CONDUCTIVITY OF MOIST AIR @ TA AND TFILM:
 C-----
 C

C CONDA=COND(TA,RH,P,W)
 C CONDAF=COND(TFILM,RH,P,W)

C
 C CALCULATE THE DIFFUSIVITY OF WATER VAPOR IN AIR:
 C-----
 C

C DIFF=0.211E-4*(101325.0/P)*(TFILM/273.15)**1.94

C ALPHA=CONDA/(RHOA*CPM)
 C C3=DIFF/ALPHA
 C C4=VAP(TA)
 C C5=VAP(TD)
 C C6=LV(TD)

C
 C WRITE(6,1000)CONDA,CONDAF,TA,TD,TFILM,VAPTF,RH,EP
 C WRITE(6,2000)CPD,CPM,RHOA,P,W,DIFF,ALPHA,C3,C4,C5,C6

C
 C CALCULATE THE AVERAGE HEAT FLUX/UNIT AREA
 C DUE TO CONVECTION:
 C-----
 C

C QC=HC*(TD-TA)
 C WRITE(6,3000)HC,QC

```

C
C CALCULATE THE AVERAGE HEAT FLUX/UNIT AREA
C DUE TO EVAPORATION:
C -----
C
C      QE=HC*(C3**(2./3.)*EP*C6*(C5-(C4*RH))/(P*CPM))
C      WRITE(6,4000)QE
C
C CALCULATE THE TOTAL HEATFLUX/UNIT AREA DUE TO
C CONVECTION AND EVAPORATION:
C -----
C
C      QCE=QC+QE
C      WRITE(6,5000)QCE
C
C CALCULATE THE TOTAL HEAT TRANSFER/UNIT AREA:
C -----
C
C      QT=HT*(TD-TA)
C      WRITE(6,6000)HT,QT
C
C FORMAT STATEMENTS:
C -----
C
1000  FORMAT('/ THERMAL CONDUCTIVITY OF MOIST AIR @ TA = ',
C          @F8.5, ' W/m-C' /
C          @
C          @F8.5, ' W/m-C' /
C          @' AIR TEMP. = ',F6.1, ' K' /
C          @' WATER TEMP.= ',F6.1, ' K' /
C          @' FILM TEMP. = ',F6.1, ' K' /
C          @' SATURATED WATER VAPOUR PRESS @TFILM = ',F8.2, ' Pa' /
C          @' RH = ',F7.2, /
C          @' EPSILON = ',F8.5)
C          @TFILM = ' ,
2000  FORMAT(' CP DRY AIR = ',F8.2, ' J/kg-K' /
C          @' CP MOIST AIR = ',F8.2, ' J/kg-K' /
C          @' DENSITY OF AIR = ',F8.5, ' kg/m**3' /
C          @' STATIC AIR PRESSURE = ',F9.1, ' Pa' /
C          @' HUMIDITY RATIO (W) = ',F8.5, /
C          @' DIFF= ',F11.8, ' m**2/s' /
C          @' ALPHA= ',F11.8, ' m**2/s' /
C          @' Pr/Sc= ',F11.8, /
C          @' VAP(TA)= ',F10.3, ' Pa' /
C          @' VAP(TD)= ',F10.3, ' Pa' /
C          @' LATENT HT VAP LV(TD)= ',F11.1, ' J/kg' /)
3000  FORMAT(' HC= ',F8.2, ' W/m**2-C' /' QC= ',F8.2, ' W/m**2' )
4000  FORMAT(' QE= ',F8.2, ' W/m**2' )
5000  FORMAT(' Q = ',F8.2, ' W/m**2' )
6000  FORMAT(' HT= ',F8.2, ' W/m**2-C' /' QT= ',F8.2, ' W/m**2' )
C
C STOP
C END

```

```

C*****
C  FUNCTION SUBROUTINE TO CALCULATE THE SATURATION
C  VAPOUR PRESSURE OF WATER VAPOUR. (LOWE, 1977)
C      VAP = VAPOUR PRESSURE. (Pa)
C      T   = TEMPERATURE. (K)
C*****

```

```

      REAL FUNCTION VAP*8(T)
      REAL*8 A0,A1,A2,A3,A4,A5,A6,T
      A0=6984.505294
      A1=-188.9039310
      A2=2.133357675
      A3=-1.2885809730D-02
      A4=4.393587233D-05
      A5=-8.023923082D-08
      A6=6.136820929D-11
      VAP=(A0+T*(A1+T*(A2+T*(A3+T*(A4+T*(A5+T*A6))))))*100.
      RETURN
      END

```

```

C*****
C  FUNCTION SUBROUTINE TO CALCULATE THE LATENT HEAT
C  OF VAPORIZATION. (PRUPPACHER AND KLETT, 1978, P.89)
C      LV = SPECIFIC LATENT HEAT OF VAPORIZATION. (J/kg)
C      T   = TEMPERATURE. (K)
C*****

```

```

      REAL FUNCTION LV*8(T)
      REAL*8 T
      LV=597.3*(273.15/T)**(0.167+3.67D-04*T)*4186.84
      RETURN
      END

```

```

C***** CONTINUED *****

```

```

C*****
C FUNCTION SUBROUTINE TO CALCULATE THE CONDUCTIVITY OF *
C MOIST AIR. (PRUPPACHER AND KLETT, 1978, P.418) *
C COND = THERMAL CONDUCTIVITY OF AIR. (W/m-C) *
C DCOND = THERMAL CONDUCTIVITY OF DRY AIR. (W/m-C) *
C VCOND = THERMAL CONDUCTIVITY OF WATER VAPOUR. *
C (W/m-C) *
C RH = RELATIVE HUMIDITY OF AIRSTREAM. *
C P = BAROMETRIC PRESSURE. (Pascals) *
C VAP = SATURATED VAPOUR PRESSURE OF WATER *
C VAPOUR. (Pa) *
C W = HUMIDITY RATIO OF MOIST AIR. *
C T = TEMPERATURE. (K) *
C*****

```

```

REAL FUNCTION COND*8(T,RH,P,W)
REAL*8 T,W
DCOND=4.186D-03*(5.69+0.017*(T-273.15))
VCOND=4.186D-03*(3.78+0.020*(T-273.15))
COND=DCOND*(1.-(1.17-(1.02*VCOND/DCOND))*
@ (W/(0.62198+W)))
RETURN
END

```

```

C*****
C  FILENAME:  QGAP
C
C  THIS PROGRAM CALCULATES THE NUSSELT NUMBER AROUND A
C  CIRCULAR CYLINDER AT 10 DEGREE INCREMENTS FROM THE
C  STAGNATION LINE.  THE CONVECTIVE HEAT FLUX IS
C  CALCULATED USING THE VOLTAGE DROP ACROSS EACH OF 10
C  HEATERS MOUNTED FROM 0 TO 10 DEGREES.  THE HEAT
C  LOSS FROM BOTH SIDES OF EACH HEATER IS CALCULATED
C  TO CORRECT FOR CIRCUMFERENTIAL HEAT FLUX ERROR.
C
C  THE PROGRAM READS A DATA FILE OF THE FORM:
C
C      DESIGNATED TEST NUMBER (I3 INTEGER)
C      REYNOLDS NUMBER, AIR VELOCITY (m/s)
C      BAROMETRIC PRESSURE ("Hg); REL. HUMIDITY (decimal)
C      SURFACE TEMPERATURE (C), AMBIENT TEMPERATURE (C)
C      LIQ. WATER CONTENT (g/m**3), MEDIAN DROP DIA. (µm)
C      ANGLE INDEX i, VOLT(i)
C      WHERE THE ANGLE INDEX i IS AN INTEGER
C      i := 1 @ 0 DEGREES.
C      i = 10 @ 90 DEGREES.
C
C  SAMPLE DATA FILE:
C  -----
C
C      22
C      101300.,30.2
C      27.3,0.25
C      37.49,25.2
C      0.27,70.0
C      1,0.547
C      2,0.563
C
C      ...
C
C      9,0.379
C      10,0.453
C
C  EXECUTION COMMAND:
C  $R -LOAD# T=3 5=DATAFILE 2=OUTPUTFILE
C*****
C
C  CONSTANTS AND VARIABLES USED IN MAIN PROGRAM:
C  -----
C
C      A  = DEPTH OF HEATERS. (m)
C      HW = WIDTH OF HEATERS. (m)
C      L  = LENGTH OF HEATERS. (m)
C      = LENGTH OF GAP BETWEEN HEATERS.
C      B2 = GAP WIDTH AT SURFACE. (mm)
C      B  = HALF THE GAP WIDTH AT SURFACE. (m)
C      K  = THERMAL CONDUCTIVITY OF MATERIAL IN THE GAPS
C      BETWEEN THE HEATERS. (W/m-C)
C***** CONTINUED *****

```

```

C*****
C
C  CONSTANTS AND VARIABLES USED: (CONTINUED)
C  -----
C  D  = CYLINDER DIAMETER. (m)
C  KA = THERMAL CONDUCTIVITY OF MOIST AIR AT THE FILM
C      TEMPERATURE. (W/m-C)
C  RH = RELATIVE HUMIDITY OF AIRSTREAM. (Decimal)
C  RE = REYNOLDS NUMBER.
C  VEL = AIR VELOCITY (m/s)
C  NUM = DESIGNATED TEST NUMBER.
C  ANGLE = ANGLE INDEX.
C          =1 @ 0 DEGREES FROM THE STAGNATION LINE.
C          =10 @ 90 DEGREES FROM THE STAGNATION LINE.
C  ANGL = ANGLE FROM STAGNATION LINE. (DEGREES)
C  TFILM = FILM TEMPERATURE AT HEATER SURFACE. (K)
C  TF     = FILM TEMPERATURE AT HEATER SURFACE. (C)
C  TS     = TEMPERATURE OF HEATER. (C)
C  TA     = AMBIENT AIR TEMPERATURE. (C)
C  H(i)   = LOCAL CONVECTIVE HEAT TRANSFER COEFFICIENT
C          AT ANGLE INDEX i. (W/m**2-C)
C          i=1 @ 0 DEGREES
C          i=10 @ 90 DEGREES
C  VOLT(i) = VOLTAGE DROP ACROSS HEATER i, i=1,2,...,10
C  R(i)   = RESISTANCE OF HEATER i. (ohms)
C  Q(i)   = TOTAL HEAT FLUX (Watts) THROUGH SEMI-GAPS
C          FROM BOTH SIDES OF THE HEATER LOCATED AT
C          ANGLE INDEX i.
C  Z(i)   = +ve ROOTS OF  $Z(i) * \tan(A * Z(i)) = H/K$ , i=1,2,3
C  NU(i)  = LOCAL NUSSELT NUMBER
C  PRESS  = BAROMETRIC PRESSURE. ("Hg)
C  WH     = RELAXATION FACTOR FOR H. (GAUSS-SEIDEL)
C  LWC    = LIQUID WATER CONTENT IN AIRSTREAM. (g/m**3)
C  MDD    = MEDIAN DROPLET DIAMETER. (microns)
C*****

```

```

      DOUBLE PRECISION Z(3),HT,DIFF
      REAL L,K,KA,H(10),Q(10),R(10),LWC,MDD,
      @ NU(10),P(10),VOLT(10)
      INTEGER ANGLE
      DATA HW/0.003175/,D/0.05997/,K/1.1344/,L/0.1524/,
      @ B2/2.0584/,WH/1.0/,A/0.0002032/
      DATA R/0.2678,0.2697,0.2697,0.2713,0.2710,
      @ 0.2676,0.2711,0.2709,0.2688,0.2685/

```

```

C  READ DATA FILE:
C  -----

```

```

      READ(5,6000)NUM
      READ(5,7000)RE,VEL,PRESS,RH,TS,TA,LWC,MDD
      DO 100 I=1,10
      READ(5,1000)ANGLE,VOLT(I)

```



```

C  CALCULATE THE AIR THERMAL CONDUCTIVITY AT THE FILM
C  TEMPERATURE AND PRINT TEST DATA IN OUTPUT FILE.
C  -----

```

```

      TF=(TS+TA)/2.
      TFILM=TF+273.
      HW1=HW*1000.
      B=B2/2000.
      A1=A*1000.
      KA=COND(TFILM,RH,PRESS)
      WRITE(2,4000)NUM,RE,VEL,TA,TS,TF,PRESS,RH,KA,LWC,
      @      MDD,D,K,HW1,L,A1,B2

```

```

C  FOR EACH POSITION FROM 0 TO 90 DEGREES
C  (ANGLE INDEX = 1 TO 10), THE 400 DO-LOOP
C  CALCULATES THE FOLLOWING:
C  1.  CALCULATE THE HEATER POWER P(i).
C  2.  CALCULATE THE INITIAL GUESS FOR H(i)
C      BASED ON THE CALCULATED POWER P(i).
C  3.  ITERATE TO DETERMINE THE VALUE OF H(i) THAT
C      SATISFIES THE EQUATION  $H=(P-Q)/(\text{AREA}*(TS-TA))$ ,
C      SINCE Q IS A FUNCTION OF H.
C      (AREA = HEATER SURFACE AREA)
C  4.  CALCULATE THE LOCAL NUSSELT NUMBER NU(i).
C  -----

```

```

      DO 400 ANGLE=1,10
      P(ANGLE)=VOLT(ANGLE)**2/R(ANGLE)
      H(ANGLE)=P(ANGLE)/(L*HW*(TS-TA))

```

```

C
C      CALL S/R BETA TO OBTAIN THE 1st 3 ROOTS OF
C       $Z*\text{TAN}(A*Z)=H/K$  USING THE CURRENT VALUE OF H:
C      -----

```

```

10      CALL BETA(Z,A,H,K,ANGLE)

```

```

C      CALCULATE HEAT FLUX THROUGH ADJACENT GAPS
C      AT EACH ANGLE:
C      -----

```

```

      SUM=0.0
      DO 200 N=1,3
      DEN=(Z(N)**2+(H(ANGLE)/K)**2)*A+(H(ANGLE)/K)
200      SUM=SUM+((DTANH(Z(N)*B))*(DTAN(Z(N)*A)))/DEN
      Q(ANGLE)=4.*L*(TS-TA)*H(ANGLE)*SUM

```

```

C      CALCULATE NEW UPDATED VALUE OF H (CALLED HT)
C      BASED ON THE PREVIOUS VALUE OF H.
C      (REQUIRED FOR GAUSS-SEIDEL ITERATION OF H):
C      -----

```

```

      HT=(P(ANGLE)-Q(ANGLE))/(L*HW*(TS-TA))
      DIFF=HT-H(ANGLE)

```

```

C      OPTIONAL WRITE STATEMENT TO PRINT DIFFERENCE
C      CALCULATED FOR EACH "H" ITERATION.
C      (SPECIFIED TOLERANCE FOR H = 0.001)
C      -----
C      WRITE(6,2000)DIFF
C
C      IF(DABS(DIFF).LE.0.001)GOTO 20
C      H(ANGLE)=H(ANGLE)+WH*(DIFF)
C      GOTO 10
C      CONTINUE
C
C      300 DO-LOOP IS AN OPTIONAL WRITE STATEMENT
C      TO PRINT FINAL CONVERGED VALUE FOR THE 1ST
C      THREE ROOTS:
C      -----
C
C      DO 300 I=1,3
C      WRITE(6,9500)I,Z(I)
C      ANGL=(ANGLE-1)*10.
C      Q(ANGLE)=Q(ANGLE)*1000.0
C      P(ANGLE)=P(ANGLE)*1000.0
C      NU(ANGLE)=H(ANGLE)*D/KA
C      WRITE(2,8000)ANGL,P(ANGLE),Q(ANGLE),H(ANGLE),
C      NU(ANGLE)
C      WRITE(2,5000)
C
C      FORMAT STATEMENTS:
C      -----
C
C      1000 FORMAT(I4,F15.5)
C      2000 FORMAT('H DIFFERENCE= ',F14.4)
C      3000 FORMAT(10X,F6.1,6X,F8.2,9X,F6.2,5X,F8.2,1X,F8.2)
C      4000 FORMAT(///// ,10X,59(' '*),/,10X,'TEST # ',I3,/,
C      @,10X,'REYNOLDS NUMBER =',F9.1,/,
C      @,10X,'AIR VELOCITY =',F6.1,' m/s' //
C      @,10X,'AMBIENT AIR TEMPERATURE =',F6.2,' C' /
C      @,10X,'HEATER (SURFACE) TEMPERATURE =',F6.2,' C' /
C      @,10X,'FILM TEMPERATURE =',F6.2,' C' //
C      @,10X,'BAROMETRIC PRESSURE =',F6.2,' "Hg'
C      @/,10X,'AIRSTREAM: RELATIVE HUMIDITY =',F6.3,/,
C      @,9X,' THERMAL CONDUCTIVITY =',F8.5,
C      @' W/m-C' /
C      @,9X,' LIQUID WATER CONTENT =',F6.1,
C      @' g/m**3' /
C      @,9X,' MEAN DROPLET DIAMETER =',F6.1,
C      @' microns' //
C      @,10X,'CYLINDER DIAMETER =',F8.5,' m' /
C      @,10X,'THERMAL CONDUCTIVITY OF EPOXY =',F8.5,
C      @' W/m-C' /
C      @,10X,'HEATER WIDTH =',F6.3,' mm' /
C      @,9X,' LENGTH =',F7.4,' m' /
C      @,9X,' DEPTH =',F6.3,' mm'

```

```

@/,10X,'GAP WIDTH AT SURFACE          =',F6.3,' mm'
@////,10X,'  ANGLE      HEATER POWER  GAP HEAT LOSS',
@'      H      NUSSELT',10X,' (DEGREES)',6X,' (mW)',11X,
@' (mW)',6X,' (W/m**2-C) NUMBER',/,10X,59(' - '))
5000  FORMAT(10X,59('*'))
6000  FORMAT(I3)
7000  FORMAT(2F15.5)
8000  FORMAT('Z(',I1,') =',F15.6)
      STOP
      END

```

```

C*****
C  SUBROUTINE TO CALCULATE THE 1ST THREE ROOTS OF *
C  Z*(TAN(Z*A)=H/K  USING  GAUSS-SEIDEL ITERATIVE *
C  METHOD WITH RELAXATION. *
C  SPECIFIED TOLERANCE FOR Z(i) = 0.0001 *
C  Z(i) = ith ROOT OF EQUATION. *
C  WZ(i)= RELAXATION FACTOR FOR Z(i). *
C  ZT   = NEW UPDATED VALUE OF Z CALCULATED *
C        USING THE PREVIOUS VALUE OF Z. *
C*****

```

```

      SUBROUTINE BETA(Z,A,H,K,ANGLE)
      DOUBLE PRECISION Z(3),ZT,DIFF
      INTEGER ANGLE
      REAL K
      DIMENSION H(10),WZ(3)
      DATA WZ/0.2,0.0001,0.0001/
      PI=3.141592654
      DO 100 I=1,3
100    Z(I)=(I-1)*PI/2./A+(((I-1)*PI/2./A)**2+
      @      (H(ANGLE)/(K*A))**0.5
      DO 200 N=1,3
10    ZT=(H(ANGLE)/K)/(DTAN(Z(N)*A))
      DIFF=ZT-Z(N)

C  OPTIONAL WRITE STATEMENT TO PRINT THE ROOT AND
C  DIFFERENCE CALCULATED FOR EACH ITERATION.
C  (SPECIFIED TOLERANCE FOR Z(i) = 0.0001)
C  -----
C      WRITE(6,1000)DIFF,Z(N)
1000  FORMAT(F13.5,2X,F15.5)

      IF(DABS(DIFF).LE.0.0001)GOTO 200
      Z(N)=Z(N)+WZ(N)*(DIFF)
      GOTO 10
200  CONTINUE
      RETURN
      END

```

```

C*****
C  FUNCTION SUBROUTINE TO CALCULATE THE CONDUCTIVITY OF      *
C  MOIST AIR AT THE SURFACE FILM TEMPERATURE (TFILM).        *
C  (PRUPPACHER AND KLETT, 1978, P.418)                        *
C      COND  = THERMAL CONDUCTIVITY OF AIR. (W/m-C)          *
C      DCOND = THERMAL CONDUCTIVITY OF DRY AIR. (W/m-C)       *
C      VCOND = THERMAL CONDUCTIVITY OF WATER VAPOUR.          *
C              (W/m-C)                                         *
C      RH    = RELATIVE HUMIDITY OF AIRSTREAM.                *
C      PRESS = BAROMETRIC PRESSURE. (Inches Hg)               *
C      PRESS1 = BAROMETRIC PRESSURE. (Pascals)                 *
C      VAP    = SATURATED VAPOUR PRESSURE OF WATER            *
C              VAPOUR. (Pa) (LOWE, 1977)                      *
C      W      = HUMIDITY RATIO OF MOIST AIR.                  *
C      T      = TEMPERATURE. (K)                              *
C*****

```

```

REAL FUNCTION COND*8(T,RH,PRESS)
REAL*8 A0,A1,A2,A3,A4,A5,A6,T,W
A0=6984.505294
A1=-188.9039310
A2=2.133357675
A3=-1.2885809730D-02
A4=4.393587233D-05
A5=-8.023923082D-08
A6=6.136820929D-11
VAP=(A0+T*(A1+T*(A2+T*(A3+T*(A4+T*(A5+T*A6)))))*100.
PRESS1=PRESS*3376.85
W=0.62198*(RH*VAP/(PRESS1-RH*VAP))
DCOND=4.186D-03*(5.69+0.017*(T-273.15))
VCOND=4.186D-03*(3.78+0.020*(T-273.15))
COND=DCOND*(1.-(1.17-(1.02*VCOND/DCOND)))*
@ (W/(0.62198+W))
RETURN
END

```

APPENDIX B

ELECTRICAL SCHEMATIC DIAGRAM
of
12 CHANNEL HEATER TEMPERATURE CONTROLLER

APPENDIX C

EXPERIMENTAL DATA

This appendix contains listings of the test conditions and reduced data for each heat transfer test performed.

 TEST # 1

REYNOLDS NUMBER = 40000.0
 AIR VELOCITY = 12.3 m/s
 TEST CONDITIONS : SMOOTH CYLINDER

AMBIENT AIR TEMPERATURE = 29.00 C
 HEATER (SURFACE) TEMPERATURE = 44.90 C
 FILM TEMPERATURE = 36.95 C

BAROMETRIC PRESSURE = 27.41 "Hg
 AIRSTREAM RELATIVE HUMIDITY = 0.24
 THERMAL CONDUCTIVITY = 0.02625 W/m-C
 LIQUID WATER CONTENT = 0.0 g/m**3
 MEDIAN DROP DIAMETER = 0.0 microns

CYLINDER DIAMETER = 0.05997 m
 THERMAL CONDUCTIVITY OF EPOXY = 1.13440 W/m-C
 HEATER WIDTH = 3.175 mm
 LENGTH = 0.1524 m
 DEPTH = 0.203 mm
 GAP WIDTH AT SURFACE = 2.058 mm

ANGLE (DEGREES)	HEATER POWER (mW)	GAP HEAT LOSS (mW)	H (W/m**2-C)	NUSSELT NUMBER
0.0	857.14	316.14	70.32	160.65
10.0	933.78	342.46	76.86	175.59
20.0	926.34	339.92	76.22	174.14
30.0	907.87	333.60	74.64	170.53
40.0	878.71	323.58	72.16	164.85
50.0	825.30	305.11	67.61	154.47
60.0	766.80	284.72	62.66	143.16
70.0	643.81	241.24	52.33	119.54
80.0	397.80	151.83	31.97	73.04
90.0	351.02	134.45	28.15	64.31

 TEST # 2

REYNOLDS NUMBER = 40000.0
 AIR VELOCITY = 12.2 m/s
 TEST CONDITIONS : SMALL ROUGHNESS (FINE SCREEN)

AMBIENT AIR TEMPERATURE = 29.20 C
 HEATER (SURFACE) TEMPERATURE = 42.53 C
 FILM TEMPERATURE = 35.86 C

BAROMETRIC PRESSURE = 27.46 "Hg
 AIRSTREAM: RELATIVE HUMIDITY = 0.36
 THERMAL CONDUCTIVITY = 0.02563 W/m-C
 LIQUID WATER CONTENT = 0.0 g/m**3
 MEDIAN DROP DIAMETER = 0.0 microns

CYLINDER DIAMETER = 0.05997 m
 THERMAL CONDUCTIVITY OF EPOXY = 1.13440 W/m-C
 HEATER WIDTH = 3.175 mm
 LENGTH = 0.1524 m
 DEPTH = 0.203 mm
 GAP WIDTH AT SURFACE = 2.058 mm

ANGLE (DEGREES)	HEATER POWER (mW)	GAP HEAT LOSS (mW)	H (W/m**2-C)	NUSSELT NUMBER
0.0	637.63	236.87	62.14	145.41
10.0	650.01	241.20	63.38	148.33
20.0	640.72	237.95	62.45	146.14
30.0	634.56	235.79	61.83	144.68
40.0	616.25	229.36	59.99	140.38
50.0	595.24	221.95	57.88	135.44
60.0	554.30	207.43	53.78	125.85
70.0	474.14	178.70	45.80	107.19
80.0	319.38	122.05	30.59	71.60
90.0	376.63	143.19	36.19	84.70

 TEST # 3

REYNOLDS NUMBER = 40000.0
 AIR VELOCITY = 12.2 m/s
 TEST CONDITIONS : SMALL ROUGHNESS (COARSE SCREEN)

AMBIENT AIR TEMPERATURE = 28.20 C
 HEATER (SURFACE) TEMPERATURE = 42.53 C
 FILM TEMPERATURE = 35.36 C

BAROMETRIC PRESSURE = 27.50 "Hg
 AIRSTREAM: RELATIVE HUMIDITY = 0.35
 THERMAL CONDUCTIVITY = 0.02607 W/m-C
 LIQUID WATER CONTENT = 0.0 g/m**3
 MEDIAN DROP DIAMETER = 0.0 microns

CYLINDER DIAMETER = 0.05997 m
 THERMAL CONDUCTIVITY OF EPOXY = 1.13440 W/m-C
 HEATER WIDTH = 3.175 mm
 LENGTH = 0.1524 m
 DEPTH = 0.203 mm
 GAP WIDTH AT SURFACE = 2.058 mm

ANGLE (DEGREES)	HEATER POWER (mW)	GAP HEAT LOSS (mW)	H (W/m**2-C)	NUSSELT NUMBER
0.0	615.52	229.97	55.60	127.88
10.0	552.45	207.48	49.75	114.42
20.0	635.51	237.05	57.47	132.17
30.0	628.71	234.64	56.83	130.77
40.0	535.65	201.45	48.20	110.85
50.0	556.79	209.04	50.15	115.35
60.0	518.72	195.36	46.63	107.26
70.0	519.10	195.50	46.67	107.34
80.0	297.95	114.30	26.49	60.92
90.0	346.46	132.37	30.88	71.02

 TEST # 4

REYNOLDS NUMBER = 40000.0
 AIR VELOCITY = 12.2 m/s
 TEST CONDITIONS : MEDIUM ROUGHNESS

AMBIENT AIR TEMPERATURE = 29.20 C
 HEATER (SURFACE) TEMPERATURE = 42.53 C
 FILM TEMPERATURE = 35.86 C

BAROMETRIC PRESSURE = 27.46 "Hg
 AIRSTREAM: RELATIVE HUMIDITY = 0.36
 THERMAL CONDUCTIVITY = 0.02563 W/m-C
 LIQUID WATER CONTENT = 0.0 g/m**3
 MEDIAN DROP DIAMETER = 0.0 microns

CYLINDER DIAMETER = 0.05997 m
 THERMAL CONDUCTIVITY OF EPOXY = 1.13440 W/m-C
 HEATER WIDTH = 3.175 mm
 LENGTH = 0.1524 m
 DEPTH = 0.203 mm
 GAP WIDTH AT SURFACE = 2.058 mm

ANGLE (DEGREES)	HEATER POWER (mW)	GAP HEAT LOSS (mW)	H (W/m**2-C)	NUSSELT NUMBER
0.0	640.72	237.95	62.45	146.14
10.0	697.50	257.74	68.18	159.56
20.0	857.14	312.32	84.47	197.67
30.0	998.23	359.29	99.06	231.82
40.0	1068.81	382.35	106.43	249.07
50.0	1084.82	387.54	108.11	252.99
60.0	1052.92	377.18	104.77	245.17
70.0	926.34	335.50	91.60	214.37
80.0	804.41	294.46	79.06	185.02
90.0	604.88	225.35	58.84	137.70

TEST # 5

REYNOLDS NUMBER = 40000.0
 AIR VELOCITY = 12.2 m/s
 TEST CONDITIONS : LARGE ROUGHNESS

AMBIENT AIR TEMPERATURE = 28.60 C
 HEATER (SURFACE) TEMPERATURE = 42.53 C
 FILM TEMPERATURE = 35.57 C

BAROMETRIC PRESSURE = 27.50 "Hg
 AIRSTREAM: RELATIVE HUMIDITY = 0.35
 THERMAL CONDUCTIVITY = 0.02609 W/m-C
 LIQUID WATER CONTENT = 0.0 g/m**3
 MEDIAN DROP DIAMETER = 0.0 microns

CYLINDER DIAMETER = 0.05997 m
 THERMAL CONDUCTIVITY OF EPOXY = 1.13440 W/m-C
 HEATER WIDTH = 3.175 mm
 LENGTH = 0.1524 m
 DEPTH = 0.203 mm
 GAP WIDTH AT SURFACE = 2.058 mm

ANGLE (DEGREES)	HEATER POWER (mW)	GAP HEAT LOSS (mW)	H (W/m**2-C)	NUSSELT NUMBER
0.0	550.62	206.56	51.05	117.35
10.0	468.60	177.02	43.26	99.45
20.0	679.21	252.04	63.38	145.70
30.0	766.44	282.32	71.83	165.12
40.0	855.51	312.77	80.52	185.11
50.0	891.75	325.03	84.08	193.29
60.0	869.46	317.50	81.89	188.25
70.0	873.69	318.93	82.30	189.21
80.0	792.34	291.22	74.35	170.92
90.0	691.85	256.45	64.60	148.50

 TEST # 6

REYNOLDS NUMBER = 80000.0
 AIR VELOCITY = 24.3 m/s
 TEST CONDITIONS : SMOOTH CYLINDER

AMBIENT AIR TEMPERATURE = 27.20 C
 HEATER (SURFACE) TEMPERATURE = 42.53 C
 FILM TEMPERATURE = 34.86 C

BAROMETRIC PRESSURE = 27.41 "Hg
 AIRSTREAM: RELATIVE HUMIDITY = 0.24
 THERMAL CONDUCTIVITY = 0.02612 W/m-C
 LIQUID WATER CONTENT = 0.0 g/m**3
 MEDIAN DROP DIAMETER = 0.0 microns

CYLINDER DIAMETER = 0.05997 m
 THERMAL CONDUCTIVITY OF EPOXY = 1.13440 W/m-C
 HEATER WIDTH = 3.175 mm
 LENGTH = 0.1524 m
 DEPTH = 0.203 mm
 GAP WIDTH AT SURFACE = 2.058 mm

ANGLE (DEGREES)	HEATER POWER (mW)	GAP HEAT LOSS (mW)	H (W/m**2-C)	NUSSELT NUMBER
0.0	1048.96	380.38	90.13	206.92
10.0	1183.39	424.80	102.27	234.79
20.0	1170.84	420.69	101.13	232.17
30.0	1162.50	417.96	100.37	230.44
40.0	1129.47	407.09	97.39	223.58
50.0	1068.81	387.00	91.92	211.02
60.0	979.05	356.92	83.87	192.55
70.0	804.41	297.19	68.38	156.99
80.0	412.53	157.10	34.44	79.06
90.0	543.48	204.86	45.65	104.80

 TEST # 7

REYNOLDS NUMBER = 80000.0
 AIR VELOCITY = 24.0 m/s
 TEST CONDITIONS : SMALL ROUGHNESS (FINE SCREEN)

AMBIENT AIR TEMPERATURE = 25.60 C
 HEATER (SURFACE) TEMPERATURE = 40.08 C
 FILM TEMPERATURE = 32.84 C

BAROMETRIC PRESSURE = 27.50 "Hg
 AIRSTREAM: RELATIVE HUMIDITY = 0.32
 THERMAL CONDUCTIVITY = 0.02595 W/m-C
 LIQUID WATER CONTENT = 0.0 g/m**3
 MEDIAN DROP DIAMETER = 0.0 microns

CYLINDER DIAMETER = 0.05997 m
 THERMAL CONDUCTIVITY OF EPOXY = 1.13440 W/m-C
 HEATER WIDTH = 3.175 mm
 LENGTH = 0.1524 m
 DEPTH = 0.203 mm
 GAP WIDTH AT SURFACE = 2.058 mm

ANGLE (DEGREES)	HEATER POWER (mW)	GAP HEAT LOSS (mW)	H (W/m**2-C)	NUSSELT NUMBER
0.0	941.25	342.68	85.43	197.46
10.0	971.43	352.82	88.29	204.07
20.0	971.43	352.82	88.29	204.07
30.0	967.63	351.54	87.93	203.24
40.0	963.84	350.27	87.57	202.41
50.0	1208.70	430.76	111.03	256.63
60.0	1547.71	537.08	144.24	333.39
70.0	1630.37	562.15	152.46	352.39
80.0	1547.71	537.08	144.24	333.39
90.0	1314.10	464.43	111.03	280.29

 TEST # 8

REYNOLDS NUMBER = 80000.0
 AIR VELOCITY = 24.2 m/s
 TEST CONDITIONS : SMALL ROUGHNESS (COARSE SCREEN)

AMBIENT AIR TEMPERATURE = 26.00 C
 HEATER (SURFACE) TEMPERATURE = 42.53 C
 FILM TEMPERATURE = 34.26 C

BAROMETRIC PRESSURE = 27.51 "Hg
 AIRSTREAM: RELATIVE HUMIDITY = 0.35
 THERMAL CONDUCTIVITY = 0.02601 W/m-C
 LIQUID WATER CONTENT = 0.0 g/m**3
 MEDIAN DROP DIAMETER = 0.0 microns

CYLINDER DIAMETER = 0.05997 m
 THERMAL CONDUCTIVITY OF EPOXY = 1.13440 W/m-C
 HEATER WIDTH = 3.175 mm
 LENGTH = 0.1524 m
 DEPTH = 0.203 mm
 GAP WIDTH AT SURFACE = 2.058 mm

ANGLE (DEGREES)	HEATER POWER (mW)	GAP HEAT LOSS (mW)	H (W/m**2-C)	NUSSELT NUMBER
0.0	892.91	329.29	70.47	162.47
10.0	812.10	301.22	63.87	147.27
20.0	960.63	352.56	76.02	175.27
30.0	1012.07	370.09	80.26	185.05
40.0	829.06	307.14	65.25	150.45
50.0	1283.24	460.41	102.88	237.18
60.0	1641.05	574.39	133.36	307.46
70.0	1803.62	624.32	147.44	339.93
80.0	1576.64	554.29	127.82	294.69
90.0	1376.77	490.76	110.77	255.40

 TEST # 9

REYNOLDS NUMBER = 80000.0
 AIR VELOCITY = 24.0 m/s
 TEST CONDITIONS : MEDIUM ROUGHNESS

AMBIENT AIR TEMPERATURE = 25.40 C
 HEATER (SURFACE) TEMPERATURE = 40.08 C
 FILM TEMPERATURE = 32.74 C

BAROMETRIC PRESSURE = 27.50 "Hg
 AIRSTREAM: RELATIVE HUMIDITY = 0.32
 THERMAL CONDUCTIVITY = 0.02594 W/m-C
 LIQUID WATER CONTENT = 0.0 g/m**3
 MEDIAN DROP DIAMETER = 0.0 microns

CYLINDER DIAMETER = 0.05997 m
 THERMAL CONDUCTIVITY OF EPOXY = 1.13440 W/m-C
 HEATER WIDTH = 3.175 mm
 LENGTH = 0.1524 m
 DEPTH = 0.203 mm
 GAP WIDTH AT SURFACE = 2.058 mm

ANGLE (DEGREES)	HEATER POWER (mW)	GAP HEAT LOSS (mW)	H (W/m**2-C)	NUSSELT NUMBER
0.0	963.84	350.64	86.33	199.57
10.0	1175.01	420.41	106.24	245.60
20.0	1620.54	560.15	149.28	345.12
30.0	1955.45	659.00	182.52	421.95
40.0	2131.88	709.08	200.30	463.07
50.0	2194.29	726.49	206.64	477.71
60.0	2120.63	705.93	199.16	460.43
70.0	1875.37	635.82	174.51	403.43
80.0	1402.51	492.98	128.04	296.02
90.0	923.66	337.10	82.58	190.90

TEST # 10

REYNOLDS NUMBER = 80000.0
 AIR VELOCITY = 24.2 m/s
 TEST CONDITIONS : LARGE ROUGHNESS

AMBIENT AIR TEMPERATURE = 26.40 C
 HEATER (SURFACE) TEMPERATURE = 42.53 C
 FILM TEMPERATURE = 34.46 C

BAROMETRIC PRESSURE = 27.51 "Hg
 AIRSTREAM: RELATIVE HUMIDITY = 0.35
 THERMAL CONDUCTIVITY = 0.02602 W/m-C
 LIQUID WATER CONTENT = 0.0 g/m**3
 MEDIAN DROP DIAMETER = 0.0 microns

CYLINDER DIAMETER = 0.05997 m
 THERMAL CONDUCTIVITY OF EPOXY = 1.13440 W/m-C
 HEATER WIDTH = 3.175 mm
 LENGTH = 0.1524 m
 DEPTH = 0.203 mm
 GAP WIDTH AT SURFACE = 2.058 mm

ANGLE (DEGREES)	HEATER POWER (mW)	GAP, HEAT LOSS (mW)	H (W/m**2-C)	NUSSELT NUMBER
0.0	849.62	313.82	68.65	158.21
10.0	784.58	291.17	63.22	145.69
20.0	1160.70	419.18	95.01	218.95
30.0	1460.63	516.34	120.99	278.82
40.0	1671.32	582.12	139.55	321.60
50.0	1786.89	617.38	149.85	345.32
60.0	1898.95	651.02	159.89	368.48
70.0	1803.62	622.43	151.34	348.77
80.0	1591.20	557.34	132.46	305.27
90.0	1309.68	467.97	107.85	248.53

 TEST # 11

REYNOLDS NUMBER = 120000.0
 AIR VELOCITY = 36.1 m/s
 TEST CONDITIONS : SMOOTH CYLINDER

AMBIENT AIR TEMPERATURE = 25.60 C
 HEATER (SURFACE) TEMPERATURE = 40.08 C
 FILM TEMPERATURE = 32.84 C

BAROMETRIC PRESSURE = 27.46 "Hg
 AIRSTREAM: RELATIVE HUMIDITY = 0.24
 THERMAL CONDUCTIVITY = 0.02600 W/m-C
 LIQUID WATER CONTENT = 0.0 g/m**3
 MEDIAN DROP DIAMETER = 0.0 microns

CYLINDER DIAMETER = 0.05997 m
 THERMAL CONDUCTIVITY OF EPOXY = 1.13440 W/m-C
 HEATER WIDTH = 3.175 mm
 LENGTH = 0.1524 m
 DEPTH = 0.203 mm
 GAP WIDTH AT SURFACE = 2.058 mm

ANGLE (DEGREES)	HEATER POWER (mW)	GAP HEAT LOSS (mW)	H (W/m**2-C)	NUSSELT NUMBER
0.0	1175.01	419.87	107.78	248.64
10.0	1379.77	485.13	127.69	294.56
20.0	1379.77	485.13	127.69	294.56
30.0	1384.30	486.55	128.13	295.59
40.0	1357.20	478.04	125.48	289.47
50.0	1299.41	459.77	119.84	276.45
60.0	1200.24	428.03	110.21	254.26
70.0	979.05	355.36	89.02	205.35
80.0	503.81	190.06	44.78	103.30
90.0	717.77	266.09	64.47	148.72

?

 TEST # 12

REYNOLDS NUMBER = 120000.0
 AIR VELOCITY = 35.0 m/s
 TEST CONDITIONS : SMALL ROUGHNESS (FINE SCREEN)

AMBIENT AIR TEMPERATURE = 23.80 C
 HEATER (SURFACE) TEMPERATURE = 37.49 C
 FILM TEMPERATURE = 30.65 C

BAROMETRIC PRESSURE = 27.93 "Hg
 AIRSTREAM: RELATIVE HUMIDITY = 0.24
 THERMAL CONDUCTIVITY = 0.02586 W/m-C
 LIQUID WATER CONTENT = 0.0 g/m**3
 MEDIAN DROP DIAMETER = 0.0 microns

CYLINDER DIAMETER = 0.05997 m
 THERMAL CONDUCTIVITY OF EPOXY = 1.13440 W/m-C
 HEATER WIDTH = 3.175 mm
 LENGTH = 0.1524 m
 DEPTH = 0.203 mm
 GAP WIDTH AT SURFACE = 2.058 mm

ANGLE (DEGREES)	HEATER POWER (mW)	GAP HEAT LOSS (mW)	H (W/m**2-C)	NUSSELT NUMBER
0.0	867.53	316.44	83.19	192.93
10.0	857.85	313.17	82.22	190.69
20.0	966.30	349.53	93.11	215.93
30.0	1082.80	387.84	104.91	243.31
40.0	1215.78	430.64	118.53	274.87
50.0	1802.43	608.46	180.24	418.00
60.0	1728.29	586.93	172.30	399.59
70.0	1649.66	563.81	163.92	380.15
80.0	1630.37	558.09	161.87	375.40
90.0	1345.25	471.39	131.92	305.93

 TEST # 13

REYNOLDS NUMBER = 120000.0
 AIR VELOCITY = 35.0 m/s
 TEST CONDITIONS : SMALL ROUGHNESS (COARSE SCREEN)

AMBIENT AIR TEMPERATURE = 24.00 C
 HEATER (SURFACE) TEMPERATURE = 37.49 C
 FILM TEMPERATURE = 30.74 C

BAROMETRIC PRESSURE = 27.93 "Hg
 AIRSTREAM: RELATIVE HUMIDITY = 0.24
 THERMAL CONDUCTIVITY = 0.02587 W/m-C
 LIQUID WATER CONTENT = 0.0 g/m**3
 MEDIAN DROP DIAMETER = 0.0 microns

CYLINDER DIAMETER = 0.05997 m
 THERMAL CONDUCTIVITY OF EPOXY = 1.13440 W/m-C
 HEATER WIDTH = 3.175 mm
 LENGTH = 0.1524 m
 DEPTH = 0.203 mm
 GAP WIDTH AT SURFACE = 2.058 mm

ANGLE (DEGREES)	HEATER POWER (mW)	GAP HEAT LOSS (mW)	H (W/m**2-C)	NUSSELT NUMBER
0.0	871.13	317.31	84.84	196.71
10.0	805.18	294.97	78.16	181.22
20.0	1010.32	363.64	99.07	229.70
30.0	1015.94	365.48	99.65	231.04
40.0	1275.81	448.94	126.68	293.70
50.0	1948.00	648.50	199.08	461.58
60.0	1807.45	608.60	183.66	425.83
70.0	1666.98	567.79	168.40	390.43
80.0	1690.01	574.55	170.89	396.21
90.0	1381.31	481.77	137.81	319.51

TEST # 14

REYNOLDS NUMBER = 120000.0
 AIR VELOCITY = 35.1 m/s
 TEST CONDITIONS : MEDIUM ROUGHNESS

AMBIENT AIR TEMPERATURE = 24.40 C
 HEATER (SURFACE) TEMPERATURE = 37.49 C
 FILM TEMPERATURE = 30.94 C

BAROMETRIC PRESSURE = 27.93 "Hg
 AIRSTREAM: RELATIVE HUMIDITY = 0.24
 THERMAL CONDUCTIVITY = 0.02588 W/m-C
 LIQUID WATER CONTENT = 0.0 g/m**3
 MEDIAN DROP DIAMETER = 0.0 microns

CYLINDER DIAMETER = 0.05997 m
 THERMAL CONDUCTIVITY OF EPOXY = 1.13440 W/m-C
 HEATER WIDTH = 3.175 mm
 LENGTH = 0.1524 m
 DEPTH = 0.203 mm
 GAP WIDTH AT SURFACE = 2.058 mm

ANGLE (DEGREES)	HEATER POWER (mW)	GAP HEAT LOSS (mW)	H (W/m**2-C)	NUSSELT NUMBER
0.0	786.71	288.06	78.73	182.44
10.0	1014.20	363.94	102.66	237.91
20.0	1504.52	517.40	155.85	361.16
30.0	1873.83	624.66	197.22	457.03
40.0	2012.48	663.23	213.02	493.65
50.0	2332.21	748.90	249.98	579.29
60.0	2058.31	675.79	218.28	505.83
70.0	1674.43	567.59	174.75	404.96
80.0	1131.52	401.88	115.20	266.96
90.0	916.26	331.66	92.30	213.89

TEST # 15

REYNOLDS NUMBER = 120000.0
 AIR VELOCITY = 35.4 m/s
 TEST CONDITIONS : LARGE ROUGHNESS

AMBIENT AIR TEMPERATURE = 24.80 C
 HEATER (SURFACE) TEMPERATURE = 40.08 C
 FILM TEMPERATURE = 32.44 C

BAROMETRIC PRESSURE = 27.93 "Hg
 AIRSTREAM: RELATIVE HUMIDITY = 0.24
 THERMAL CONDUCTIVITY = 0.02597 W/m-C
 LIQUID WATER CONTENT = 0.0 g/m**3
 MEDIAN DROP DIAMETER = 0.0 microns

CYLINDER DIAMETER = 0.05997 m
 THERMAL CONDUCTIVITY OF EPOXY = 1.13440 W/m-C
 HEATER WIDTH = 3.175 mm
 LENGTH = 0.1524 m
 DEPTH = 0.203 mm
 GAP WIDTH AT SURFACE = 2.058 mm

ANGLE (DEGREES)	HEATER POWER (mW)	GAP HEAT LOSS (mW)	H (W/m**2-C)	NUSSELT NUMBER
0.0	913.11	334.48	78.26	180.70
10.0	899.36	329.79	77.04	177.87
20.0	1443.74	508.08	126.55	292.20
30.0	1732.07	596.71	153.56	354.56
40.0	2026.13	683.27	181.63	419.36
50.0	2624.23	848.40	240.19	554.58
60.0	2267.27	751.54	205.01	473.35
70.0	1813.96	621.19	161.33	372.49
80.0	2115.01	708.71	190.21	439.17
90.0	1861.64	635.31	165.86	382.97

 TEST # 16

REYNOLDS NUMBER = 40000.0
 AIR VELOCITY = 11.8 m/s
 TEST CONDITIONS : WATER SPRAY COOLING

AMBIENT AIR TEMPERATURE = 28.40 C
 HEATER (SURFACE) TEMPERATURE = 34.99 C
 FILM TEMPERATURE = 31.69 C

BAROMETRIC PRESSURE = 27.98 "Hg
 AIRSTREAM: RELATIVE HUMIDITY = -
 THERMAL CONDUCTIVITY = 0.02549 W/m-C
 LIQUID WATER CONTENT = 0.1 g/m**3
 MEDIAN DROP DIAMETER = 37.6 microns

CYLINDER DIAMETER = 0.05997 m
 THERMAL CONDUCTIVITY OF EPOXY = 1.13440 W/m-C
 HEATER WIDTH = 3.175 mm
 LENGTH = 0.1524 m
 DEPTH = 0.203 mm
 GAP WIDTH AT SURFACE = 2.058 mm

ANGLE (DEGREES)	HEATER POWER (mW)	GAP HEAT LOSS (mW)	H. (W/m**2-C)	NUSSELT NUMBER
0.0	821.80	279.56	170.05	400.04
10.0	864.30	291.93	179.50	422.26
20.0	736.70	254.24	151.30	355.93
30.0	610.21	215.21	123.87	291.41
40.0	482.14	173.88	96.67	227.42
50.0	388.13	142.32	77.09	181.35
60.0	332.59	123.17	65.68	154.51
70.0	271.21	101.54	53.21	125.17
80.0	148.81	56.96	28.80	67.76
90.0	161.13	61.54	31.23	73.47

 TEST # 17

REYNOLDS NUMBER = 40000.0
 AIR VELOCITY = 11.8 m/s
 TEST CONDITIONS : WATER SPRAY COOLING

AMBIENT AIR TEMPERATURE = 28.80 C
 HEATER (SURFACE) TEMPERATURE = 34.99 C
 FILM TEMPERATURE = 31.90 C

BAROMETRIC PRESSURE = 27.98 "Hg
 AIRSTREAM: RELATIVE HUMIDITY = ---
 THERMAL CONDUCTIVITY = 0.02550 W/m-C
 LIQUID WATER CONTENT = 0.3 g/m**3
 MEDIAN DROP DIAMETER = 24.7 microns

CYLINDER DIAMETER = 0.05997 m
 THERMAL CONDUCTIVITY OF EPOXY = 1.13440 W/m-C
 HEATER WIDTH = 3.175 mm
 LENGTH = 0.1524 m
 DEPTH = 0.203 mm
 GAP WIDTH AT SURFACE = 2.058 mm

ANGLE (DEGREES)	HEATER POWER (mW)	GAP HEAT LOSS (mW)	H (W/m**2-C)	NUSSELT NUMBER
0.0	1125.37	360.00	255.54	600.97
10.0	1150.06	366.36	261.65	615.35
20.0	1005.95	328.42	226.21	531.99
30.0	797.50	270.06	176.10	414.14
40.0	625.37	218.45	135.86	319.51
50.0	531.56	188.92	114.40	269.04
60.0	466.21	167.72	99.66	234.37
70.0	376.21	137.64	79.65	187.31
80.0	226.97	85.43	47.25	111.13
90.0	281.66	104.92	59.01	138.78

 TEST # 18

REYNOLDS NUMBER = 40000.0
 AIR VELOCITY = 11.9 m/s
 TEST CONDITIONS : WATER SPRAY COOLING

AMBIENT AIR TEMPERATURE = 28.20 C
 HEATER (SURFACE) TEMPERATURE = 32.55 C
 FILM TEMPERATURE = 30.38 C

BAROMETRIC PRESSURE = 27.46 "Hg
 AIRSTREAM: RELATIVE HUMIDITY = 0.64
 THERMAL CONDUCTIVITY = 0.02543 W/m-C
 LIQUID WATER CONTENT = 0.6 g/m**3
 MEDIAN DROP DIAMETER = 49.3 microns

CYLINDER DIAMETER = 0.05997 m
 THERMAL CONDUCTIVITY OF EPOXY = 1.13440 W/m-C
 HEATER WIDTH = 3.175 mm
 LENGTH = 0.1524 m
 DEPTH = 0.203 mm
 GAP WIDTH AT SURFACE = 2.058 mm

ANGLE (DEGREES)	HEATER POWER (mW)	GAP HEAT LOSS (mW)	H (W/m**2-C)	NUSSELT NUMBER
0.0	3757.53	727.61	1439.51	3394.74
10.0	3908.57	743.65	1503.64	3546.00
20.0	3428.57	691.12	1300.55	3067.05
30.0	2380.95	556.79	866.65	2043.80
40.0	1388.84	388.82	475.11	1120.43
50.0	787.20	252.04	254.25	599.60
60.0	604.20	202.35	190.92	450.23
70.0	427.53	149.81	131.94	311.16
80.0	330.37	118.76	100.54	237.09
90.0	341.93	122.54	104.23	245.81

 TEST # 19

REYNOLDS NUMBER = 80000.0
 AIR VELOCITY = 23.2 m/s
 TEST CONDITIONS : WATER SPRAY COOLING

AMBIENT AIR TEMPERATURE = 25.80 C
 HEATER (SURFACE) TEMPERATURE = 32.55 C
 FILM TEMPERATURE = 29.18 C

BAROMETRIC PRESSURE = 28.10 "Hg
 AIRSTREAM: RELATIVE HUMIDITY = ---
 THERMAL CONDUCTIVITY = 0.02539 W/m-C
 LIQUID WATER CONTENT = 0.1 g/m**3
 MEDIAN DROP DIAMETER = 34.5 microns

CYLINDER DIAMETER = 0.05997 m
 THERMAL CONDUCTIVITY OF EPOXY = 1.13440 W/m-C
 HEATER WIDTH = 3.175 mm
 LENGTH = 0.1524 m
 DEPTH = 0.203 mm
 GAP WIDTH AT SURFACE = 2.058 mm

ANGLE (DEGREES)	HEATER POWER (mW)	GAP HEAT LOSS (mW)	H (W/m**2-C)	NUSSELT NUMBER
0.0	2148.81	602.08	473.57	1118.47
10.0	2380.95	647.25	530.81	1253.67
20.0	2092.63	590.75	459.84	1086.04
30.0	1645.18	494.33	352.36	832.21
40.0	1125.37	365.77	232.57	549.29
50.0	733.39	254.00	146.78	346.66
60.0	528.75	189.56	103.85	245.28
70.0	402.68	147.52	78.12	184.51
80.0	214.29	81.13	40.77	96.28
90.0	281.66	105.38	53.97	127.46

APPENDIX D

FINITE DIFFERENCE ANALYSIS OF THE HEAT CONDUCTION IN A TYPICAL CYLINDER SECTOR

This study assumes that the steady state heat conduction from the bottom of each heater is negligible compared with the heat loss from the sides of the heaters. In order to verify this assumption, a finite difference model of a typical 5 degree sector of the cylinder is represented here.

D.1 Cylinder Geometry

The test cylinder used for this study consists of a 59.97 mm diameter expanded polystyrene foam cylinder with a 31.75 mm plexiglass tube core. The plexiglass tube was filled with expanded polyurethane foam. The 3.2 mm wall thickness of the plexiglass tube was neglected in this numerical analysis and the thermal conductivities of both types of foam are approximately equal at the mean test temperature.

Nine nichrome strip heaters (each 3.175 mm wide) were mounted on the surface from 0° to 90° from the stagnation line. This results in nine gaps between the heaters at the surface. The gaps were filled with an epoxy having a thermal conductivity of 1.1344 W/m·°C. The calculated gap width at the surface is:

$$\frac{\pi(59.97)/4 - 9(3.175)}{9.0} = 2.058 \text{ mm}$$

Therefore the semi-gap width utilized in this analysis is 1.029 mm.

Due to symmetry, the finite difference model incorporates half the width of one heater and half the gap adjacent to the heater, as shown in Figure D.1.

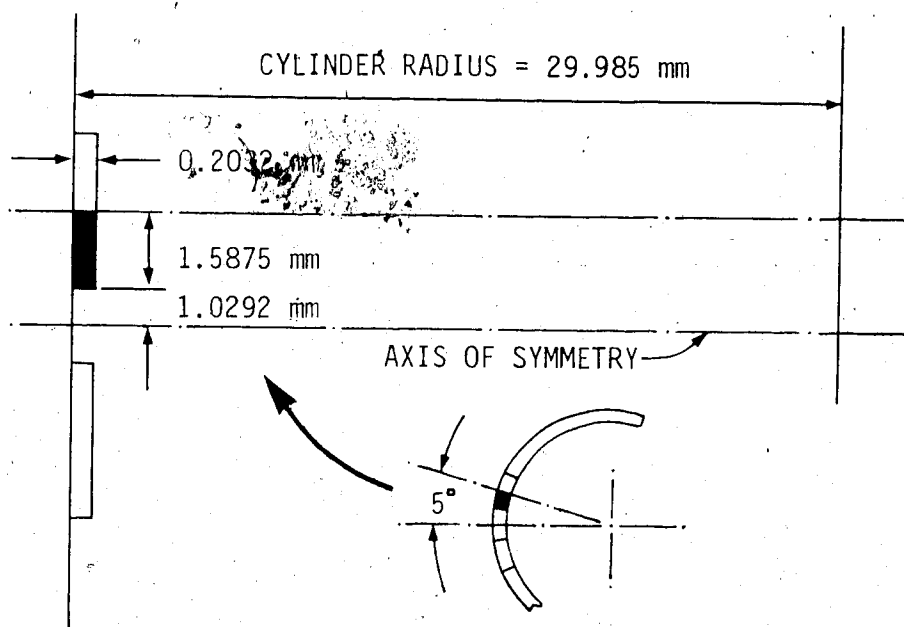


Figure D.1 Geometry of the finite difference model.

The cylinder sector is approximated by a rectangular grid with a constant temperature corner and a convective boundary condition at the surface. A constant temperature boundary condition (ambient temperature) is assumed for

the side of the grid associated with the cylinder center.

D.2 Finite Difference Equations

The temperature field is divided into a rectangular grid with increments in the radial (x) and circumferential (y) directions (see Figure D.2). For this analysis $\Delta x = \Delta y$.

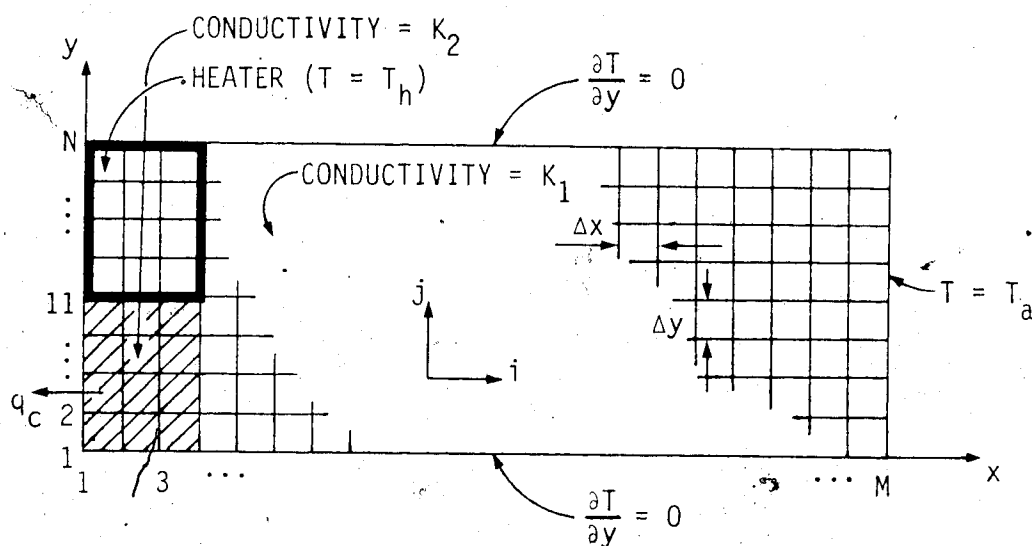


Figure D.2 Nodal numbering scheme for the finite difference grid.

The coordinates i and j are used to locate grid points in the x and y directions respectively. The material in the region $i = 1, 2, 3$ and $j = 1, 2, \dots, 10$ is epoxy with a thermal conductivity specified as K_1 and the remainder of the grid corresponds to foam with a thermal conductivity specified as K_2 . The following finite difference

equations, derived in detail by Holman (1976, P.75-76), are used in this analysis:

i) interior nodes ($i=2$ or $i>4$):

$$T_{i,j} = \frac{T_{i,j+1} + T_{i-1,j} + T_{i,j+1} + T_{i,j-1}}{4.0} \quad (D.1)$$

ii) convective boundary ($i=1$):

$$T_{i,j} = \frac{(T_{i,j+1} + T_{i,j-1}) + 2(T_{i+1,j} + hT_a\Delta y/K_1)}{4 + 2h\Delta y/K_1} \quad (D.2)$$

iii) insulated boundary:

$$(j = 1): T_{i,j} = \frac{T_{i-1,j} + T_{i+1,j} + 2T_{i,j+1}}{4.0} \quad (D.3)$$

$$(j = N): T_{i,j} = \frac{T_{i-1,j} + T_{i+1,j} + 2T_{i,j-1}}{4.0} \quad (D.4)$$

Three nodal equations remain to be defined for this numerical analysis:

iv) Node (1,1):

Node (1,1) represents a corner with a convective boundary and an insulated boundary (see Figure D.3). Under steady state conditions, the net heat flow per unit area into any node from its surrounding nodes is zero. The energy

balance for node (i,j) in Figure D.3 is:

$$\frac{K_1}{2\Delta x}(T_{i+1,j} - T_{i,j}) + \frac{K_2}{2\Delta y}(T_{i,j+1} - T_{i,j}) + h(T_a - T_{i,j}) = 0$$

Solving for $T_{i,j}$ with $\Delta x = \Delta y$:

$$T_{i,j} = \frac{T_{i+1,j} + T_{i,j+1} + hT_a\Delta x/K_1}{2 + h\Delta x/K_1} \quad (D.5)$$

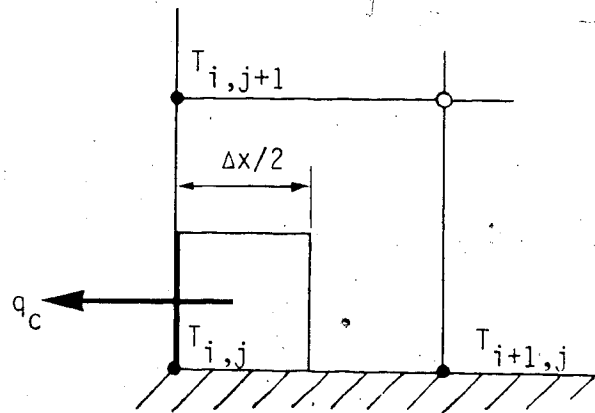


Figure D.3 Corner node with a convective boundary and an insulated boundary.

v) Interface boundary ($i=3$):

The boundary $i=3$ separates two regions with different thermal conductivities; therefore, nodes along this interface require a unique finite difference equation. The heat flux along this boundary consists of two

components. One component is based on the thermal conductivity of epoxy (K_1), and the other component is based on the conductivity of foam (K_2) (see Figure D.4).

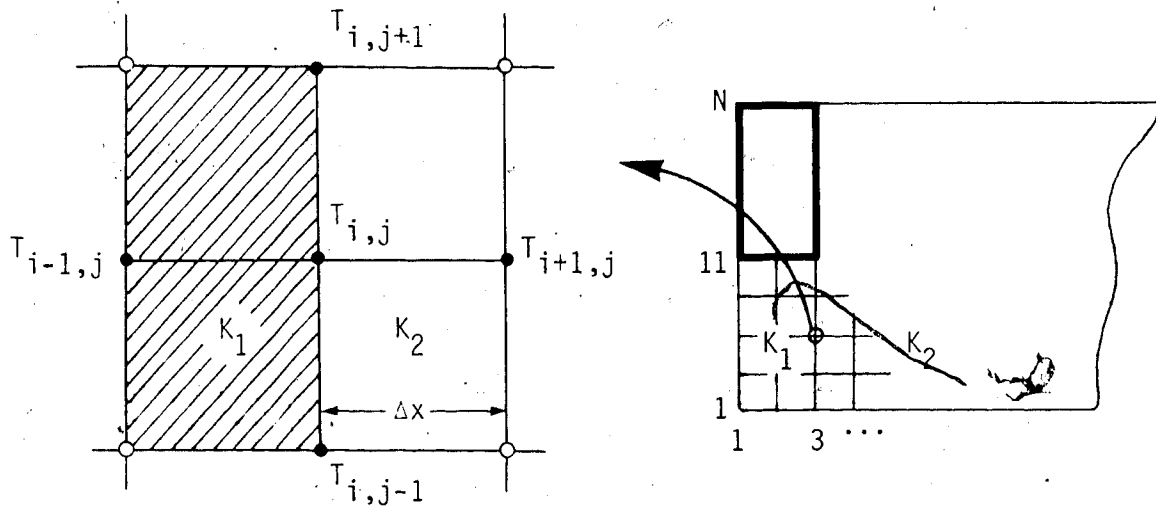


Figure D.4 Node on a boundary separating regions with different thermal conductivities.

The energy balance for node (i, j) in Figure D.4 is:

$$\begin{aligned} & \frac{K_1}{\Delta x}(T_{i-1,j} - T_{i,j}) + \frac{K_2}{\Delta x}(T_{i+1,j} - T_{i,j}) + \frac{K_1}{2\Delta y}(T_{i,j+1} - T_{i,j}) \\ & + \frac{K_2}{2\Delta y}(T_{i,j+1} - T_{i,j}) + \frac{K_1}{2\Delta y}(T_{i,j-1} - T_{i,j}) + \\ & \frac{K_2}{2\Delta y}(T_{i,j-1} - T_{i,j}) = 0 \end{aligned}$$

Solving for $T_{i,j}$ with $\Delta x = \Delta y$,

$$T_{i,j} = \frac{K_1(2T_{i-1,j} + T_{i,j+1} + T_{i,j-1})}{4(K_1 + K_2)} + \frac{K_2(2T_{i+1,j} + T_{i,j+1} + T_{i,j-1})}{4(K_1 + K_2)} \quad (D.6)$$

vi) Node (3,1):

Node (3,1) represents a node bounded on one side by an insulated boundary and located on the interface between two regions with different thermal conductivities (see Figure D.5).

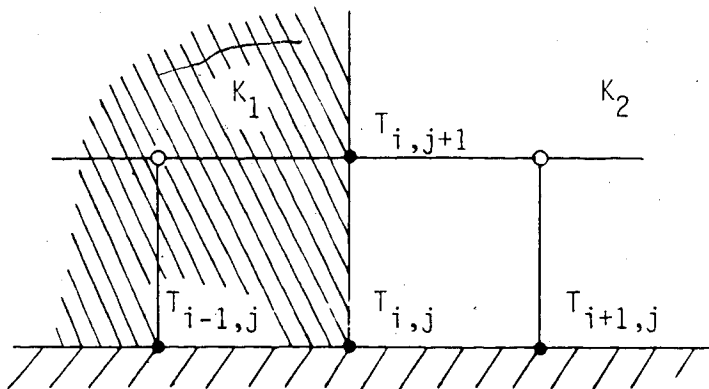


Figure D.5 Node intersecting an insulated boundary and two regions with different thermal conductivities.

The energy balance for node (i,j) in Figure D.5 is:

$$\begin{aligned} \frac{K_1}{2\Delta x}(T_{i-1,j} - T_{i,j}) + \frac{K_1}{2\Delta y}(T_{i,j+1} - T_{i,j}) + \\ \frac{K_2}{2\Delta y}(T_{i,j+1} - T_{i,j}) + \frac{K_2}{2\Delta x}(T_{i+1,j} - T_{i,j}) = 0 \end{aligned}$$

Solving for $T_{i,j}$ with $\Delta x = \Delta y$,

$$T_{i,j} = \frac{K_1(T_{i-1,j} + T_{i,j+1}) + K_2(T_{i,j+1} + T_{i+1,j})}{2(K_1 + K_2)} \quad (D.7)$$

The temperature distribution in the grid was solved numerically using the following constants and sample boundary conditions:

$$\begin{aligned} T_a &= 23.8^\circ\text{C} \\ \Delta x &= \Delta y = 0.016 \text{ mm} \\ T_h &= 38.0^\circ\text{C} \\ h &= 132.62 \text{ W/m}^2\cdot^\circ\text{C} \\ K_1 &= 1.1344 \text{ W/m}\cdot^\circ\text{C} \\ K_2 &= 0.026 \text{ W/m}\cdot^\circ\text{C} \end{aligned}$$

A coarse grid of 296 x 27 nodes was utilized initially to solve for the temperature distribution. The FORTRAN computer program entitled COND detailing the algorithm is included in Appendix A. Gauss-Seidel iteration with relaxation was used to solve for the nodal temperatures with a specified tolerance of 0.0005°C.

In order to obtain a more accurate numerical solution in the vicinity of the heater, this procedure was repeated using a smaller grid spacing. The output from

the coarse grid solution was used as the initial guess for the fine grid solution. The fine grid algorithm is detailed in the FORTRAN program called COND.B included in Appendix A.

The area of the coarse grid represented by nodes $i=1$ to 160 and $j=1$ to 27 was analyzed in detail using a fine grid of 319 x 53 nodes (see Figure D.6). Each node along column $i=160$ of the coarse grid solution had a steady state temperature of 23.878°C. This value was used for the right hand boundary condition for the fine grid analysis. The grid spacing utilized for the fine grid was $\Delta x = \Delta y = 0.0508$ mm. The results of this finite difference analysis are shown as a contour plot in Figure D.8.

D.3 Heat Flux Calculations

Using the nodal temperature distribution obtained from the finite difference analysis, the following heat transfer data was calculated:

a) Surface heat flux between heaters.

The heat loss due to convection in the gap between the heaters was calculated using the temperatures of the surface nodes, $i=1$. The convective boundary condition defined in the finite difference analysis includes convective heat transfer to the air from nodes $j=1$ to 20 inclusive (see Figure D.7).

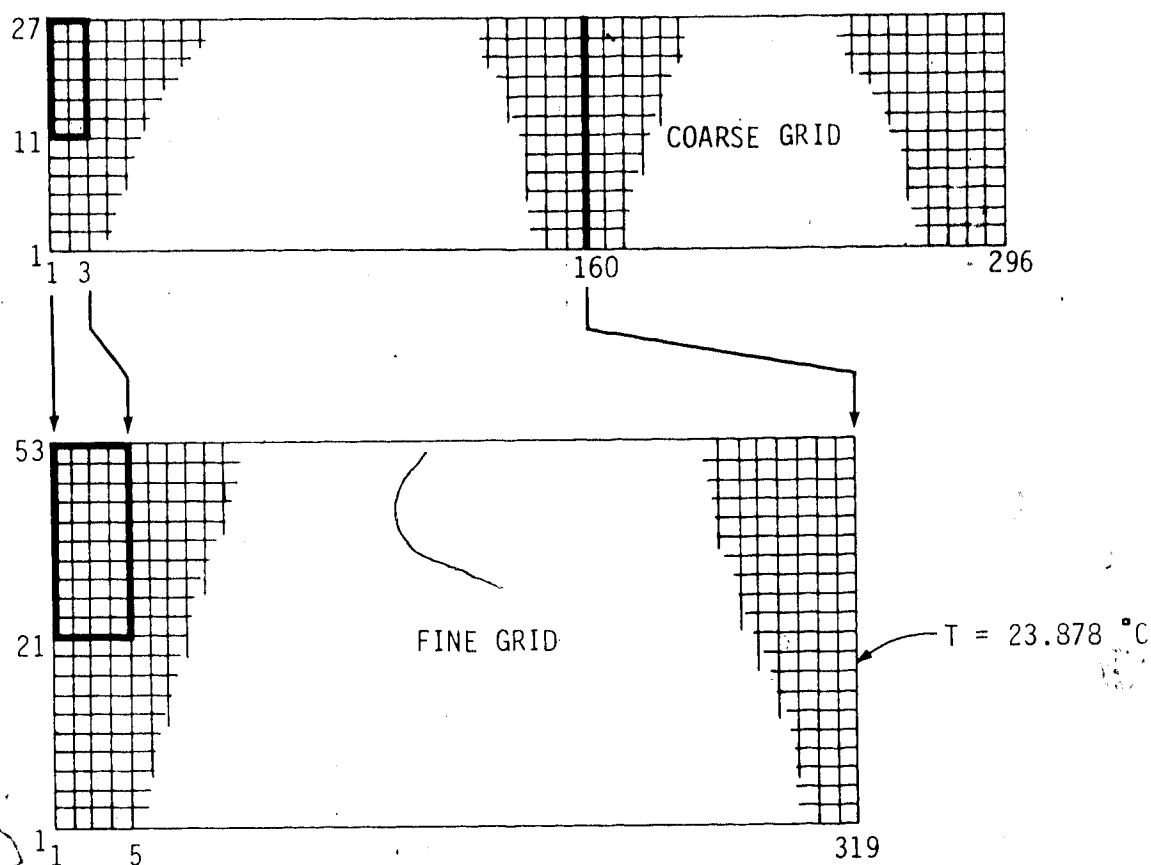


Figure D.6 Nodal numbering scheme used with smaller grid increments.

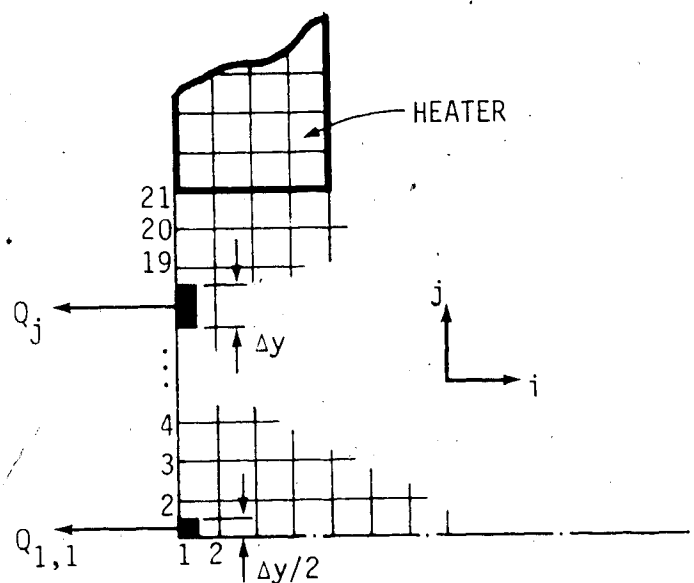


Figure D.7 Nodes on the convective boundary.

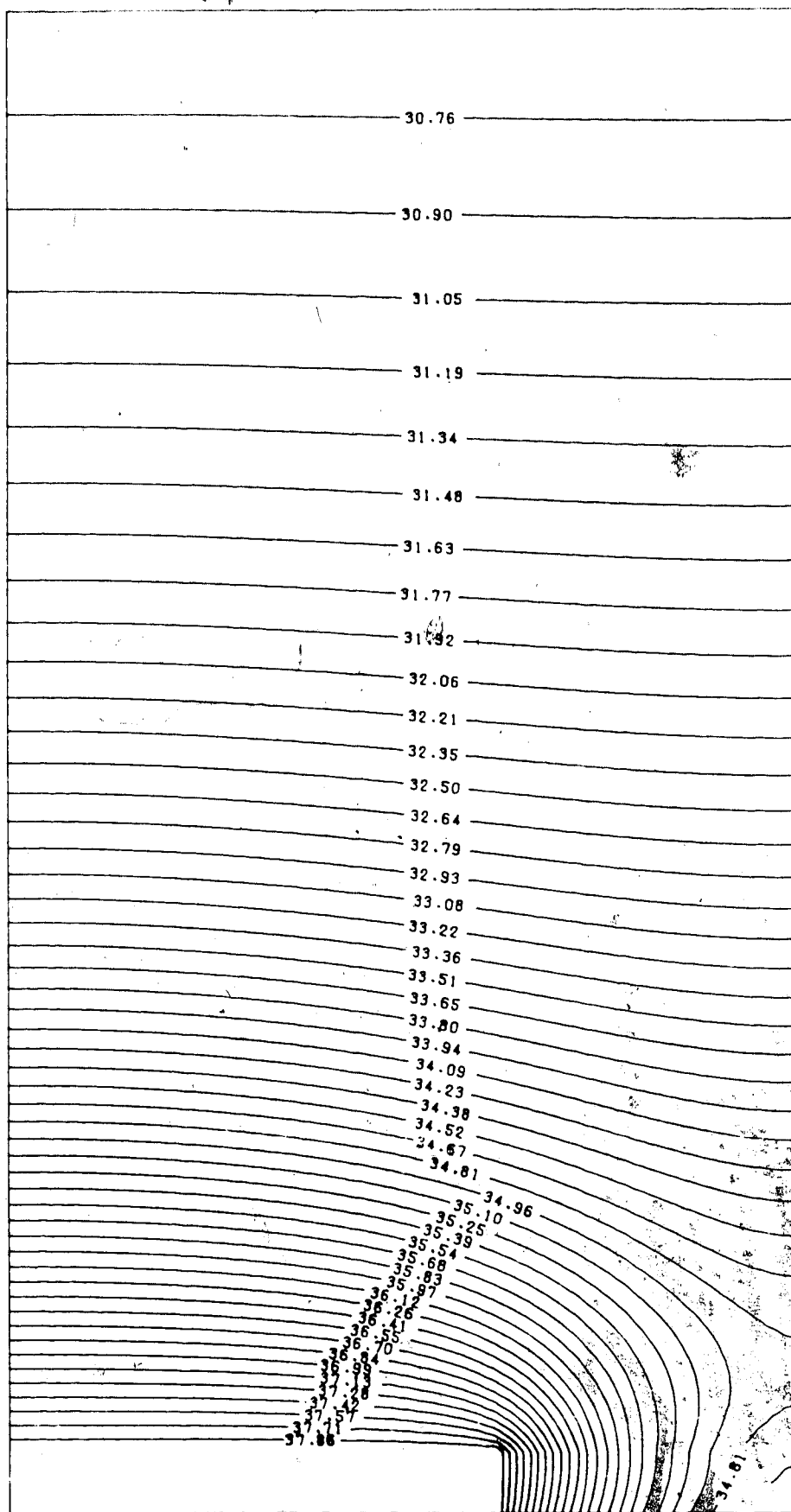


Figure D.8 Contour plot solution of the finite difference analysis showing the temperature distribution in a typical cylinder sector.

For any node $(1,j)$, $j=2,3,\dots,20$.

$$Q_j = h(L\Delta y)(T_{1,j} - T_a)$$

where L = length of the gap between heaters.

The corner node $(1,1)$ includes only half the heat flux area:

$$Q_{1,1} = hL\frac{\Delta y}{2}(T_{1,1} - T_a)$$

Recall that the finite difference analysis only models half the width of one heater and half of the gap adjacent to the heater. All the heat losses calculated are multiplied by 2.0 to represent the losses associated with one entire heater width and the entire gap width between heaters. The total convective heat loss in the entire gap between adjacent heaters is:

$$Q_s = 2hL\Delta y \left[\sum_{j=2}^{20} (T_{1,j} - T_a) + 0.5(T_{1,1} - T_a) \right] \quad (D.8)$$

where Q : [W] h : [$W/m^2 \cdot ^\circ C$] T : [$^\circ C$]
 y : [m] L : [m]

b) Heat loss from the bottom and side of the heater.

As indicated in Figure D.9, the total heat loss from the interior side of the heater is:

$$Q_I = 2K_2L \left\{ \sum_{22}^{52} (T_h - T_{6,j}) + 0.5(T_h - T_{6,21}) + 0.5(T_h - T_{6,53}) \right\} \quad (D.9)$$

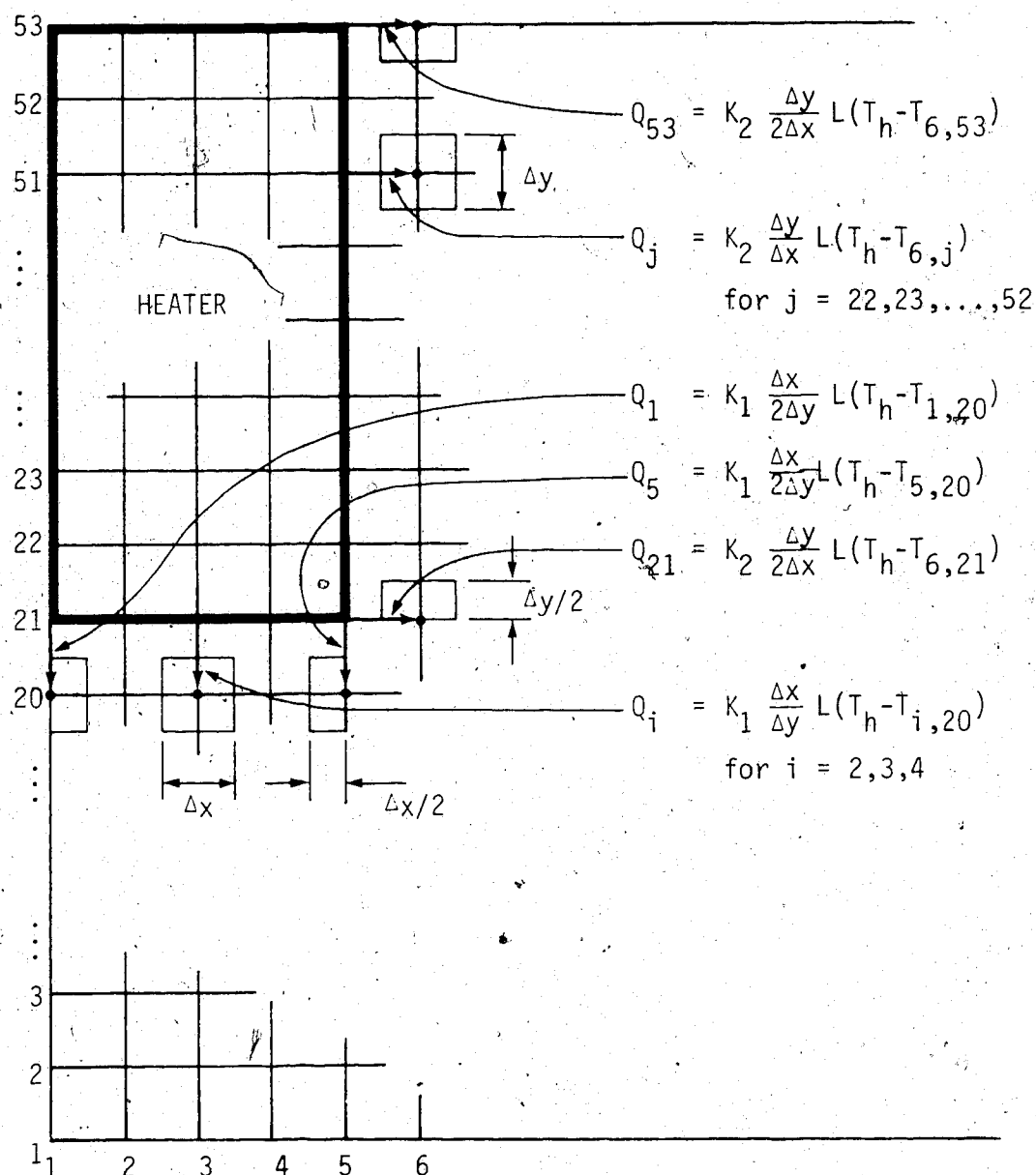


Figure D.9 Equations used in the numerical solution to calculate the heat loss from the side and bottom of the nichrome strip heater.

The total heat loss from both sides of the heater is:

$$Q_J = 2K_1L \left\{ \sum_{i=2}^4 (T_h - T_{i,20}) + 0.5(T_h - T_{1,20}) + 0.5(T_h - T_{5,20}) \right\} \quad (D.10)$$

where Q : [W] T : [°C]
 K_1 : [W/m·°C] K_2 : [W/m·°C]
 L : [m]

A FORTRAN program entitled HEATFLUX (see Appendix A) was written to calculate the heat losses around a typical heater using equations (D.8), (D.9), and (D.10). The output from this program including the constants used in this analysis are presented in Table D.1.

Table D.1 Finite difference solution. Summary of the steady state heat losses from a typical nichrome strip heater.

Finite Difference Solution	
Convective heat transfer coefficient = 132.62 W/m ² ·°C	
Ambient temperature = 23.8°C	
Heater temperature = 38.0°C	
Gap thermal conductivity (epoxy) = 1.134 W/m·°C	
Cylinder thermal conductivity (foam) = 0.026 W/m·°C	
Heat Loss Summary	
A. Heat loss from the surface of the gap	= 471.7 mW
B. Heat loss from the bottom of heater	= 47.6 mW
C. Loss from both sides of the heater	= 481.1 mW
D. Total (B+C)	= 528.7 mW
E. Loss to the interior of the cylinder	= 48.3 mW
F. Loss from the surface of the heater	= 911.2 mW
Gap loss represents 51.76% of the heater's surface loss.	

APPENDIX

STEADY STATE CONDUCTION HEAT LOSS IN THE GAP BETWEEN HEATERS. (ANALYTICAL SOLUTION)

The steady state conduction heat loss from the edge of the strip heaters can be estimated by solving the Laplace equation for two dimensional heat flow in the region between the heaters.

Due to symmetry, consider half the gap contained between two heaters as shown in Figure E.1.

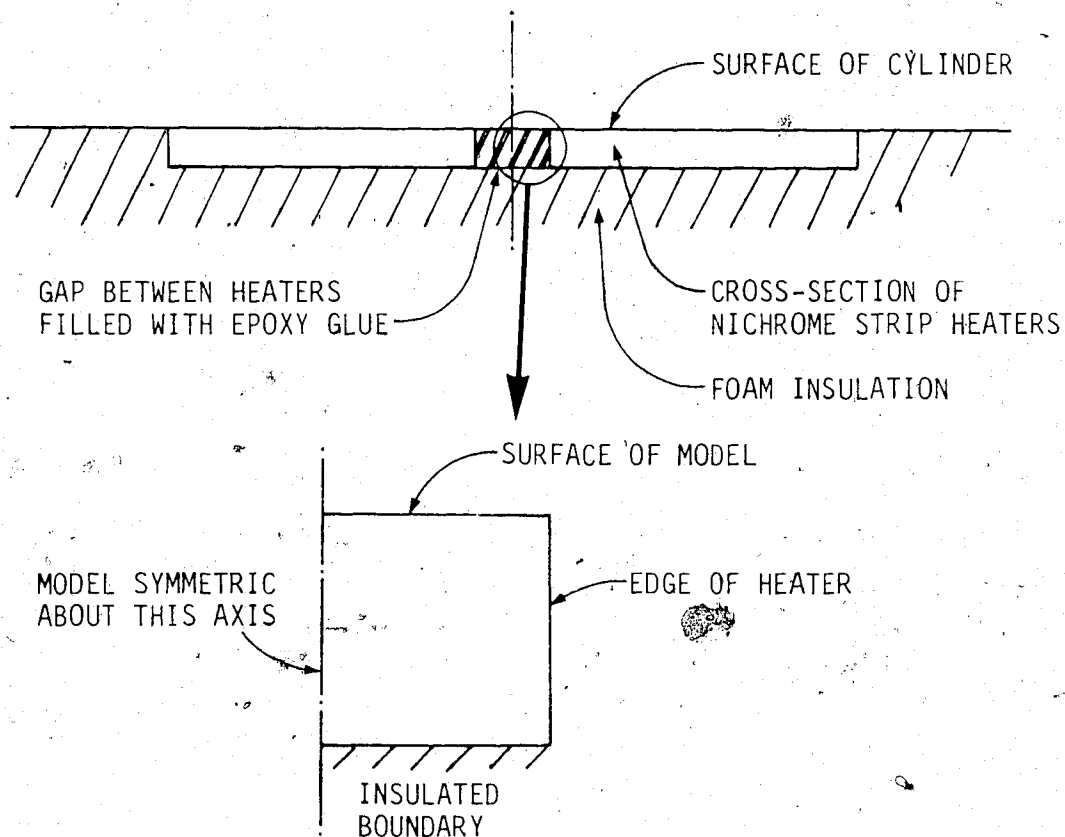


Figure E.1 Geometry for the analytical model.

The method of separation of variables was used to solve the Laplace equation for two-dimensional heat conduction subject to the boundary conditions shown in Figure E.2.

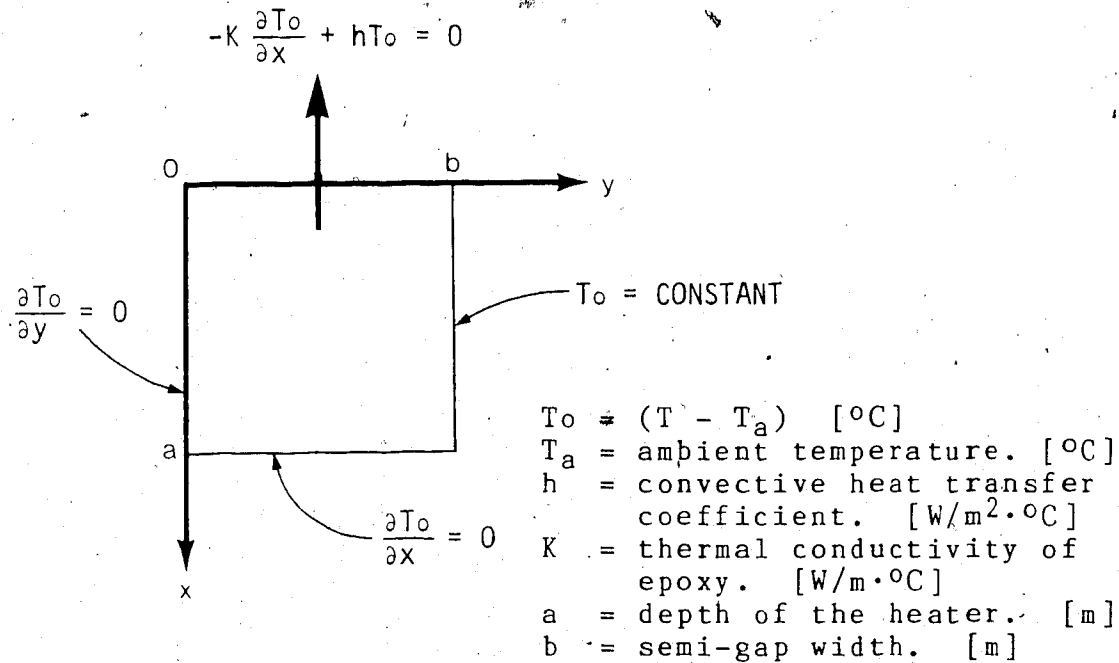


Figure E.2 Boundary conditions for the analytical model.

The Laplace equation for this problem is:

$$\frac{\partial^2 T_o}{\partial x^2} + \frac{\partial^2 T_o}{\partial y^2} = 0 \quad (\text{E.1})$$

To solve equation (E.1), the solution is assumed to take the form:

$$T_o(x, y) = X(x)Y(y)$$

$$\frac{\partial^2 T_o}{\partial x^2} = X''Y \quad \text{and} \quad \frac{\partial^2 T_o}{\partial y^2} = XY''$$

from Equation E.1 $X''Y + XY'' = 0$

or

$$\frac{1}{X} \frac{\partial^2 X}{\partial x^2} = - \frac{1}{Y} \frac{\partial^2 Y}{\partial y^2} = -\lambda^2$$

$$\frac{\partial^2 X}{\partial x^2} + \lambda^2 X = 0 \quad (E.2)$$

$$\frac{\partial^2 Y}{\partial y^2} - \lambda^2 Y = 0 \quad (E.3)$$

from Equation E.2 $X = C_1 \cos \lambda x + C_2 \sin \lambda x$

from Equation E.3 $Y = C_3 e^{-\lambda y} + C_4 e^{\lambda y}$

therefore $T_o(x,y) = (C_1 \cos \lambda x + C_2 \sin \lambda x)(C_3 e^{-\lambda y} + C_4 e^{\lambda y}) \quad (E.4)$

Boundary Conditions:

i) at $y=0$, $\frac{\partial T_o}{\partial y} = 0$

using Equation E.4 $(C_1 \cos \lambda x + C_2 \sin \lambda x)(\lambda C_4 - \lambda C_3) = 0$

therefore $C_3 = C_4$

and $T_o(x,y) = (C_1 \cos \lambda x + C_2 \sin \lambda x)C_3 \cosh \lambda y$

ii) at $x=a$, $\frac{\partial T_o}{\partial x} = 0$

using Equation E.4 $(C_2 \lambda \cos \lambda a - C_1 \lambda \sin \lambda a) C_3 \cosh \lambda y = 0$

$$C_2 = C_1 \frac{\sin \lambda a}{\cos \lambda a} = C_1 \tan \lambda a$$

therefore $T_o(x,y) = (C_1 \cos \lambda x + C_1 \tan \lambda a \sin \lambda x) C_3 \cosh \lambda y$

or $T_o(x,y) = C(\cos \lambda x + \tan \lambda a \sin \lambda x) \cosh \lambda y$ (E.5)

iii) at $x=0$, $-K \frac{\partial T_o}{\partial x} + h T_o = 0$

using Equation E.5 $-K(C \lambda \tan \lambda a \cosh \lambda y) + h C \cosh \lambda y = 0$

or $K \lambda \tan \lambda a = h$

Eigenvalues λ_n are the positive roots of $\lambda_n \tan \lambda_n a = \frac{h}{K}$

therefore $T_o(x,y) = \sum_{n=1}^{\infty} C_n (\cos \lambda_n x + \tan \lambda_n a \sin \lambda_n x) \cosh \lambda_n y$

iv) at $y=b$, $T_o = (T_h - T_a)$

$$T_h - T_a = \sum_{n=1}^{\infty} C_n (\cos \lambda_n x + \tan \lambda_n a \sin \lambda_n x) \cosh \lambda_n b$$

$$= \sum_{n=1}^{\infty} C_n (\cos \lambda_n a \cos \lambda_n x + \sin \lambda_n a \sin \lambda_n x) \frac{\cosh \lambda_n b}{\cos \lambda_n a}$$

or $T_h - T_a = \sum_{n=1}^{\infty} C_n \cos \lambda_n (a-x) \frac{\cosh \lambda_n b}{\cos \lambda_n a}$ (E.6)

multiply both sides of Equation E.6 by $\cos \lambda_m(a-x)$ and integrate both sides of the equation from $x=0$ to $x=a$:

$$(T_h - T_a) \int_0^a \cos \lambda_m(a-x) dx = \sum_{n=1}^{\infty} C_n \frac{\cosh \lambda_n b}{\cos \lambda_n a} \int_0^a \cos \lambda_n(a-x) \cos \lambda_m(a-x) dx$$

if $\lambda_m \neq \lambda_n$ the right hand integral is equal to zero.

if $\lambda_m = \lambda_n$ the right hand integral becomes:

$$\begin{aligned} \int_0^a \cos^2 \lambda_n(a-x) dx &= \frac{1}{2} \int_0^a \{1 + \cos 2\lambda_n(a-x)\} dx \\ &= \frac{1}{2} \left(x + \frac{\sin 2\lambda_n(a-x)}{-2\lambda_n} \right) \Big|_0^a \\ &= \frac{a}{2} + \frac{\sin 2\lambda_n a}{4\lambda_n} \end{aligned}$$

therefore:

$$-(T_h - T_a) \frac{\sin \lambda_n(a-x)}{\lambda_n} \Big|_0^a = C_n \frac{\cosh \lambda_n b}{\cos \lambda_n a} \left(\frac{a}{2} + \frac{\sin 2\lambda_n a}{4\lambda_n} \right) \quad (E.7)$$

but

$$\begin{aligned} \frac{\sin 2\lambda_n a}{4\lambda_n} &= \frac{2\sin \lambda_n a \cos \lambda_n a}{4\lambda_n} \\ &= \frac{\sin \lambda_n a \cos \lambda_n a}{2\lambda_n (\cos^2 \lambda_n a + \sin^2 \lambda_n a)} \\ &= \frac{1}{2\lambda_n} \left(\frac{\cos \lambda_n a}{\sin \lambda_n a} + \frac{\sin \lambda_n a}{\cos \lambda_n a} \right)^{-1} \\ &= \frac{1}{2\lambda_n} \left(\frac{1}{\tan \lambda_n a} + \tan \lambda_n a \right)^{-1} \\ &= \frac{\tan \lambda_n a}{2\lambda_n (1 + \tan^2 \lambda_n a)} \end{aligned}$$

or

$$\frac{\sin 2\lambda_n a}{4\lambda_n} = \frac{\lambda_n \tan \lambda_n a}{2\lambda_n^2 (1 + \tan^2 \lambda_n a)}$$

$$= \frac{\lambda_n \tan \lambda_n a}{2(\lambda_n^2 + \lambda_n^2 \tan^2 \lambda_n a)}$$

but

$$\lambda_n \tan \lambda_n a = \frac{h}{K}$$

therefore

$$\frac{\sin 2\lambda_n a}{4\lambda_n} = \frac{h/K}{2\{\lambda_n^2 + (h/K)^2\}}$$

Equation E.7 becomes:

$$(T_h - T_a) \frac{\sin \lambda_n a}{\lambda_n} = C_n \frac{\cosh \lambda_n b}{\cosh \lambda_n a} \left(\frac{a}{2} + \frac{h/K}{2\{\lambda_n^2 + (h/K)^2\}} \right)$$

therefore

$$C_n = (T_h - T_a) \frac{\sin \lambda_n a \cosh \lambda_n a}{\lambda_n \cosh \lambda_n b} \left(\frac{2\{\lambda_n^2 + (h/K)^2\}}{a\{\lambda_n^2 + (h/K)^2\} + h/K} \right)$$

substituting for C_n the expression for T_o becomes:

$$T_o(x,y) = (T_h - T_a) \sum_{n=1}^{\infty} \frac{2 \sin \lambda_n a \cosh \lambda_n a}{\lambda_n \cosh \lambda_n b} \left(\frac{\lambda_n^2 + (h/K)^2}{\{\lambda_n^2 + (h/K)^2\}a + h/K} \right) (\cos \lambda_n x +$$

$$+ \tan \lambda_n a \sin \lambda_n x) \cosh \lambda_n y$$

but

$$\frac{2 \sin \lambda_n a \cosh \lambda_n a}{\lambda_n} = 4 \left(\frac{\sin 2\lambda_n a}{4\lambda_n} \right)$$

$$= 4 \left(\frac{h/K}{2\{\lambda_n^2 + (h/K)^2\}} \right)$$

$$= 2 \left(\frac{h/K}{\lambda_n^2 + (h/K)^2} \right)$$

therefore:

$$\begin{aligned} T_o(x,y) &= 2 \frac{h}{K} (T_h - T_a) \sum_{n=1}^{\infty} \frac{(\cos \lambda_n x + \tan \lambda_n a \sin \lambda_n x) \cosh \lambda_n y}{\cosh \lambda_n b \left[\{\lambda_n^2 + (h/K)^2\} a + h/K \right]} \\ &= 2 \frac{h}{K} (T_h - T_a) \sum_{n=1}^{\infty} \frac{(\cos \lambda_n x \cos \lambda_n a + \sin \lambda_n a \sin \lambda_n x) \cosh \lambda_n y}{\cos \lambda_n a \cosh \lambda_n b \left[\{\lambda_n^2 + (h/K)^2\} a + h/K \right]} \end{aligned}$$

or:

$$T_o(x,y) = 2 \frac{h}{K} (T_h - T_a) \sum_{n=1}^{\infty} \frac{\cos \lambda_n (a-x) \cosh \lambda_n y}{\left[\{\lambda_n^2 + (h/K)^2\} a + h/K \right] \cos \lambda_n a \cosh \lambda_n b} \quad (E.8)$$

Surface heat flux

To evaluate the heat flux at the surface, the temperature gradient at $x = 0$ is evaluated using Equation E.8:

$$Q_s = -KA \left. \frac{\partial T_o}{\partial x} \right|_{x=0} \quad (E.9)$$

The total heat flux area through two semi-gaps (both sides of the heater) is:

$$A = 2bL$$

where b = semi-gap width. [m]

L = length of the gap between heaters. [m]

Therefore Equation (E.9) can be rewritten as:

$$Q = -2KL \int_0^b \left. \frac{\partial T_o}{\partial x} \right|_{x=0} dy \quad (E.10)$$

substituting Equation E.8 into Equation E.10

$$Q = -2KL \int_0^b \left(2 \frac{h}{K} (T_h - T_a) \sum_{n=1}^{\infty} \frac{-\sin(\lambda_n a) \lambda_n \cosh(\lambda_n y)}{[\{\lambda_n^2 + (h/K)^2\}a + h/K] \cos \lambda_n a \cosh \lambda_n b} \right) dy$$

$$= 4KL(T_h - T_a) \sum_{n=1}^{\infty} \frac{\tan \lambda_n a \lambda_n \sinh \lambda_n y}{[\{\lambda_n^2 + (h/K)^2\}a + h/K] \cosh(\lambda_n b) \lambda_n} \bigg|_{y=0}^b$$

or

$$Q = 4Lh(T_h - T_a) \sum_{n=1}^{\infty} \frac{\tan \lambda_n a \tanh \lambda_n b}{\{\lambda_n^2 + (h/K)^2\}a + h/K} \quad (E.11)$$

APPENDIX F

DERIVATION OF THE HEAT TRANSFER DUE TO EVAPORATION OF WATER VAPOUR FROM THE CYLINDER SURFACE

The total heat transfer per unit area due to evaporation of water vapour can be expressed as:

$$Q_e = \frac{\dot{m}_e l_v}{A} \quad (F.1)$$

where \dot{m}_e = evaporative mass flux per unit time. [kg/s]
 l_v = latent heat of vaporization. [J/kg]
 Q_e = heat transfer per unit area. [W/m²]
 A = mass flux area. [m²]

Holman (1976, P.433) shows that the mass flux can be expressed in terms of the mass-transfer coefficient (h_D) defined as:

$$\dot{m}_e = h_D A (\rho_{vs} - \rho_{va}) \quad (F.2)$$

where ρ_{vs} = water vapour density at the cylinder surface temperature. [kg/m³]
 ρ_{va} = water vapour density at ambient air temperature. [kg/m³]

If water vapour is assumed to behave as an ideal gas,

$$\rho_v = \frac{p_v}{R_v T} \quad (F.3)$$

where ρ_v = water vapour density. $[\text{kg}/\text{m}^3]$
 p_v = partial pressure of water vapour. $[\text{Pa}]$
 R_v = specific gas constant for water vapour.
 $[\text{J}/\text{kg}\cdot\text{K}]$
 T = temperature. $[\text{K}]$

Similarly for dry air,

$$\rho_d = \frac{p_d}{R_d T} \quad (\text{F.4})$$

where p_d = partial pressure of dry air. $[\text{Pa}]$
 R_d = specific gas constant for dry air. $[\text{J}/\text{kg}\cdot\text{K}]$
 ρ_d = density of dry air. $[\text{kg}/\text{m}^3]$

Combining Equations F.3 and F.4 gives:

$$\frac{\rho_v}{\rho_d} = \frac{p_v R_d}{p_d R_v} \quad (\text{F.5})$$

Using Dalton's law of partial pressures, the static air pressure (P) can be expressed in terms of the partial pressure of dry air and the partial pressure of water vapour. Therefore:

$$p_d = P_{\text{stat}} - p_v \quad (\text{F.6})$$

Substituting Equation F.6 into Equation F.5 gives:

$$\frac{\rho_v}{\rho_d} = \frac{p_v \epsilon}{(P_{\text{stat}} - p_v)} \quad \text{where } \epsilon = \frac{R_d}{R_v}$$

or

$$p_v \approx \rho_d \epsilon \frac{p_v}{p_{stat}} \quad (F.7)$$

Substituting Equations F.7 and F.2 into Equation F.1 gives:.

$$Q_e = h_D \rho_d \epsilon \frac{l_v}{p_{stat}} (p_{vs} - p_{va}) \quad (F.8)$$

where p_{vs} = partial pressure of water vapour at the cylinder surface. [Pa]
 p_{va} = partial pressure of water vapour at ambient air temperature. [Pa]

Recall that the relative humidity (RH) is defined as:

$$RH = \frac{p_v}{e} \quad (F.9)$$

Assuming that the relative humidity of the air at the cylinder surface is approximately equal to 1.0, Equation F.8 can be rewritten using Equation F.9 as:

$$Q_e = h_D \rho_d \epsilon \frac{l_v}{p_{stat}} [e_s - (RH)e_a] \quad (F.10)$$

where e_a , e_s = saturation vapour pressure of water vapour at ambient air temperature and the cylinder surface temperature respectively, [Pa]

Holman (1976, P.435) has shown that by using Reynolds

analogy, the mass-transfer coefficient can be expressed in terms of the friction factor (f) as follows:

$$\left(\frac{h_D}{u_m} \right) Sc^{2/3} = \frac{f}{8} \quad (F.11)$$

Similarly for heat transfer problems, the heat transfer coefficient can also be expressed in terms of the friction factor as:

$$\left(\frac{h}{u_m C_{pa} \rho_d} \right) Pr^{2/3} = \frac{f}{8} \quad (F.12)$$

Eliminating "f" from Equations F.11 and F.12 gives;

$$\frac{h}{h_D} = \rho_d C_{pa} \left(\frac{Sc}{Pr} \right)^{2/3} \quad (F.13)$$

where C_{pa} = specific heat capacity of moist air at constant pressure. [J/kg.K]
 Sc = Schmidt number for water vapour in air.
 Pr = Prandtl number for air.
 h = local convective heat transfer coefficient. [W/m².°C]

Eliminating h_D from Equation F.10 using Equation F.13 gives the final expression for the heat transfer per unit area due to evaporation:

$$Q_e = h \left(\frac{Pr}{Sc} \right)^{2/3} \frac{1_v \epsilon}{C_{pa} P_{stat}} [e_s - (RH)e_a] \quad (F.14)$$

The following constants are required to evaluate Equation F.14:

(i) h = local convective heat transfer coefficient. $[W/m^2 \cdot ^\circ C]$

(ii) ϵ = ratio of the specific gas constants for dry air and water vapour.
= ratio of the molecular weights of water vapour and dry air.

$$\epsilon = \frac{M_v}{M_d} = \frac{18.01534}{28.9645}$$

(iii) l_v = specific latent heat of vaporization. $[J/kg]$
(Pruppacher and Klett, 1978, p.89)

$$l_v = 4186.84 \left[597.3 \left(\frac{273.15}{T} \right)^{(0.167 + 0.000367T)} \right]$$

(iv) P_{stat} = static air pressure. $[Pa]$

(v) e_a, e_s = saturation vapour pressure of water at ambient air temperature and cylinder surface temperature respectively. $[Pa]$ (Lowe, 1977)

$$e = 100(A_0 + T(A_1 + T(A_2 + T(A_3 + T(A_4 + T(A_5 + TA_6))))))$$

where

$$\begin{aligned} A_0 &= 6984.505294 \\ A_1 &= -188.9039310 \\ A_2 &= 2.133357675 \\ A_3 &= -1.2885809730 \text{ E-02} \\ A_4 &= 4.393587233 \text{ E-05} \\ A_5 &= -8.023923082 \text{ E-08} \\ A_6 &= 6.136820929 \text{ E-11} \\ T &= \text{temperature. } [K] \end{aligned}$$

(vi) C_{pa} = specific heat capacity of moist air at constant pressure. $[J/kg \cdot K]$

$$C_{pa} = C_{pd} \left[1.0 + \left(\frac{C_{pv}}{C_{pd}} - 1.0 \right) \frac{W}{W + 1} \right] \quad (F.15)$$

where C_{pd} = constant pressure specific heat capacity of dry air.
 = 1005 J/kg·K.
 C_{pv} = constant pressure specific heat capacity of water vapour.
 = 1850 J/kg·K.
 W = humidity ratio for moist air. (see below)

The humidity ratio (W) in Equation F.15 is given by ASHRAE (1977, P.5.3) as:

$$W = 0.62198 \left[\frac{(RH)_e}{P - (RH)_e} \right] \quad (F.16)$$

where P_{stat} = static air pressure. [Pa]
 RH_e = relative humidity. [decimal]
 P_e = saturation vapour pressure of water vapour. [Pa]

(vii) $\frac{Pr}{Sc}$ = ratio of the Prandtl number to the Schmidt number

$$Pr = \frac{\nu}{\alpha}, \quad Sc = \frac{\nu}{D}$$

therefore
$$\frac{Pr}{Sc} = \frac{D}{\alpha}$$

where D = diffusivity of water vapour in air. [m^2/s]
 α = thermal diffusivity. [m^2/s]

Pruppather and Klett (1978) estimate the diffusivity of water vapour in air for temperatures between -40°C and +40°C as:

$$D = 2.11 \times 10^{-5} \left(\frac{101325.0}{P} \right) \left(\frac{T}{273.15} \right)^{1.94}$$

where T = temperature. [K]
 P_{stat} = static air pressure. [Pa]

$$\alpha = \frac{k_a}{\rho_a C_p} \quad (\text{F.17})$$

where k_a = thermal conductivity of moist air. [W/m·°C]
 ρ_a = density of moist air. [kg/m³]

An expression for the thermal conductivity of moist air is given by Pruppacher and Klett (1978, P.418) which is based on the thermal conductivity of dry air (k_d) and the conductivity of water vapour (k_v). The expression reported by Pruppacher and Klett has a typographical error and should read:

$$k_a = k_d \left[1 - \left(1.17 - 1.02 \frac{k_v}{k_d} \right) \right] x_v \quad (\text{F.18})$$

where x_v = mole fraction for water vapour in moist air.

$$k_d = 4.1868 \times 10^{-3} [5.69 + 0.017(T - 273.15)]$$

$$k_v = 4.1868 \times 10^{-3} [3.78 + 0.020(T - 273.15)]$$

To eliminate x_v in Equation F.17, ASHRAE (1977, P.5.2) defines the humidity ratio (W) in terms of the mole fraction x_v as:

$$W = 0.62198 \frac{x_v}{x_a}$$

but

$$x_v + x_a = 1.0$$

therefore

$$W = 0.62198 \frac{x_v}{1 - x_v}$$

or

$$x_v = \frac{W}{0.62198 + W} \quad (F.19)$$

Substituting Equation F.19 into F.18 gives:

$$k_a = k_d \left[1 - \left(1.17 - 1.02 \frac{k_v}{k_d} \right) \right] \frac{W}{W + 0.62198}$$

An expression for the density of moist air (ρ_a) in Equation F.17 can be determined if both dry air and water vapour are assumed to obey the perfect gas equation of state.

$$\rho_a = \frac{(\text{mass of dry air}) + (\text{mass of water vapour})}{(\text{total volume of the mixture})} = \frac{(m_d + m_v)}{V}$$

$$\rho_a = \frac{m_d}{V} \left(1 + \frac{m_v}{m_d} \right)$$

but

$$W = \frac{m_v}{m_d}$$

therefore

$$\rho_a = \frac{m_d}{V} (1 + W) \quad (F.20)$$

ASHRAE (1977) shows that the specific volume of a moist

air mixture expressed in terms of a unit mass of dry air as:

$$v = \frac{V}{m_d} = \frac{R_a T}{P_{stat} - P_v} \quad (F.21)$$

Substituting Equation F.21 into Equation F.20 gives:

$$\rho_a = \frac{P_{stat} - P_v}{R_a T} (1 + W)$$

The humidity ratio (W) given by Equation F.16 can be expressed in terms of the partial pressure of water vapour (p_v) as:

$$W = 0.62198 \frac{P_v}{P_{stat} - P_v}$$

Solving for p_v gives:

$$P_v = \frac{1.6078 W P_{stat}}{1 + (1.6078)W} \quad (F.22)$$

Substituting Equations F.21 and F.22 into Equation F.20 gives the density of moist air as:

$$\rho_a = \frac{P_{stat} (1 + W)}{R_a T [1 + (1.6078)W]}$$

but

$$R_a = \frac{R}{M_d} = 287.055 \text{ J/kg-K}$$

therefore

$$e_a = \frac{P_{\text{stat}} (1 + W)}{(287.055) T [1 + (1.6078)W]}$$